PEDRO MANUEL FORTES NASCIMENTO

Study of Matrix Gla Protein (MGP) deficiency in the zebrafish and its interaction with Elastin.

Contribution to the study of Keutel syndrome

Universidade do Algarve

Faculdade de Ciências e Tecnologias

2022

PEDRO MANUEL FORTES NASCIMENTO

Study of Matrix Gla Protein (MGP) deficiency in the zebrafish and its interaction with Elastin.

Contribution to the study of Keutel syndrome

Master's in Biotechnology

Work conducted under scientific tutoring of: Doctor João Santos
Doctor Paulo Gavaia

Universidade do Algarve

Faculdade de Ciências e Tecnologias

2022

Study of Matrix Gla Protein (MGP) deficiency in the zebrafish and its interaction with Elastin. Contribution to the study of Keutel syndrome

Declaração de autoria de trabalho

Declaro ser o autor deste trabalho, que é original e inédito. Autores e trabalhos consultados estão devidamente citados no texto e constam da listagem de referências incluída.

_____

Pedro Manuel Fortes Nascimento

"Sometimes Science is more art than Science."

Sanchez, Rick

"Happiness can be found, even in the darkest of times, if one only remembers to turn on the light."

Rowling, J.K.

Agradecimentos

Em primeiro lugar, quero agradecer à Professora Doutora Leonor Cancela pela oportunidade dada em realizar este trabalho no laboratório BIOSKEL.

Um agradecimento aos meus orientadores, Doutor Paulo Gavaia e Doutor João Santos, pelo apoio prestado ao longo deste trabalho. Em especial agradecer, pelos ensinamentos tutorados, pela paciência no esclarecimento de dúvidas e pelo pragmatismo na resolução dos problemas que foram surgindo.

A todos os colegas de laboratório, em especial à Rita e Carolina, que para além colegas de laboratório e bancada com o qual partilhei bons momentos, foram sempre incansáveis na ajuda e disponibilidade que me prestaram durante todo o fluxo de trabalho e pessoal.

À minha família, em especial à minha mãe e irmã, por sempre acreditarem em mim e me apoiarem em todos os momentos, sobretudo aqueles mais conturbados. Por todo o esforço que sempre fizeram para que eu tenha a oportunidade de singrar no que sempre almejei. Obrigado por 27 anos de vida privilegiados ao vosso lado.

Ao meu avô, um dos maiores pilares da minha vida e que de forma tão incansável contribuiu para o meu crescimento pessoal e académico. Espero que me estejas a ver, pois as promessas feitas estão em marcha e continuarão a ser cumpridas com a mesma força de vontade a que me habituaste.

Aos meus amigos, que têm acompanhado o meu crescimento pessoal e académico, que estiveram lá muitas vezes quando mais era necessário e por terem contribuído mais do que pensam para que este trabalho fosse desenvolvido.

Agradecer também, a tudo e todos aqueles que contribuíram igualmente para o meu sucesso pessoal e académico ao longo deste período, que sem os quais não seria a pessoa na qual hoje me ergo.

Muito Obrigado,

Pedro

Abstract

The Keutel Syndrome (KS) is a rare autosomal recessive disorder that manifests in humans due to loss-of-function mutations in the *MATRIX GLA PROTEIN* (*MGP*) gene, which is correlated with ectopic calcification within cartilaginous and vascular tissues. The mechanisms by which MGP inhibits calcium deposition are still poorly understood, thus contributing to a major limitation in the comprehension of the disease pathophysiology and therefore the development of effective therapies. The Mgp-deficient mice model has been very used to favor the understanding of the disease. However, the symptomatology in Mgp-deficient mice is far more severe from what is observed in KS patients, which generates interest in the development of new animal models that can mimic the disease. The objectives of this work were to contribute to the establishment for the first time of a zebrafish model to study KS pathophysiology and to investigate whether MGP is a crucial inhibitor of vascular and cartilage calcification in the zebrafish model. For that, we identified and characterized an *mgp* zebrafish through RT-PCR and sequencing, and found an 18-nucleotide deletion at exon 4. Next, we performed a morphometric analysis at the larval and adult stages of development, where we found that the homozygous *mgp* mutant larvae are smaller than their wild-type siblings. To investigate the impact of the mutation in the process of ectopic mineralization, the zebrafish mutants were treated with warfarin, a potent inhibitor of the vitamin K cycle that induces ectopic calcification, and we found that the homozygous mutants die more. To determine the pathological accumulation of calcium, we performed Alizarin red S and von Kossa stainings, and we found that the *mgp* homozygous mutants have an extensive accumulation of calcium in the abdominal intervertebral space, caudal fin ray area, heart and parasphenoidal carotid artery. To confirm that these effects were due to the loss of expression of Mgp, we performed an immunohistochemistry analysis with an anti-BGP lab produced antibody and found a reduction in the expression of Mgp in the *mgp* mutants.

In conclusion, we characterized a zebrafish mutant for *mgp* and found that they have a reduced size and extensive accumulation of calcium in bone and soft tissues. The *mgp* zebrafish mutant mimics the conditions observed in human KS patients suggesting that it might be a good model to study the pathophysiology of the KS.

Keywords: Ectopic calcification, Keutel Syndrome, Matrix Gla protein (MGP), zebrafish.

Resumo

A Síndrome de Keutel (KS) foi caracterizada pela primeira vez em 1972 por Keutel e colegas. A (KS) é uma doença autossómica recessiva rara que se manifesta em humanos devido a mutações que levam à perda de função da proteína Gla de Matriz (MGP). A sua prevalência é rara, afetando 1 em 1 000 000 pessoas e, até hoje, apenas 43 casos de KS foram relatados. Contudo, devido às semelhanças sintomáticas com outras doenças e baixa letalidade da KS, espera-se que o número de casos de KS seja maior do que até então tem sido relatado. Apesar da KS ser uma doença rara, possui um quadro de sintomas muito vasto, desde atrasos no desenvolvimento e anormalidades nas estruturas faciais como a hipoplasia da face intermédia, braquitelefalangismo, a sintomas mais severos que condicionam progressivamente a sua saúde, tais como, a calcificação ectópica a nível do trato respiratório, vascular e cartilaginoso. O diagnóstico primordial da KS é frequentemente específico para a sintomatologia e/ou características morfológicas observadas. O braquitelefalangismo e a calcificação coronária da válvula aórtica são frequentemente identificados através de abordagens radiográficas como a tomografia computorizada (TC). As estenoses simples podem ser observadas através da endoscopia e outros sintomas, tais como perda de audição, convulsões ou atraso de desenvolvimento devem ser avaliados muito cedo durante o desenvolvimento, antes que a calcificação anormal inicie nessses tecidos. A esperança média de vida dos pacientes de KS é dependente de muitos fatores, sobretudo a gravidade das complicações associadas ao pulmão, que muitas vezes preveem o prognóstico dos pacientes. No entanto, não existe atualmente nenhuma terapia específica para a KS.

A MGP é uma pequena proteína da matriz extracelular (ECM) que tem um papel importante na prevenção da deposição de cálcio e na prevenção de problemas de calcificação ectópica nos tecidos cartilaginosos e vasculares. A MGP pertence à família das proteínas Gla nas quais também estão incluídas outras proteínas esqueléticas da ECM, incluindo a osteocalcina, fatores de coagulação tais como os fatores II, VII, IX e X, e fatores anticoagulantes como as proteínas S e C. A perda de função na MGP leva à calcificação anormal de tecidos moles *in vivo*, como é observado nos humanos e nos ratinhos. No ratinho, a perda de função da MGP resulta na morte prematura, poucas semanas depois de nascerem, devido a uma extensa calcificação da aorta e consequentemente, a sua ruptura. A MGP desempenha um papel importante na regulação da calcificação da ECM, ligando-se a iões de cálcio com elevada afinidade, evitando assim que estes

se acumulem nos locais das fibrilhas de colagénio e elastina. Os mecanismos pelos quais a MGP inibe a deposição do cálcio ainda são pouco compreendidos, contribuindo assim para uma grande limitação na compreensão da patofisiologia da doença e, portanto, no desenvolvimento de terapias eficazes. O modelo de ratinho deficiente da MGP tem sido muito usado para favorecer a compreensão da doença. No entanto, a sintomatologia expressa nos ratos é muito mais grave do que é observado em pacientes com KS.

O peixe-zebra (Danio rerio) é um pequeno peixe teleósteo de água doce com inúmeras características que o torna num bom modelo de estudo para doenças humanas, tais como o seu rápido desenvolvimento, translucência dos embriões e os baixos requisitos necessários para a sua manutenção. Os peixes-zebra são pequenos, exigindo assim apenas espaço mínimo de manutenção. Os peixes-zebra desenvolvem-se muito rapidamente, em comparação com outros peixes teleósteos e outras espécies de peixes marinhos, permitindo-lhes ser manuseados facilmente para a investigação genética e biomédica, uma vez que podem ser geridos e estudados em fases iniciais do desenvolvimento. Os peixes-zebra têm o seu genoma completamente sequenciado e mapeado, e partilham uma homologia significativa com o genoma humano. A MGP é expressa nos peixes-zebra através de um único gene, e a proteína matura tem 36 aminoácidos totalmente conservados quando comparados com os mamíferos, e dentro destes, estão incluídos os três resíduos Gla que são essenciais para a ativação da proteína.

Uma vez que o mutante de ratinho apresenta limitações para o estudo e compreensão da KS, procuramos perceber se o peixe-zebra poderia ser uma boa alternativa para colmatar algumas das suas limitações. Os objetivos deste trabalho delinearam-se em contribuir para o estabelecimento pioneiro de um modelo de peixe-zebra para estudar a patofisiologia da KS e investigar se a MGP é um inibidor crucial da calcificação vascular e cartilagem no modelo do peixe-zebra.

A forma mutante da Mgp nos mutantes de peixe-zebra foi identificada e caracterizada através de RT-PCR e sequenciação. Identificámos a mutação como uma deleção de 18 nucleótidos no exão 4 do gene *mgp*, que prediz uma deleção de 6 aminoácidos na região terminal-C da Mgp. Esta região terminal é altamente conservada entre os vertebrados, e sendo que a mutação ocorreu nesta região, três desses aminoácidos bastante conservados foram removidos. Em seguida,

realizámos análises morfométricas nas fases larvares e adultas de desenvolvimento, e observámos que as larvas homozigóticas dos mutantes *mgp* são mais pequenas do que os seus irmãos wild-type. Para investigar o impacto provocado pela mutação no processo de mineralização ectópica, os peixes-zebra mutantes foram tratados com varfarina, um potente inibidor do ciclo da vitamina K que induz calcificação ectópica e, descobrimos que os mutantes homozigóticos apresentam maior letalidade. Para determinar a acumulação patológica de cálcio, realizámos técnicas específicas de coloração como a de Alizarina vermelha S e von Kossa, e identificámos que os mutantes homozigóticos para o *mgp* possuem uma extensa acumulação de cálcio no espaço intervertebral abdominal, na área do raio da barbatana caudal, no coração e na artéria carótida adjacente à cartilagem parasfenoidal. Para confirmar que os efeitos observados se deviam à perda de expressão da MGP, realizámos uma análise imunohistoquímica com um anticorpo anti-BGP produzido em laboratório e observámos uma redução na expressão da Mgp nos mutantes homozigóticos para o *mgp*.

Em conclusão, caracterizámos um mutante de peixe-zebra para o *mgp* e descobrimos que eles têm um tamanho reduzido e acumulação extensiva de cálcio nos tecidos ósseos e moles. O mutante de peixe-zebra *mgp* imita as condições observadas em pacientes de KS humanos sugerindo que poderia ser um bom modelo para estudar a fisiopatologia do KS.

Palavras-chave: Calcificação ectópica, Sindrome Keutel, peixe-zebra, Proteína Gla de Matriz (MGP).

Table of Contents

Agradecimentos i

Abstract ii

Resumo iii

List of Figures ix

List of Tables xi

Abbreviations xii

Chapter 1 - Introduction 1

1.1. Keutel Syndrome 2

a. General characterization 2

b. Current prognosis and treatment 5

1.2. MGP 5

c. General characterization 5

d. Genetic and molecular profile 7

e. Expression profile and putative regulatory factors 8

f. Post-translational modifications and the role of VK 10

g. VK antagonists 12

i. Role of MGP in calcification 13

1.3. Ectopic calcification in the vascular system and cartilaginous tissues 16

a. Ectopic calcification 16

I. Cardiovascular system 17

II. Cartilage 20

1.4. Elastin 21

a. General characterization 21

b. Elastin's correlation with calcification 21

1.5. Zebrafish 23

a. General characterization 23

b. Model establishment and detailed characterization 23

c. Genetic, organ and tissue homology to human 24

d. Developmental characterization 24

e. *mgp* expression in zebrafish 25
f. *eln* expression in zebrafish 26
g. Ectopic calcification in zebrafish 27
h. Transgenic zebrafish lines to study ectopic mineralization 27
i. Knockout and knockdown mutation approaches 28

Chapter 2 - Objectives 30
2.1. Objectives 31

Chapter 3 - Materials and Methods 32
3.1. Zebrafish lines and husbandry 33
3.2. Biological sample acquisition 33
3.3. Genomic DNA extraction and yield concentration analysis 33
3.4. Real-time qPCR 34
3.5. Sequencing Alignment and Peptide Bioinformatic Analysis 35
3.6. Morphometric analysis 35
3.7. Hatching rate, egg mortality and larvae mortality 36
3.8. Warfarin treatment 36
3.9. Alizarin Red *in vivo* Staining 37
3.10. Immunohistochemistry 39
3.11. von Kossa's staining and toluidine coloring 41
3.12. Statistical analysis 41

Chapter 4 – Results and Discussion 43
4.1. Identification and genomic characterization of the *mgp* mutants 44
4.2. *mgp* mutant larvae developmental characterization 48
4.3. Morphometric analysis of the *mgp* mutants 51
4.4. Inducing ectopic calcification to the *mgp* mutants 54
4.5. Analysis of ectopic calcification in the *mgp* mutant zebrafish 56
4.5.1. Abdominal vertebrae 56
4.5.1.1. Distances between vertebrae 57
4.5.1.2. Area of the vertebrae 58
4.5.1.3. Mineralization quantification of the vertebrae 59
4.5.2. Caudal fin rays 60
4.5.2.1. Area of the caudal fin rays 62

4.5.2.2. Mineralization quantification of the caudal fin rays 63
4.6. Mgp expression 64
4.7. Ectopic calcification assessment in the *mgp* mutants 66
Chapter 5 - Conclusion 70
Bibliography 74
Appendix 83

List of Figures

Figure 1.1. Typical KS patient features 4
Figure 1.2. Chronological illustration of the MGP mutations identified in KS patients 5
Figure 1.3. Human MGP gene, transcripts and protein isoforms 8
Figure 1.4. MGP expression in human tissues and organs 10
Figure 1.5. VK cycle scheme 12
Figure 1.6. Role of MGP in ectopic calcification 15
Figure 1.7. Human organs and tissues where abnormal calcification occur 16
Figure 1.8. Arterial wall transversely cut illustration.. 18
Figure 1.9. Human heart and section of the human heart wall.. 19
Figure 1.10. Relationship between vitamin K and elastin degradation 22
Figure 1.11. Zebrafish life cycle and each developmental stage 25
Figure 1.12. Mgp expression in the zebrafish organ and tissues systems 26
Figure 1.13. Genetic editing approaches scheme 29
Figure 3.1. Genomic DNA extraction 34
Figure 3.2. Real Time-qPCR protocol used to identify the zebrafish mutants 35
Figure 3.3. Morphological measured parameters of zebrafish 36
Figure 3.4. Treatment with warfarin 37
Figure 3.5. Experimental layout of the Alizarin red staining 38
Figure 3.6. F3 generation larvae in polypropylene embedding molds with GMA monomer and 2% catalyst 40
Figure 3.7. Von Kossa staining and toluidine coloring protocol to the zebrafish sections 41
Figure 4.1.1. qPCR melting curve of the F1 *mgp* zebrafish mutants 45
Figure 4.1.2. Chromatogram of the *mgp* exon 4 in the *mgp* zebrafish mutants 47
Figure 4.1.3. MGP peptide sequence alignment with other vertebrates 47
Figure 4.2.1. Impact of the loss of *mgp* function in embryo mortality 49
Figure 4.2.2. Impact of the loss of *mgp* function in the hatching rate at 48 hpf 50
Figure 4.2.3. Larval mortality of the *mgp* mutants between 7 and 11 dpf 51
Figure 4.3.1. Morphometric analysis of the F1 *mgp* mutation carriers at 5 mpf 52
Figure 4.3.2. Morphometric analysis of the F3 *mgp* mutants until 30 dpf 53
Figure 4.3.3. Morphometric analysis of the F3 *mgp* mutants at 5 mpf 54

Figure 4.4.1. Inducing ectopic calcification to the *mgp* mutants at 19 dpf 56
Figure 4.5.1.1. *In vivo* alizarin red staining of *mgp* mutant larvae at 22 dpf 57
Figure 4.5.1.2. Intervertebral measurement of the *mgp* mutants at 22 dpf 58
Figure 4.5.1.3. Vertebrae area of the *mgp* mutants at 22 dpf 59
Figure 4.5.1.4. Calcification quantification of the abdominal vertebrae of the *mgp* mutants at 22 dpf 60
Figure 4.5.2.1. Alizarin red staining *in vivo* of the *mgp* mutant larvae at 22dpf 61
Figure 4.5.2.2. Area of the caudal fin rays of the *mgp* mutants at 22 dpf 62
Figure 4.5.2.3. Calcification quantification of the caudal fin rays of *mgp* mutants at 22 dpf 64
Figure 4.6.1. Immunohistochemistry for Bgp in the *mgp* mutants at 33 dpf, *ex vivo* 65
Figure 4.7.1. Ectopic calcification on the *mgp* mutants at 33 dpf, *ex vivo* 67
Figure 4.7.2. Ectopic calcification on the *mgp* mutants at 33 dpf, *ex vivo* 68
Figure 4.7.3. Ectopic calcification on the *mgp* mutants at 33 dpf, *ex vivo* 69
Figure A.1. Crossings of the *mgp* mutants to obtain the F3 generation zebrafish 84
Figure A.2. Summary image of the knockout *mgp* mutant generation 85

List of Tables

Table 1.1. Symptoms and features of KS patients and their frequency 3
Table 1.2. MGP expression in different tissues of different vertebrates 6
Table 5.1. KS features comparison between KS human patients and the *mgp* mutants 72

Abbreviations

ALK-1	Activin receptor-like kinase type 1
BA	Branchial arch
BCF	Bottom lobe caudal fin
Bgp	Bone Gla protein
BMP	Bone morphogenetic protein
cDNA	complementary Desoxyribonucleic acid
CDPX1	Brachytelephalangic X-linked chondrodysplasia punctata
CM	Cardiac muscle
cMGP	Carboxylated MGP
COO^-	Carboxyl group
COPD	Chronic obstructive pulmonary disease
CRISPR-Cas9	Clustered regularly interspaced short palindromic repeat- associated protein 9
CT	Computed tomography
CTCF	Corrected Total Cell Fluorescence
CV	Caudal vertebrae
DAB	Diaminebenzidine
ddH_2O	Deionized distilled water
dgf	*dragonfish*
DNA	Desoxyribonucleic acid
Dpf	Days post fertilization
dpMGP	dephosporylated MGP
dp-ucMGP	dephosporylated and uncarboxylated MGP
E	Erythrocytes
ECM	Extracellular matrix
ED	Eye diameter
EDTA	Ethylenediamine tetraacetic acid
EDPs	Elastin-derived peptides
ELN	Elastin
elna	Elastin gene a
elnb	Elastin gene b

ENU	Ethyl-nitrosourea
fbn1	*fibrillin-1*
FGF	fibroblast growth factor
FL	Fork length
GGCX	γ-glutamyl carboxylase
Gla	γ-carboxyglutamic acid
Glu	Glutamate
GMA	Glycidyl methacrylate
GOI	Gene of interest
HL	Head length
HP	Heart periphery
hpf	Hours post-fertilization
HT	Heart Tissue
IL-1	Interleukin type 1
IP	Inferior parasphenoidal cartilage
KH_2	vitamin K_2 reduced form
KP	Kidney periphery
KS	Keutel syndrome
KT	Posterior kidney tissue
MGP	Matrix Gla Protein
Mgp $^{-/-}$	Mgp-deficient
mgp $^{+/+}$	*mgp* wild type siblings
mgp $^{+/m}$	*mgp* heterozygous mutant
mgp $^{m/m}$	*mgp* homozygous mutant
MO	Morpholino
mpf	months post fertilization
MV's	Matrix vesicles
N	Number of specimens
NHEJ	non-homologous end joining
NK	Natural killer
npMGP	non-phosphorylated Matrix Gla Protein
NT	Non-treated

OA	Osteoarthritis
PAM	Protospacer adjacent motif
PBS	Phosphate buffer saline
PCR	Polymerase chain reaction
PFA	Paraformaldehyde
P_i	Inorganic phosphorus
PKD1*/*PDK2	Polycystin-1/polycystin-2
PKP	Posterior kidney periphery
pMGP	phosphorylated Matrix Gla Protein
polr2f	RNA polymerase II subunit F
PXE	Pseudoxanthoma elasticum
qPCR	Quantitative Polymerase Chain Reaction
RFU	Relative fluorescence units
RNA	Ribonucleic acid
RNA_i	RNA interference
SD	Standard deviation
sgRNA	synthetic single guided RNA
SL	Standard Length
SP	Superior Parasphenoidal cartilage
sox10	SRY-Box Transcription Factor 10
T	Treated
TAGLN	*TRANSGELIN*
TALENs	Transcription activator-like effector nucleases
TCT	Tampon coons with Tris
TCF	Top lobe Caudal Fin
TGF-β1	Transforming Growth Factor-beta type 1
TL	Total Length
TNF-α	Tumor Necrosis Factor-α
ucMGP	uncarboxylated MGP
UTR	Untranslated region
VK	Vitamin K
VKDP	Vitamin K-dependent proteins

VKO	Vitamin K epoxide
VKOR	Vitamin K epoxide reductase
VSMC	Vascular smooth muscle cells
W	Width
WT	Wild type
-/-	Homozygous
(w/v)	Weight per volume

Chapter 1 - Introduction

1.1. Keutel Syndrome

a. General characterization

Keutel syndrome (KS) is an autosomal recessive disorder, i.e., both mutated alleles must be present for KS to develop [1]. Its prevalence is rare, and it is likely to affect 1 in 1 000 000 people and to this day, only 43 KS cases have been reported. Due to symptoms similarities to other diseases, it was until recently difficult to separate KS patients from other diseases. The symptoms of KS that are shared with other diseases include abnormal cartilage calcification, peripheral pulmonary stenosis, midface hypoplasia and brachytelephalangism. Some of these symptoms overlap with other diseases such as Vitamin K (VK) deficiency embryopathy, brachytelephalangic X-linked chondrodysplasia punctata (CDPX1), mutation disorders associated with VK dependent gamma-glutamyl carboxylase (GGCX), warfarin embryopathy, and warfarin sodium therapy-induced complications. Since KS symptoms are similar to other diseases and associated with low lethality, the number of KS cases is expected to be higher but go undisclosed. Improvement in molecular approaches and the lowering price of sequencing methodologies allowed KS easier diagnose [2]. Table 1.1 describes the symptoms of reported observations in KS patients, although it is likely that KS patients had other associated problems not reported or overlooked.

Table 1.1. Symptoms and features of KS patients and their frequency [2,3].

Very Frequent (>80% of cases)	Frequent (20-80% of cases)	Rare (<20% of cases)
Developmental abnormalities: • Brachytelephalangism • Depressed nasal bridge • Midface hypoplasia • Tracheal atresia **Cardiovascular defects :** • Peripheral pulmonary stenoses (PPS) **Ectopic calcification:** • Cartilaginous calcification • Respiratory tract calcification **Respiratory issues:** • Wheezing and Dyspnea	**Developmental abnormalities:** • Physical and psychomotor developmental delay • Mild mental retardation • Underdeveloped alae nasae • Sloping forehead • Short stature **Cardiovascular defects :** • Ventricular septum hypertrophy • Pulmonary artery hypertension **Ectopic calcification:** • Vascular calcification • Ribs calcification **Respiratory issues:** • Persistent respiratory infections **Other defects/causes:** • Hearing loss • Ear infections and sinusitis • Teeth abnormalities	**Developmental abnormalities:** • Infertility • Abortions **Cerebral defects :** • Seizures • Brain damages • Memory loss **Ectopic calcification:** • Brain calcification **Respiratory issues:** • Nasaled and breathless speech **Skin/glandular issues:** • Skin lesions • Flabby and pasty skin • Thyroid nodules **Other defects/causes:** • Alopecia • Optic atrophy

KS was first characterized in 1972 by Keutel and co-authors [4]. Patients features include abnormalities in cartilage calcification, tracheobronchial narrowing, and peripheral pulmonary artery stenoses [1]. Abnormal calcification on cartilaginous tissues can lead to or results from impaired formation of skeletal tissues, subsequently leading to midface hypoplasia [2]. Other phenotypic features identified include brachytelephalangism, neural hearing loss, depressed nasal bridge, midface retrusion, calcified auricles, and short stature [4,5].

KS primordial diagnosis is often specific to symptomatology and/or morphological features seen in Figure 1.1. Brachytelephalangism is often identified through radiographic approaches, and aortic valve and coronary calcification can be detected by computed tomography (CT) [3,6]. Simple stenosis can be observed through endoscopy [7] and other symptoms such as hearing loss, seizures or developmental delay can be assessed during early development before abnormal calcification initiates in the tissues [2]. As KS is similar with other human disorders such as pseudoxanthoma elasticum (PXE), further confirmation by mutational analysis is often necessary before the diagnosis can be made [8].

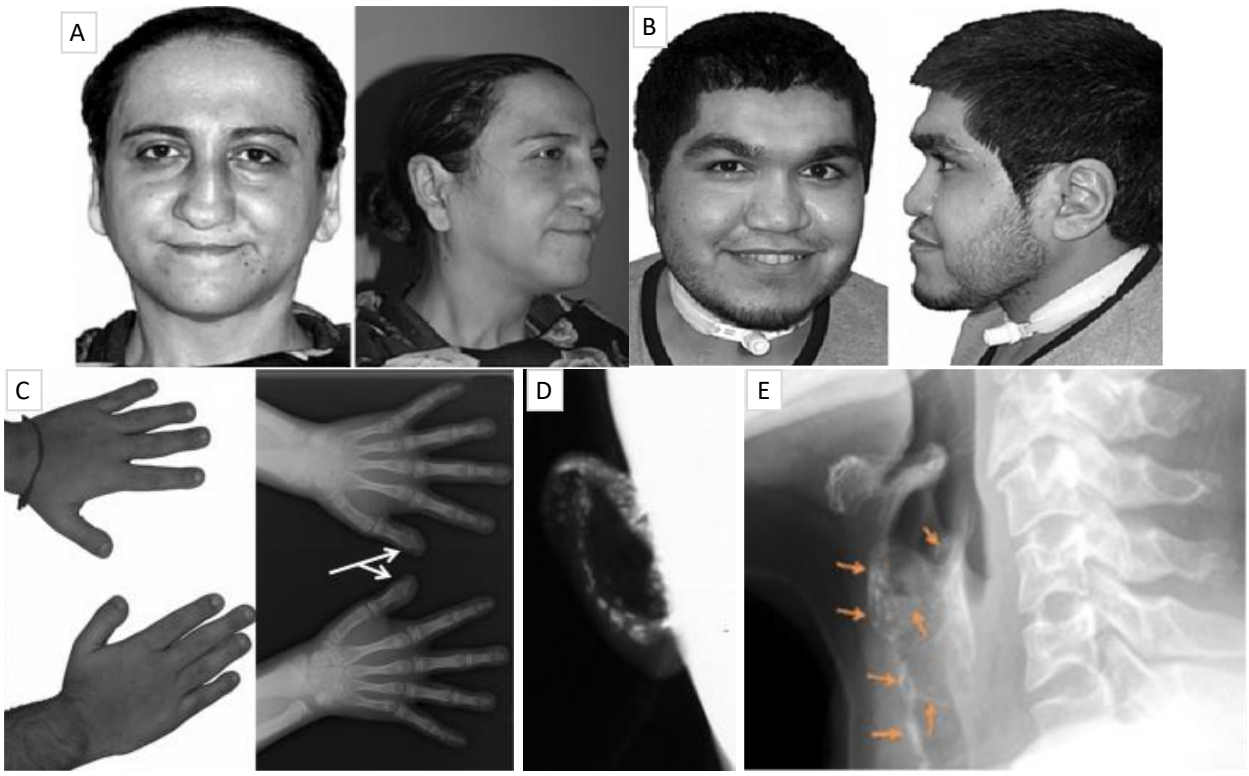

Figure 1.1. Typical KS patient features. (A and B) Frontal pictures of two diagnosed KS patients. (C) Hand brachytelephalangism (left) and radiographic image (right), (D) abnormal calcification of auricle and (E) laryngotracheal calcification (adapted from [5,9,10]).

The candidate causal gene, behind the KS disease development, was identified 27 years after KS first diagnose. In 1999, Munroe et al. first identified mutations in the *MATRIX GLA PROTEIN* (*MGP*) gene from two Turkish consanguineous families [9]. According to Munroe and co-authors, all KS patients displayed mutations in the MGP gene, and these mutations were associated with the absence or non-functional activity of MGP [9]. Figure 1.2. illustrates the chronological identification of all *MGP* mutations in KS patients described so far. Nowadays, through morphological and clinical examinations followed by sequencing of the *MGP* alleles, KS can be readily distinguished. Of the total KS cases, around 74% occurred in consanguineous families and are mainly diagnosed in children and adolescences, from 5 to 15 years of age [2,5].

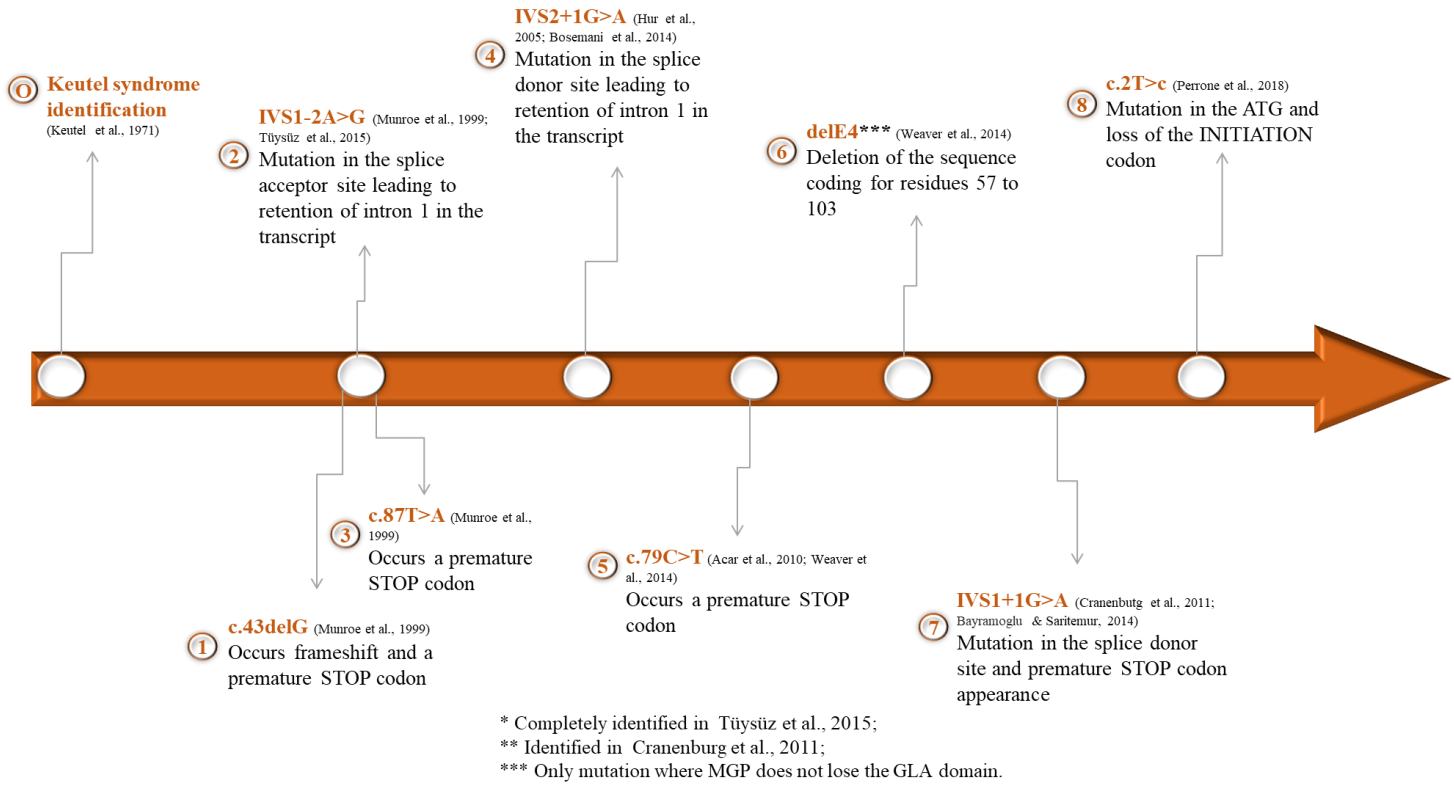

Figure 1.2. Chronological illustration of the MGP mutations identified in KS patients (adapted from [2]).

b. Current prognosis and treatment

KS prognosis is usually good and diagnosed children survive through adulthood. Although life expectancy is dependable on many factors, the severity of lung associated complications often predicts patients' prognostic. In general, KS patients suffer from their abnormal displayed features, a discomfort that is spread to their relatives [2].

Treatment options for KS include angiographic dilation for peripheral pulmonary artery stenosis, chemical bronchodilation for dyspnea and wheezing, reconstructive surgery for midface hypoplasia, and antihypertensive agents for hypertension [2,8]. However, there is currently no specific therapy for KS.

1.2. MGP

c. General characterization

MGP is a small extracellular matrix (ECM) protein that appears to be correlated with ectopic calcification [11]. MGP belongs to the Gla protein family in which are also included other

skeletal ECM proteins including osteocalcin, coagulation factors such as factors II, VII, IX and X, and anticoagulation factors proteins S and C [9]. Loss-of-function mutations in *MGP* can lead to abnormal calcification of soft tissues *in vivo*, as seen in human and mice [12,13]. MGP plays an important role in the regulation of the ECM calcification, by binding calcium ions with high affinity, thus preventing calcium ions from accumulating within collagen and elastin fibrils' sites [14]. Additionally, other functions have been attributed to MGP including the regulation of transforming growth factor-beta type 1 (TGF-β1) activity, the maintenance of endothelial cells normal function, and BMP and Notch signaling regulation, by inhibiting bone morphogenetic proteins (BMP) 2, 4 and 7 activities [15]. MGP tends to accumulate in the ECM of calcified cartilage and is mostly expressed by vascular smooth muscle cells (VSMC), chondrocytes and mesenchymal stem cells [16,17]. MGP can be synthesized in lungs, cartilage, heart, kidneys, spleen, and arterial vessel walls [18,19]. MGP is expressed in all vertebrates, beginning at early developmental stages in most vertebrates and at the embryonic stage (24 hours post-fertilization) in zebrafish [20,21]. Table 1.2 shows tissues in which MGP expression has been previously reported.

Table 1.2. MGP expression in different tissues of different vertebrates. N/A= not available (adapted from [22]).

	Mammals	**Chicken**	***Xenopus laevis***	**Teleost fishes**
Embryonic tissues	Present	Present	N/A	N/A
Cartilaginous tissues	Present	Present	Present	Present
Muscles and connective tissues	N/A	Present	Absence	Present
Cardiovascular tissues	Present	Present	N/A	Present in the heart

d. Genetic and molecular profile

Cancela et al. identified that the human *MGP* gene is found at locus 12p13.1-p12.3 [23]. MGP is encoded by one single gene in all vertebrates [20]. Until early in 2014, it was believed that MGP gene was consisted of four exons and three introns, comprising a total length of 3,9 kilobases [24]. Exon 1 encodes the 5'- untranslated region (UTR) and transmembrane signal peptide. Exon 2 is translated into the α-helical domain. Exons 3 and 4 encode the putative γ-carboxylation recognition sites and the domains containing Gla residues, respectively [23]. MGP is now known to span a 5th exon, discovered from cDNA sequences of human fetal brain precursor tissue, seen in Figure 1.3 A [20]. Figure 1.3 B shows the possible two human MGP transcripts. MGP was first isolated from urea extracts of bovine bone matrix in 1983 by Price *et. al.* [18]. MGP is a 10-14kDa protein with a theoretical isoelectric point of 9.7 and the mature protein consists of 84 amino acids [18,20,24,25]. Despite the low amount of hydrophobic amino acids in its content, mature MGP seems to poorly solubilize in water-based buffers, reinforcing its highly insolubility [11,26]. Figure 1.3 C illustrates human MGP possible isoforms. One of the two isoforms of MGP putatively have the novel exon that is only expressed in primates, between exon 1 and 2, whose function has yet to be addressed [20]. Interestingly, recent studies performed by Leurs and co-authors have detected the presence of two *mgp* genes (*mgp1* and *mgp2*) in the small-spotted catshark (*Scyliorhinus canicula*), a class of cartilaginous fishes [22].

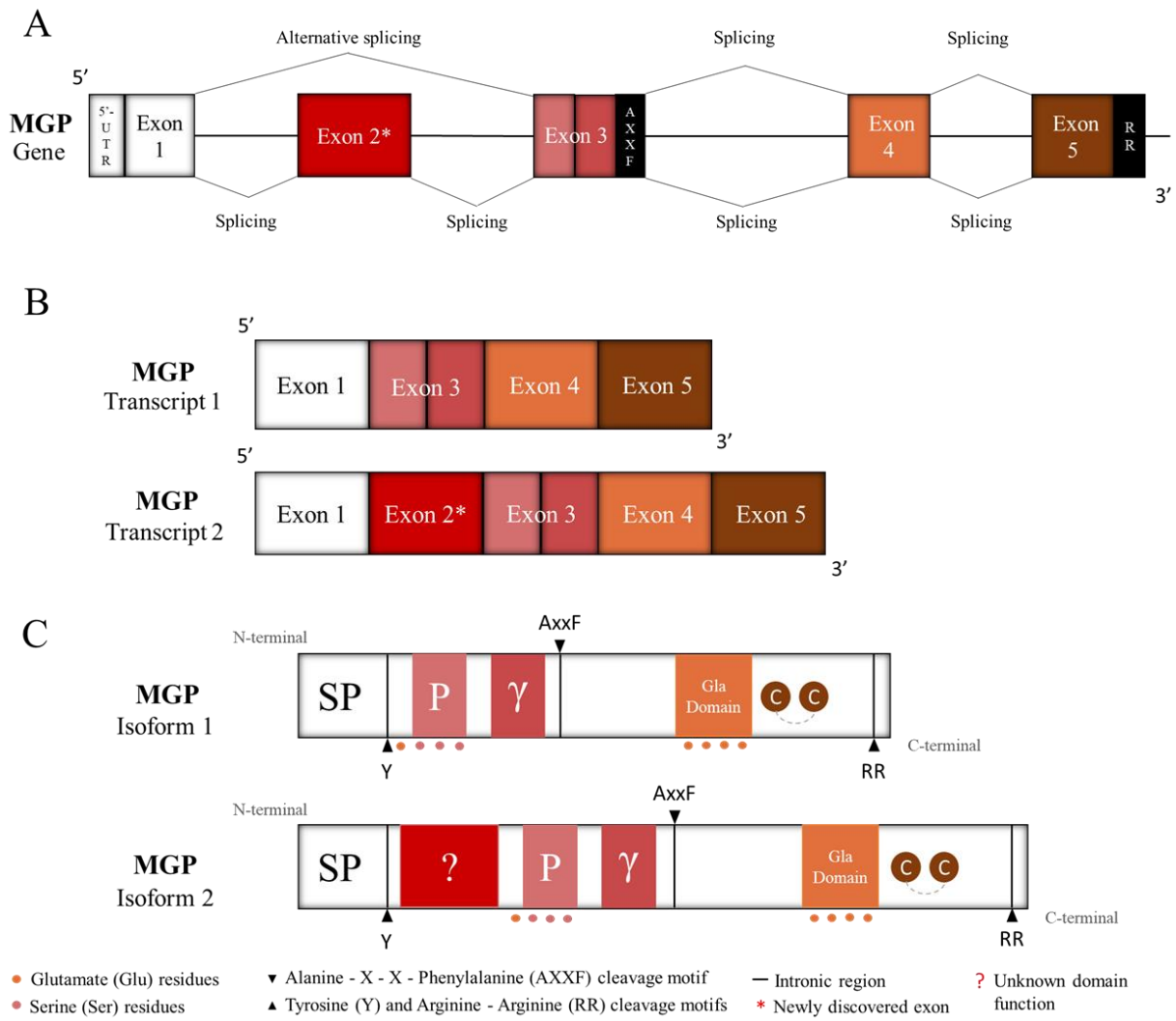

Figure 1.3. Human MGP gene, transcripts and protein isoforms. (A) Human *MGP* gene and splicing sites, (B) human MGP transcript 1 (most common form) and transcript 2 (discovered in primates) and (C) human MGP isoform 1 corresponding to the most expressed form and isoform 2, that possess a newly unknown function domain between the signal peptide and the phosphorylation domain. C-C=cysteine dissulfide bond at positions 54 and 60 (according to the 4 exon transcript); γ=gamma-carboxylase recognition site; P=phosphorylation domain; SP=signal peptide; *= last discovered exon 2; ?= unknown domain function (adapted from [2,20]).

e. Expression profile and putative regulatory factors

Studies performed by Speer and co-authors *in vitro* suggest that MGP might be strongly expressed by endothelial cells [27]. Yagami and co-authors demonstrated that either MGP absence or overexpression in *in vivo* chick limbs impact cartilage mineralization, ossification, and chondrocyte maturation [28]. Despite MGP expression in the vascular and cartilage tissues, it is mostly expressed in the gallbladder and adrenal and salivary glands. Additionally, MGP is also

expressed in the lungs and prostate [29–31]. MGP expression within the human anatomy can be seen in Figure 1.4. MGP activation is key to inhibit mineral deposition, preventing abnormal calcification. MGP inhibits BMP-2 and BMP-4 vascular calcification activity, by directly binding to their receptor [32,33]. To date, studies suggest that MGP is regulated by 1,25-dihidroxy vitamin D_3, extracellular calcium levels, fibroblast growth factor (FGF), retinoic acid, and epigenetic factors [2,34]. For instance, a study conducted by Fraser and peers observed a 15-fold increase in *Mgp* expression in rat bone cells after 1,25-dihydroxy vitamin D_3 treatment.[14]. Interestingly, MGP promoter has putative binding sites for vitamin D_3 and retinoic acid, highlighting their putative regulation role on MGP expression [17]. According to Proudfoot and co-author, vitamin D_3 increases MGP expression in mice VSMC. Additionally, high levels of vitamin D_3 lead to vascular calcification *in vivo* [35]. Upon MGP deficiency, there is an abnormal activation of signaling pathways involving *Notch*, bone morphogenetic protein (BMP), interleukin type 1 (IL-1) and tumor necrosis factor-α (TNF- α), favoring activation of transcription factors that are important to osteoblast differentiation and maturation, which induce expression of bone related proteins (e.g., osteocalcin), resulting in vascular calcification [36].

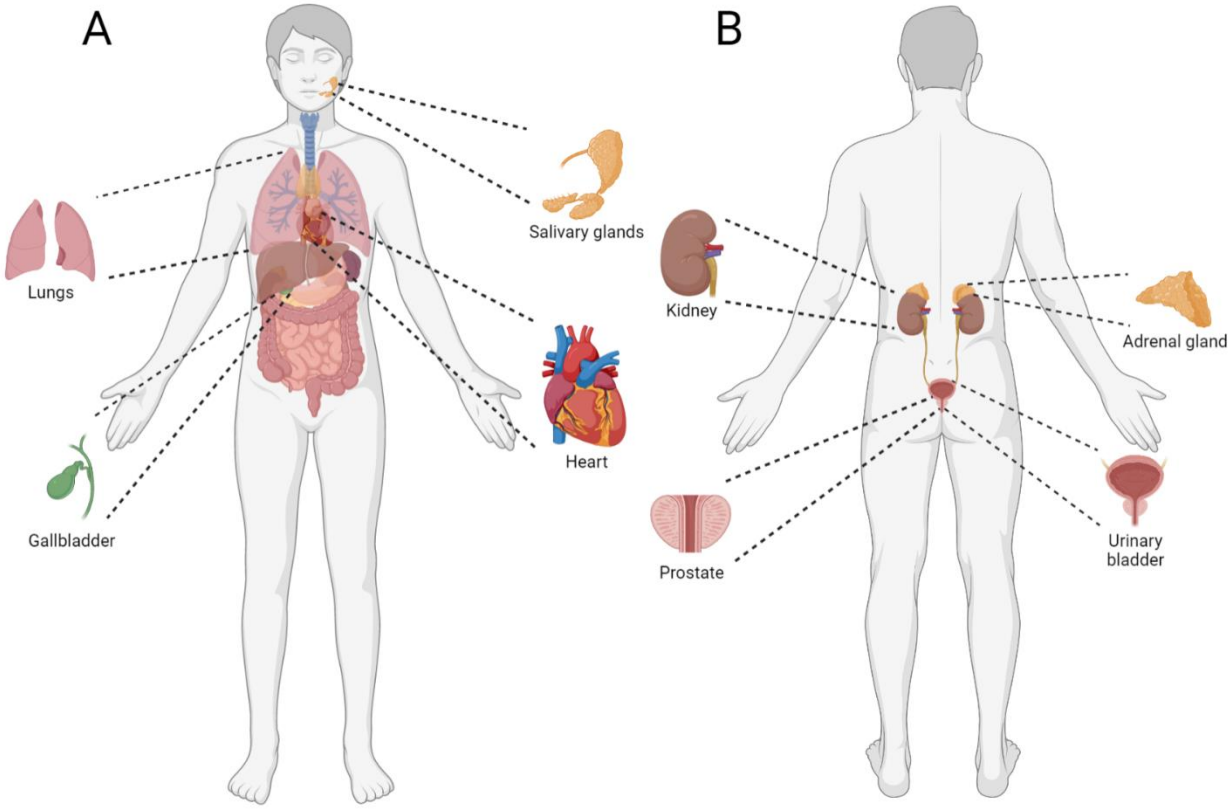

Figure 1.4. MGP expression in human tissues and organs. (A) Frontal illustration of the human organ and tissue anatomy and (B) posterior illustration of the organs and tissues found on the back of the human anatomy where MGP is expressed (adapted from [14,29,30]).

Furthermore, some genes putatively regulate MGP activity or expression. Most notably *polycystin-1* and *polycystin-2* (*PKD1*, *PDK2*) which are involved in the regulation of calcium permeable channels across cell membranes, and *activin receptor-like kinase type 1* (*ALK-1*) that may upregulate the expression of dephosporylated and uncarboxylated MGP (dp-ucMGP), although the mechanism is still unclear. In VSMC, *ALK1* increases the expression of MGP through a negative feedback mechanism [37,38].

f. Post-translational modifications and the role of VK

MGP can undergo two different post-translational modifications: the phosphorylation of the serine residues and VK-dependent γ-carboxylation of the glutamate (Glu) residues [16]. After mRNA processing is complete, the immature MGP goes for Golgi apparatus where the post-translational modifications occur. Here, a VK-dependent enzyme or kinase recognizes the signal peptide leading to conformational changes due to carboxylation of Glu residues into Gla and activation of MGP [39]. MGP carboxylation, is a process in which a carboxyl group (COO^-) is added

to five Glu residues out of nine [26]. COO^- binds to glutamate residues at positions 2, 37, 41, 48 and 52 [24]. Accordingly, MGP phosphorylation is a process in which a phosphate group binds at the serine residues 3, 6 and 9, specifically at the Ser-X-Glu motif at MGP N-terminal, thus conferring MGP its full function [31]. Data suggests that only after MGP's serine phosphorylation and γ-carboxylation, MGP is secreted to the extracellular environment [39]. Each post-translational modification changes MGP at different levels, leading to different MGP species such as: phosphorylated (pMGP), non-phosphorylated (desphospho, dpMGP), carboxylated (cMGP) or uncarboxylated (ucMGP) [16]. Studies suggest that the carboxylation of Glu residues is essential for prevention of mineral crystal formation [2]. Also, studies suggest that the phosphorylation process may be catalyzed by the enzyme casein kinase [31]. Although the role of MGP phosphorylation is not completely uncovered it appears to also be important for preventing mineral deposition [40]. Schurgers and co-authors found that *Mgp* expression in normal human vessels was predominantly carboxylated, whereas in calcified vessels *Mgp* expression was predominantly uncarboxylated, which supports the important role of carboxylation in vascular calcification [41]. Another study from Schurgers and co-authors, suggested that pMGP prevented calcium deposition while non-phosphorylated MGP (npMGP) did not prevent calcification [42]. MGP carboxylation is mediated by VK_2, which contributes to changes in the protein increasing its affinity for mineral ions like calcium and hydroxyapatite crystals, a process schematized in Figure 1.5 A [26]. When VK_2 is in its reduced form (KH_2), GGCX enzyme uses it as a co-factor to covert the Glu into γ-carboxyglutamic acid (Gla) residues. GGCX facilitates the addition of COO- to glutamic acid γ-carbon, thus generating Gla residues [43]. After that, VK_2 is converted into VK epoxide (VKO) which in time can be converted back to its initial form due to the action of VK epoxide reductase (VKOR) enzyme [44]. According to Danziger, VK_2 supplementation showed to indirectly prevent peripheral arterial calcification, probably by increasing active MGP concentration, while VK_1 supplementation did not prevent abnormal calcification. These findings suggest that VK_2 may be involved in the carboxylation of Gla proteins, thus protecting vasculature from calcifying [43].

g. VK antagonists

VK antagonists are frequently used for anticoagulation therapies. A well-known VK antagonist is warfarin, which stops the VK cycle by inhibiting VKO reduction back to VK_2, that can be seen in Figure 1.5 B [45]. Warfarin is a widely prescribed anticoagulant for treating arterial and venous thromboembolic disorders, stroke, atrial fibrillation, and hypercoagulable conditions [45]. Warfarin was discovered in the decade of 1950s [46]. The effect on the VK cycle was first demonstrated by Matschiner et al. in 1970. Their studies showed high increase in VKO in rats treated with warfarin, suggesting its interference in the reduction of VKO into VK_2 [47]. Nowadays, coumarin derivatives, other than warfarin, are clinically used for anticoagulation therapy purposes [48]. By preventing VK reduction, γ-carboxylation of VK-dependent proteins (VKDP) like MGP never occurs, which leads to an increase in ucMGP polymorphisms, resulting in mineral deposition [45].

Several studies have indicated some risks associated with warfarin treatment. According to different authors, chronic warfarin treatment leads to high ectopic calcification in coronary arteries, peripheral blood vessels, and cardiac valves [6,49–52]. Interestingly, warfarin usage during pregnancy carries major risks for both fetus and pregnant women. The coumarin derivative can cross the placenta, preventing the fetus of synthesizing VK-dependent proteins. This can lead to spontaneous abortion, central nervous system abnormalities and warfarin embryopathy for the fetus [53,54].

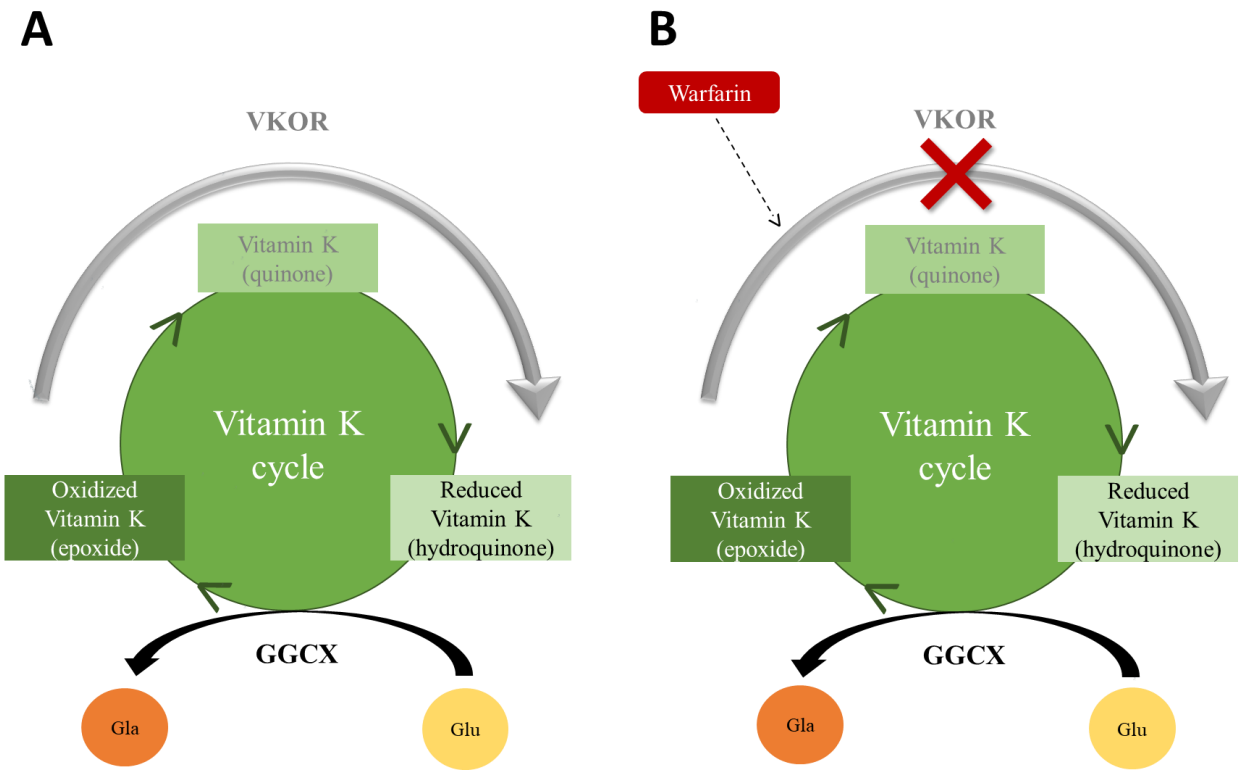

Figure 1.5. VK cycle scheme. VK cycle in (A) normal physiological conditions where it converts Glu into Gla residues and (B) during warfarin treatment, where oxidized VK is not reduced to its functional reduced form, therefore stopping the conversion of Glu into Gla amino acids. GGCX= γ-glutamyl carboxylase; VKOR= VK epoxide reductase.

h. MGP Knockout mice

In MGP-deficient (*Mgp* $^{-/-}$) mice, calcification aggravates quickly, being prominent in vasculature and cartilage at initial stages of development. According to a study from Luo and co-authors, an *Mgp* $^{-/-}$ mice model die prematurely by two months of age from severe arterial calcification and develop slowly which reflects on their short stature compared with their wild type siblings. Calcification defects, particularly in the aorta, become evident at 2-3 weeks post-gestation [13]. Murshed et al., used the *Mgp* $^{-/-}$ mice model developed by Luo et. al [13], in which the absence of MGP did not prevent mineral deposition, reinforcing its role on the anti-mineralization process [55].

i. Role of MGP in calcification

MGP acts as an important inhibitor of vascular and cartilage calcification [25]. MGP prevents ectopic calcification after serine phosphorylation and Glu γ-carboxylation, by forming complexes with fetuin-A, calcium and phosphorus ions [37]. Calcium deposition is prevented by MGP through

regulation of calcification by VSMC-derived matrix vesicles (MVs) and apoptotic bodies [31] and by inhibiting VSMC transdifferentiation [56]. VSMC-MVs concentrate phosphate and calcium, thus inhibiting mineral deposition [56]. Apoptotic bodies can act as a natural receptacle for calcium crystal formation. Increased apoptotic bodies formation in VSMCs nodules lead to an increase in *MGP* expression, which suggests a correlation between MGP and apoptosis. One of the possible mechanisms is that MGP sequesters calcium from apoptotic bodies [35]. VSMCs of the arterial wall switch from their contractile phenotype to an osteogenic phenotype, showing resemblance to chondrocytes and osteoblasts. This transdifferentiation may occur due to stress caused by high extracellular levels of calcium and phosphate, or absence of calcification inhibitors such as MGP [57]. Interestingly, a study from Parashar and co-authors using the mice model demonstrated that only pMGP peptides prevented mineral deposition, while cMGP peptides did not prevent mineral deposition. This suggests that serine phosphorylation is necessary to prevent mineral deposition and glutamate γ-carboxylation alone cannot prevent mineral deposition [58]. A general summary of MGP functions, expression pathway and role in preventing ectopic calcification is shown in Figure 1.6.

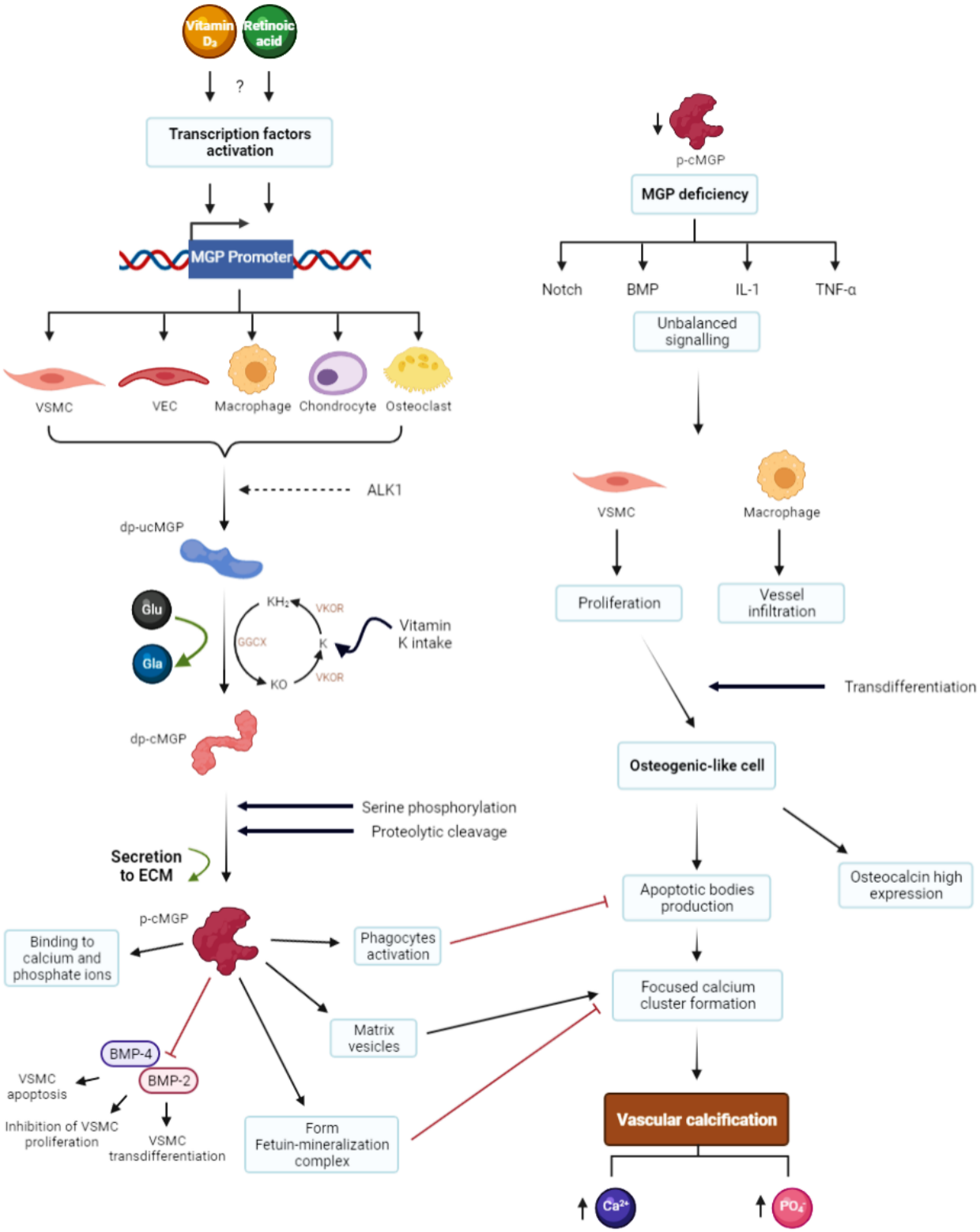

Figure 1.6. Role of MGP in ectopic calcification. BMP-2 and -4=bone morphogenetic protein 2 and 4, respectively; dp- and p-cMGP/ucMGP=dephosphorylated and phosphorylated forms of cMGP/ucMGP; KH_2=VK hydroquinone; KO=VK epoxide; VEC=vascular endothelial cells; VSMC=vascular smooth muscle cell (adapted from [15–17,36,37,59,60])

1.3. Ectopic calcification in the vascular system and cartilaginous tissues

a. Ectopic calcification

Calcification is a normal physiological process that occurs in skeletal tissues such as bones and teeth. However, under pathological conditions, organs and arteries such as the aorta are prone to calcification [55]. Briefly, this process converts the soft ECM into a firm component that can endure strong mechanical forces [13]. Despite its importance in hard tissues, calcification can occur in soft tissues and organs, as a pathological imbalance of calcium. These imbalances can occur in most soft tissues but particularly affecting the vascular and cartilaginous systems [9,13,47,61], as seen in Figure 1.7.

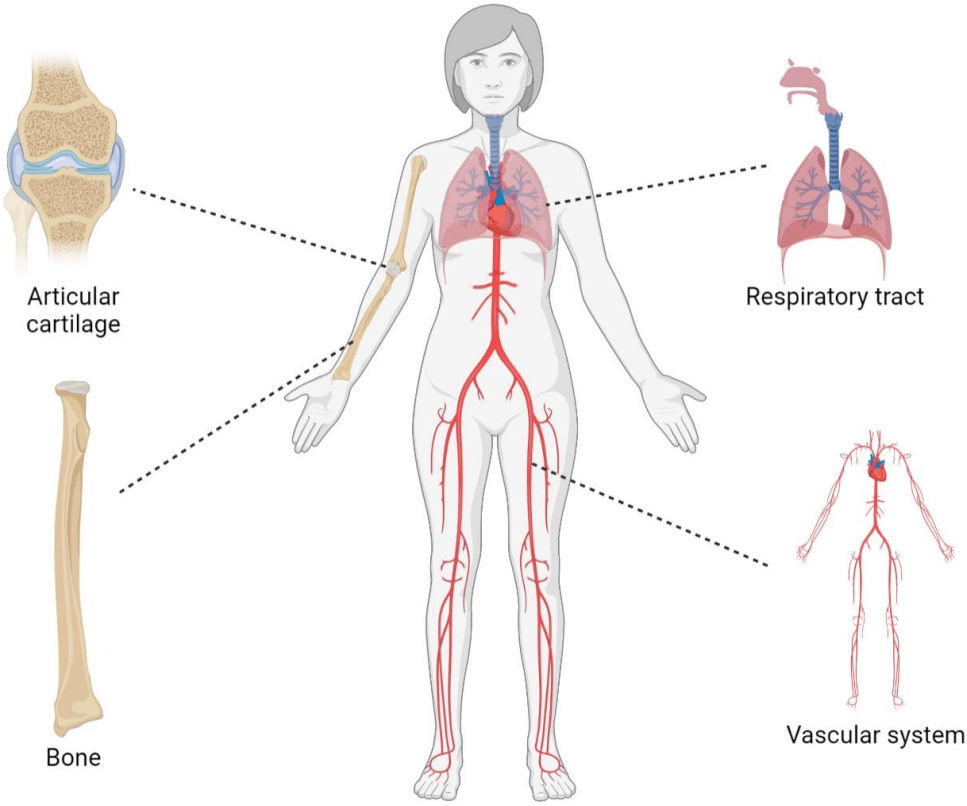

Figure 1.7. Human organs and tissues where abnormal calcification occur (adapted from [9,13,47,61]).

Imbalances in mineralization of calcium lead to ectopic mineralization, which is an intricate process in which calcium phosphate complexes deposit in the ECM [62]. Several genes are associated with anti-mineralization properties like *β-Glucosidase*, *Fetuin*, *Osteoprotegrin*, *Osteopontin*, and *MGP* [63]. Two mechanisms of ectopic calcification in the ECM have been

disclosed, dystrophic and metastatic calcification. Dystrophic calcification happens when normal calcium and phosphate homeostasis is disrupted as a result of an insult, which usually occurs in the form of injury or damage. In contrast, metastatic calcification results from the accumulation of high levels of serum phosphate and/or calcium [62]. Increasing evidence has been built in the involvement of MVs in soft tissue calcification. MVs are important in normal physiological mineralization processes. These vesicles can initiate mineralization in a two-stage process. First, after hydroxyapatite formation in the MVs, alkaline phosphatase activity induces an increase in inorganic phosphorus (P_i) concentration in the ECM. Thereafter, Pi enters the MV, followed by calcium influx to the vesicles. Secondly, due to these influxes, hydroxyapatite crystals continue to form and grow, thus breaking the MV membrane. This contributes to the crystals' exposure, which allows further expansion and increasing calcification [33].

I. Cardiovascular system

Vasculature is a complex system composed of a multitude of vessels, that are responsible for the blood movement throughout the circulatory system [64]. Cardiovascular system formation occurs during early embryonic stages [65]. It is comprised by the heart, arteries, capillaries, and veins in a complex and organized network, which is also responsible for providing oxygen and nutrients to every organ and tissue in the body [64,66].

The vascular system consists of three different layers: tunica *intima*, tunica *media*, and tunica *adventitia* [67]. The tunica *intima* is a thin single layer of endothelial cells that are supported by an organized layer of elastic lamina, that provides the flexibility and stability. The tunica *media* is a highly organized layer, responsible for the movement of large blood volumes, and it is composed of smooth muscle cells and elastin fibers. The tunica *adventitia* is structurally supported by external elastic lamina. Figure 1.8 shows the organization of the vascular layers and the localization of their constituent cells [64].

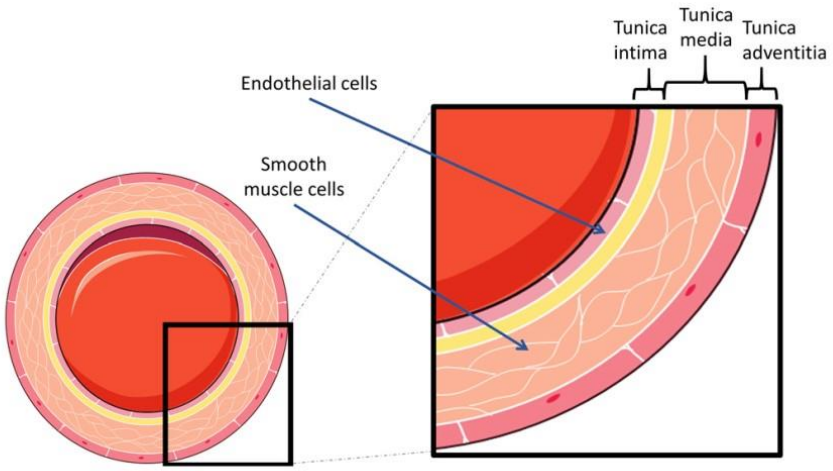

Figure 1.8. Arterial wall transversely cut illustration. Anatomical localization of the endothelial and smooth muscle cells within the arterial wall. Arterial wall histological regions schematized: tunica *intima*, tunica *media*, and tunica *adventitia* (adapted from [66]).

The heart is responsible to pump blood and their important associated nutrients to tissues and organs throughout the body. The heart is the first organ to be formed in humans concomitantly to vasculature development and it is also one of the first organs where mineral deposition begins to accumulate during abnormal calcification conditions. The heart wall is composed of endocardial cells (specialized endothelial cells) in the inner layer, myocytes that constitute the muscular medial layer or myocardium, and the epicardium that forms the outer layer, as shown in Figure 1.9 by a representative illustration of a sectioned human heart wall. Reciprocal molecular communication between both layers is crucial for proper heart formation [68].

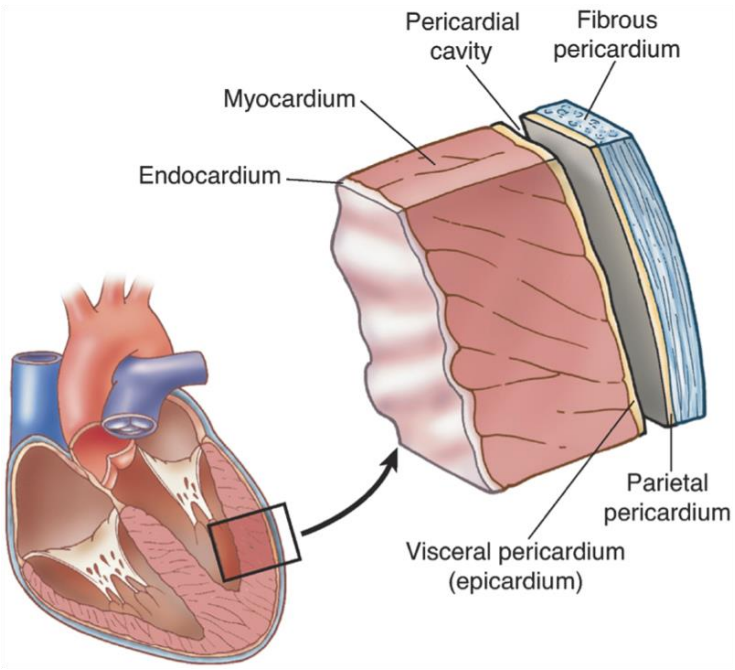

Figure 1.9. **Human heart and section of the human heart wall.** Anatomic location of the endocardial, myocardial and pericardial cell layers (adapted from [69]).

The aorta is an elastic artery composed of many elastic membrane layers, and it is flexible to the shifting blood volume pumped from the beating heart [64]. The aorta is the largest artery in the human body, it begins at the left ventricle and spreads throughout the body to supply oxygen through blood. The arterial wall is primarily made up of elastin, myofibroblasts, and collagen, and jointly they form the ECM. This major artery, as like the heart, is one of the first tissues prone to abnormal calcification [66].

Vascular calcification was thought to be a passive process, resulting from aging and disease. Nowadays, vascular calcification is known to be a pathological consequence of the imbalance in one or more biological pathways. Vascular calcification can occur in heart valves, in the tunica media and tunica intima of the vasculature [47]. Calcification of the tunica intima occurs due to macrophage infiltration and lipid accumulation in the vessel wall, and VSMC proliferation [36,60]. Calcification of tunica media begins when calcium crystals start to form deposits at the elastic lamellae site. Tunica *media* calcification develops throughout the aging process, thus leading to vessel stiffening and rupture [47].

Loss-of-function of MGP leads to vascular calcification. O'Rourke and co-authors used VSMC of the *Mgp* $^{-/-}$ mice model *in vitro* and verified an increase in VSMC transdifferentiation into an osteogenic phenotype, which leads to vascular calcification. Also, through *in vitro* studies

of human VSMC, the authors found that in the absence of MGP, calcification highly increased in VSMC, but when MGP expression increased, calcification within VSMC decreased, which suggests that MGP may actively regulate the vascular calcification process [36].

II. Cartilage

Cartilage is an elastic, flexible, and tough connective tissue, which lack direct irrigation from blood vessels and innervation from nerves. Cartilage is found in joints, ribs, nose, ear, vertebral disks intercalation, throat, epiphyseal growth plate, larynx, epiglottis, tendons, articulations, and ligaments [70,71]. Cartilage is mainly maintained by chondrocytes, which are derived from mesenchymal stem cells, through chondrogenesis [71,72]. A major portion of cartilage composition is water, that contributes to the high permeability within cartilaginous tissues [73]. The solid phase of cartilage is comprised by the ECM of collagen, proteoglycans, and glycosaminoglycans [72].

Cartilage major purpose is to provide scaffolding for mineral deposition [70]. Moreover, it can resist compressive forces in bony tissues, comprise spongy flexibility in the ears and nose, and confer a friction free surface within joints to allow correct movement and prevent articular attrition [70,71].

Cartilage possesses inefficient regeneration when injured or damaged, mostly due to its surrounding layer of perichondrium-like fibrous membrane. Other implication in cartilage slow recovery is due to the lack of irrigation of blood vessels[71,72]. Efforts have been made to better understand how to address these issues and the mechanisms underlying chondrogenesis. For example, El-Maadawy and co-authors investigated if other mesenchymal stem cells could originate chondrocytes and therefore originate cartilage. By using the *Mgp* $^{-/-}$ mice model, the authors demonstrated that VSMCs of the arterial media could differentiate into chondrocytes, and that these chondrocytes could produce an ECM typically found in hyaline cartilage, thus leading to calcification [74].

Cartilage calcification is a pathological process that increases as aging progresses and occurs mainly in the cartilage associated with joints [75]. In abnormal conditions, osteoblasts are overrecruited to cartilage sites, where abnormal mineral deposition occurs [13]. Abnormal calcification of cartilaginous tissues has been reported in the synovial fluid, meniscal

fibrocartilage, hyaline articular cartilage matrix and knee cartilage [75]. A study from Luo and co-authors, using the *Mgp* $^{-/-}$ mice model, demonstrated that in the absence of MGP these mice endured abnormal calcification of the growth plate, which lead to a disruption in chondrocyte columns, resulting in fractures and short stature [13]. Ectopic calcification of cartilaginous tissues is often linked to osteoarthritis (OA), which is responsible for the degradation of the cartilage matrix and increase of calcified cartilage thickness [75,76].

1.4. Elastin

a. General characterization

Elastin is an extracellular matrix protein that is a preponderant component of many tissues within vertebrates such as elastic cartilage, tendon, skin, lung, arteries, and ligaments. This insoluble and very durable biopolymer confers elasticity and resilience to these tissues. Elastin makes up the internal core and accounts for 90% of elastic fibers [77]. Elastin is synthesized by VSMCs and acts as a mineral nucleator [78]. Additionally, elastin is secreted and synthesized by fibroblasts, chondroblasts, endothelial cells, and mesothelial cells [77]. Elastin fibers are mainly formed before birth and in neonatal period [79]. Its presence within the circulation and respiratory system is a necessary requirement to provide elastic properties to these organs. Furthermore, elastin possesses high affinity for calcium ions, and the calcium content within elastic fibers tends to improve as aging progresses [79].

b. Elastin's correlation with calcification

Elastin calcification is intrinsically associated with elastin degradation. In this directly proportional process, elastin degradation promotes elastin-derived peptides (EDPs) to be released in the ECM, causing *MGP* upregulation and instigate cells to differentiate into osteoblast phenotypes [79]. Medial elastin calcification is related with vascular disorders linked with aging, renal failure and diabetes [60]. In *Mgp* $^{-/-}$ mice model ectopic calcification first occurs in the arterial elastic lamina, a place in which MGP typically localizes. Additionally, due to MGP absence, vascular ECM at elastin-rich elastic lamina sites, is prone to ectopic calcification in the *Mgp* $^{-/-}$ mice. Furthermore, Khavandgar and co-authors showed that elastin haploinsufficiency in *Mgp* $^{-/-}$ mice, reduced mineral deposition within arterial elastin-rich sites. This novel insight reinforces the importance of elastin in ectopic calcification, and its synergy with MGP [78].

Eln $^{-/-}$ mice dies in the perinatal period due to severe arterial obstruction. Also, *Eln* $^{+/-}$ in neonatal mice, is associated with aortic valve malformation and the development of cardiovascular diseases [80]. Finally, a study by Janssen and co-author suggested that there is a strong correlation between vitamin K deficiency and elastin degradation. VK deficiency increase inactive MGP levels (dp-unMGP), which therefore leads to calcification within elastin-rich sites and the activation of elastases, responsible for elastin degradation. Elastin degradation was detected due to the presence of high levels of plasma desmosine (elastin amino acid constituent) in patients with chronic obstructive pulmonary disease (COPD), seen in Figure 1.10 [79].

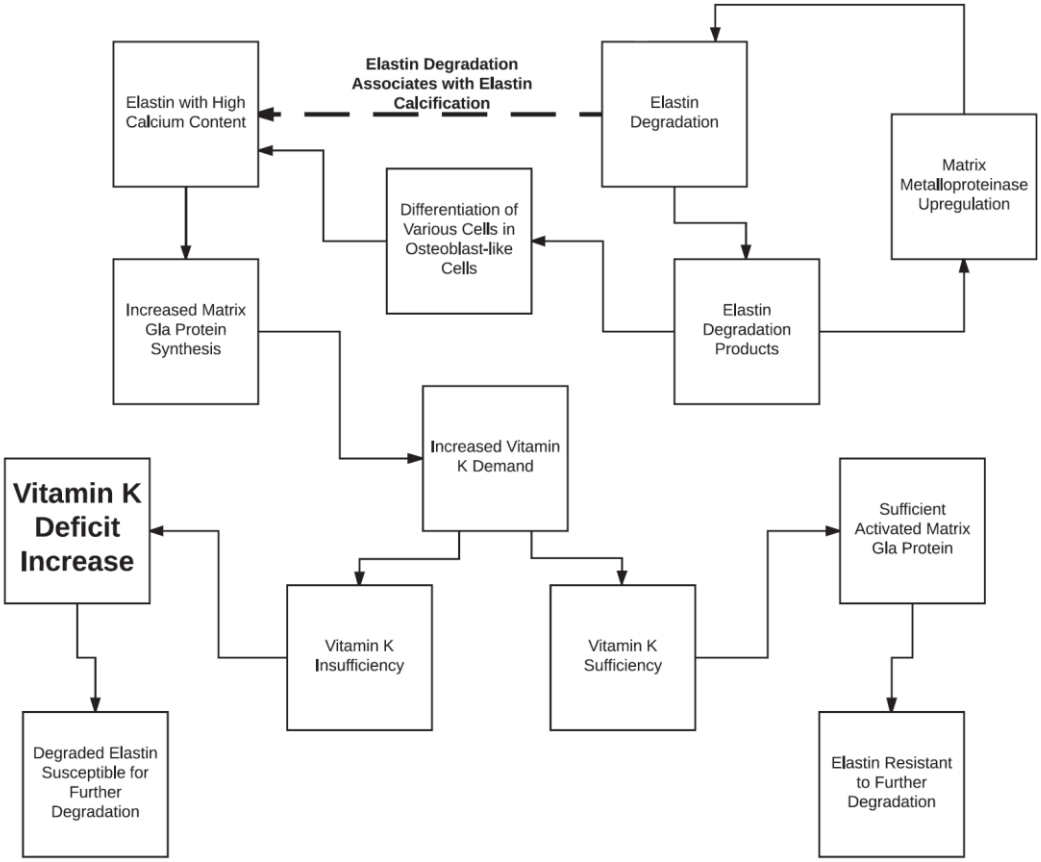

Figure 1.10. Relationship between vitamin K and elastin degradation (adapted from [79]).

1.5. Zebrafish

a. General characterization

Zebrafish (*Danio rerio*) is a small freshwater teleost fish that possess a multitude of positive characteristics that makes them a great study model for human diseases, such as their fast development, translucent embryos, and low maintenance requirements [81]. Zebrafish are small thus requiring only minimal keeping space [82]. Zebrafish also develops very rapidly compared with other teleost fish and other marine fish species, allowing them to be used for genetic and biomedical research with ease as they can be managed and studied at early developmental stages [83]. Translucency of specific structures and external development allow the entire development to be observed in real time [82]. Zebrafish can survive several days without a heart, which for example poses great advantages for studying pathologies associated with cardiovascular anomalies [84]. Zebrafish are used in studies from different scientific sub-areas such as embryonic development [83], regenerative medicine [85], toxicology and drug discovery [86], and bone and muscle deformities research [82].

b. Model establishment and detailed characterization

Zebrafish are native to river basins in East India. They were first used for laboratory purposes by Streisinger and collaborators in the 1960s [85]. Subsequently, this group helped establishing zebrafish as a viable organism to increase knowledge on molecular genetics, development and physiological processes [87]. In 1981, zebrafish was finally acknowledged as a viable biological model for genetic and developmental studies. Nowadays, zebrafish are used in medical research such as cancer, blindness, digestive disease, hematopoiesis, neural disorders, diabetes, and infectious diseases [88]. Zebrafish mature rapidly and embryos hatch 48-56 hours post-fertilization (hpf) into the larvae stage [89]. Zebrafish can regrow a variety of tissues such as fins that have been amputated, or even lesioned brain, retina, heart, spinal cord, and others. At the skeletal level, the key to their regeneration lies within their dermal bone rays, which are composed by osteoblasts [85]. In general, zebrafish is cheap and easy to maintain, due to their size, reasonably low condition requirements, and their high reproduction rate [81].

c. Genetic, organ and tissue homology to human

Zebrafish have their genome completely sequenced and mapped, and they share significant homology with the human genome [90]. Studies suggest that around 71% of human protein coding genes, have one ortholog in zebrafish [89]. Reciprocally, 69% of zebrafish genes have at least one human ortholog [91]. In mice, 80 to 90% of human protein coding genes, have at least ortholog [82]. Also, 82% of human morbidity-associated genes possess at least one zebrafish ortholog [89]. As zebrafish develop externally, a whole batch can be injected easily and rapidly with plasmid constructs of interest, at 1-2 cell stage, which present advantages because the probability of the plasmid construct to pass on the daughter cells is higher in early stages of development. Consequently, this artificial manipulation allows for efficient genesis of induced mutations or substitutions at specific genetic loci [82]. Zebrafish possesses a diploid genome consisted of 25 chromosomes. Around 20% of human genes have two orthologs in zebrafish [88]. Furthermore, forward and reverse genetic approaches can be performed to identify new genes of interest [90].

Zebrafish have functionally and morphologically similar tissues and organs to human. Zebrafish heart at 24 hpf is almost identical to the human fetus heart at three weeks of gestation. Despite the functionality difference of bone in zebrafish and human, the cellular, protein matrix, and molecular signaling pathways involved are similar [92]. Zebrafish have a circulatory system like mammals, which contributes to mimic the human physiology regarding vascular calcification and MGP activity [89,93]. Furthermore, zebrafish develop an innate immune system at 48 hpf composed by natural killer (NK) cells, macrophages and neutrophiles, and a complete adaptative immune system between 4 to 6 weeks post-fertilization [90].

d. Developmental characterization

Zebrafish embryos are around 4 mm in size and several dozens of fertilized eggs can be obtained from a single mating. During development, cell duplication occurs approximately every 15 minutes. Embryonic development starts at the zygotic phase where one cell-stage can be visualized. At 24 hours post fertilization (hpf), segmentation phase occurs, which is characterized by the formation of rudimentary organs. Between 48-56 hpf, pharyngula phase occurs and embryos hatch, and in this stage the heartbeat, body pigmentation, retinal pigmentation, and spontaneous tail movement can be seen. At 5 days post fertilization (dpf) larvae mouth opens and they can

already be feed, not depending only on the nutrients from the yolk sac. Approximately at 3 mpf, zebrafish reach sexual maturity and are ready to generate new progeny [94]. Figure 1.11 shows the zebrafish developmental stages from one cell stage to adulthood.

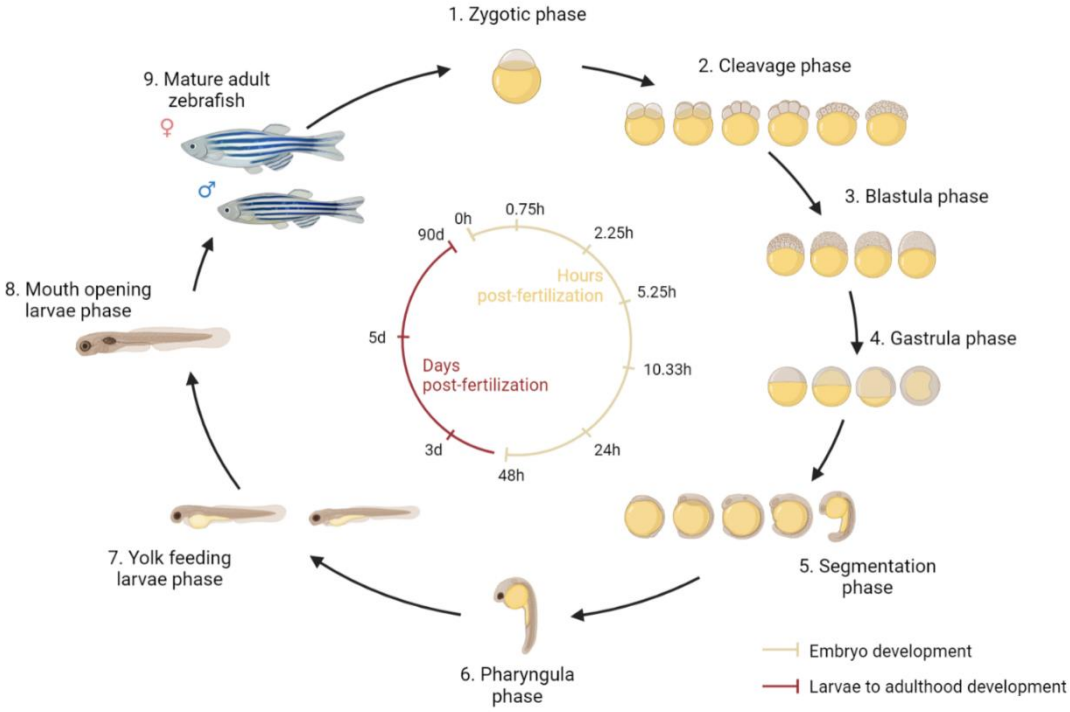

Figure 1.11. Zebrafish life cycle and each developmental stage.

e. *mgp* expression in zebrafish

Mgp was first purified from a cartilaginous fish, the soupfin shark, in 1994 by Rice and peers and from a teleost fish named *Argyrosomus regius*, in 2003. In the zebrafish, the mature Mgp possesses 84 amino acids, 36 of which are totally conserved when compared to mammals, and these include three Gla residues that are essential for the protein's activation [83,95,96]. Similar to human MGP peptide, zebrafish Mgp is composed by a signal peptide at the N-terminal region and the protein chain made by the phosphorylated serines and Gla domains, and the cysteines that form the disulfide bond responsible for the protein dimensional structure [97]. In zebrafish, Mgp is encoded by one single gene that is present at chromosome 3 [22,95]. Mgp is expressed at the caudal fin, respiratory system, skeletal system, and cardiovascular system, as shown in Figure 1.12. Mgp starts to be expressed very early at pharyngula (24-48 hpf) developmental stage and maintains expression throughout its entire life cycle [83,98]. *mgp* coding sequence has 338 bp within 5 exons

and it was demonstrated to be highly conserved since cartilaginous fish like the blue shark (*Prionace glauca*) to tetrapods and teleost fish including zebrafish [22,95].

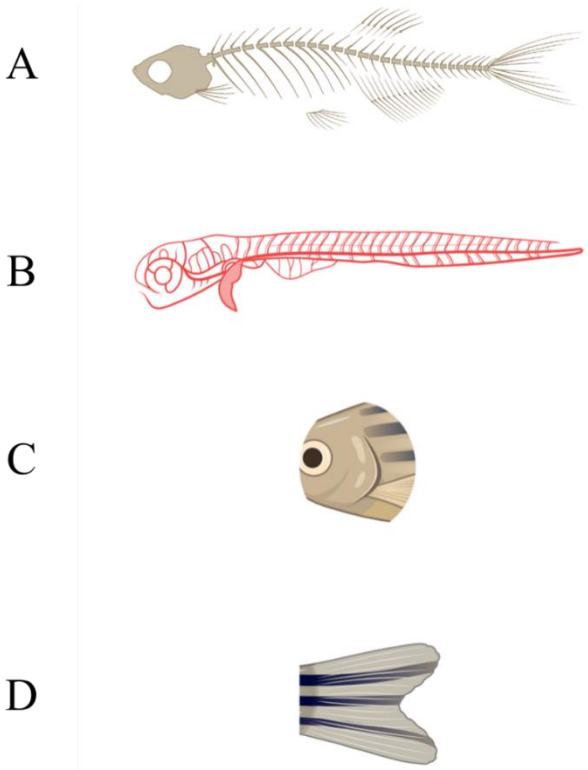

Figure 1.12. Mgp expression in the zebrafish organ and tissues systems. Mgp expression in (A) the skeletal system, (B) the cardiovascular system, (C) the respiratory system and (D) the caudal fin (adapted from [98]).

f. *eln* expression in zebrafish

Similarly, to Mgp, Eln is also expressed in zebrafish. Zebrafish elastin gene a (*elna*) coding sequence accounts for 3 633 bp, composed by 57 exons, located at chromosome 15. Elastin protein possesses 1 210 amino acids [99]. Zebrafish elastin gene b (*elnb)* has 6 246 bp, 59 exons and it is found at chromosome 21 [100]. A study from Miao and group, identified the expression of two tropoelastin genes (*eln*) in zebrafish. The co-expression of the two genes affects the elastin protein physical properties, either in crosslinking or coacervation phases, and *eln* expression occurred at very early stages of zebrafish development, achieving its peak 6-7 dpf. According to the study, elastin was expressed early in heart, particularly in ventral aorta and bulbus arteriosus, cranial skeletal cartilage, and swim bladder wall [101].

g. Ectopic calcification in zebrafish

Zebrafish share most of the features of chondrogenesis and osteogenesis with other vertebrates. Both processes are associated with calcification in humans. Ectopic calcification in zebrafish was reported by Hong and co-authors to have occurred in zebrafish scales, specifically at the dermo-epidermal junctions, where large amounts of calcium are maintained and subsequently contribute to calcification, and expression of calcification-related markers such as BMP-4, osteocalcin, β-catenin, and osteopontin [102]. Additionally, ectopic calcification was reported by Apschner and co-authors in *dragonfish* (*dgf)* zebrafish mutants, in the skin, heart, notochord sheet, intracranial space, eye, bulbus arteriosus and cartilage, some of which are also observed in PXE patients, which is another rare autosomal recessive disorder that leads to ectopic calcification in several tissues including the arteries [103]. Furthermore, Czimer and co-authors used a zebrafish model to induce mutations in the *abcc6* genes, which is the gene linked to the development of PXE. The authors demonstrated that the clustered regularly interspaced short palindromic repeat (CRISPR)-associated protein 9 (Cas9) indel mutations at the target gene of zebrafish, led to a phenotypic change, contributing to a potential parallel solution to study this and other diseases that affect normal tissue mineralization [104].

Ectopic calcification can be detected in zebrafish through different techniques. The von Kossa staining is a staining approach performed *ex vivo*, that stains in black or dark brown sites of high calcium and phosphate ions concentration. Alizarin red and Alcian-blue are staining approaches that can be performed *in vivo* or *ex vivo*. Alizarin red allows to observe every site rich in calcium ions through red staining and Alcian-blue stains glycosaminoglycans and saccharides at cartilaginous tissues in alcian blue [83].

h. Transgenic zebrafish lines to study ectopic mineralization

Throughout the years several zebrafish transgenic lines have been created, adding to more than 48 000 different transgenic lines [105]. A commonly used zebrafish line to investigate cartilage associated phenotypes is the transgenic *Tg(sox9:EGFP)* [106]. Sox9 regulates the expression of *Col2a1*, responsible for encoding most of the cartilage's collagen. Additionally, Yan and peers found that two orthologs of *SOX9*, were found in zebrafish and were named *sox9a* and *sox9b* [107]. The transgenic line *Tg(bglap:mCherry)* is of major importance to study osteogenesis, because

osteoblasts are marked with *mCherry* reporter gene. Additionally, this line may be of importance to study VSMC phenotypic changing into osteogenic-like cells, like osteoblasts [108]. Finally, *GATA1* and *FLI1* were merged to provide the transgenic zebrafish line *fli-gata*. *FLI1* is a transcription factor found in endothelial cells that interacts with *GATA1*, thus activating megakaryocyte-specific genes responsible for the platelets' formation. The convergence of these lines has been used to understand vasculogenesis [109]. Additionally, *TRANSGELIN* (*TAGLN*) is highly expressed in VSMCs, therefore is widely used as a marker for this cell type, as it is one of the major MGP producer cells [110].

i. Knockout and knockdown mutation approaches

Several approaches have been used to generate knockout and knockdown mutations in zebrafish. Ethyl-nitrosourea (ENU) has been a widely used tool to generate point knockout mutations. According to Shin and Fishman, until 2002, 7000 mutations were performed in 600 genes using ENU's approach [93]. Transcription activator-like effector nucleases (TALENs) is an efficient approach to inactivate a gene of interest (GOI). These nucleases are artificially produced by merging Xanthomonas' TAL effector DNA-binding domain with a DNA-cleavage domain. TALENs produce low off-target activity and it is easy to design and optimize [92]. Furthermore, the recently discovered tool, CRISPR-Cas9, has been applied successfully in genome editing across several species. Particularly in zebrafish, CRISPR-Cas9 has allowed to generate mutants for human disorders such as genetic cardiovascular and liver diseases, and autism [111]. In brief, CRISPR-Cas9 system consists of creating a synthetic single guided RNA (sgRNA) with a sequence complementary to the sequence of the GOI, where the nuclease Cas9 can induce the double-strand nick at the protospacer adjacent motif (PAM), a cleavage site, leading to the site repairing through non-homologous end joining (NHEJ), where different repair approaches can take place, such as adding or deleting nucleotides, resulting in the gene knockout, seen in Figure 1.13 [112,113]. As an example, Yin and co-authors have successfully generated a zebrafish model through CRISPR-Cas9 methodology for *fibrillin-1* (*fbn1*), a gene responsible for Marfan's syndrome [111].

As for knockdown mutations, approaches like morpholino antisense technology (MO), RNA interference (RNA_i) and dominant-negative, are often used. MO is applied by injection at 1-4 cell stage of zebrafish embryos, knocking down GOIs. Although RNAi is widely used as a knockdown approach, so far it has not been totally effective due to some non-specific effects

displayed. Several novel approaches in RNAi have been tested, by using micro RNAs and small harpin RNAs, which increased efficiency in knocking down the GOI, but its activity decreases over time. Finally, the dominant-negative approach consists in introducing a mutant gene to wild-type zebrafish, which will affect the wild-type gene product, reducing its level of expression [88,92]. Successfully, Lanham and group applied the dominant-negative approach to protect the development of dioxin toxicity in zebrafish [114].

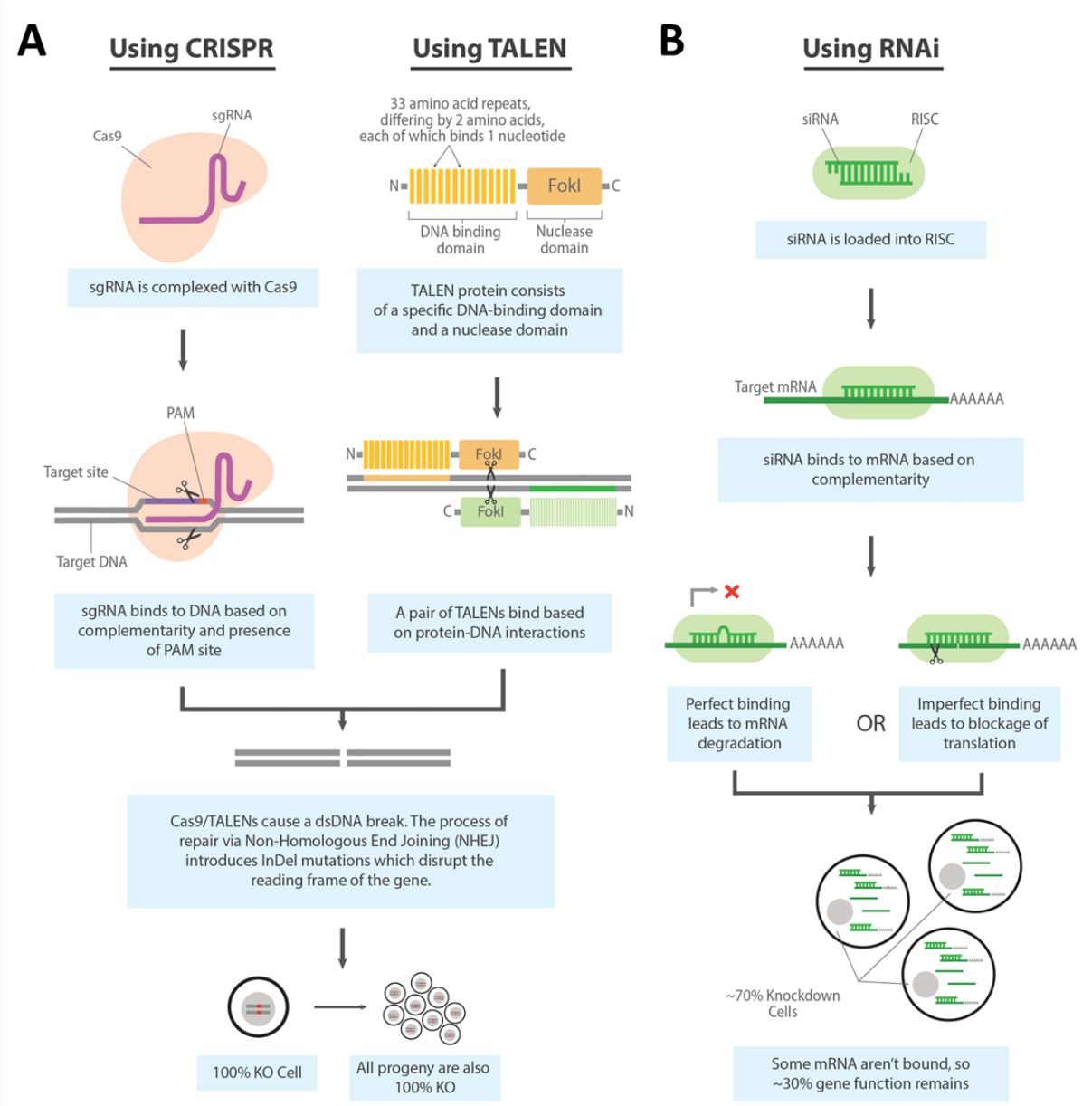

Figure 1.13. Genetic editing approaches scheme. (A) Knockout approaches CRISPR-Cas9 and TALEN and (B) knockdown approach RNA interference (RNAi) (retrieved from [115]).

Chapter 2 - Objectives

2.1. Objectives

KS is a non-curable rare recessive genetic disorder, with insufficient treatment options. Over the years, the *Mgp* $^{-/-}$ mice model has been used to unveil important cues regarding KS pathophysiology, particularly the importance of MGP as a key mechanism in the regulation of ectopic calcification. As important as this model continues to be, *Mgp* $^{-/-}$ mice model still presents some limitations regarding the wider view of the KS pathophysiology. Contrarily to humans, *Mgp* $^{-/-}$ mice suffers from severe arterial obstruction due to ectopic calcification within 2-3 weeks after birth, dying shortly after. Due to their premature death, the *Mgp* $^{-/-}$ mice poses a strong limitation to understand the mechanisms behind the ectopic calcification and the development of KS. Additionally, as the *Mgp* $^{-/-}$ mice shows exacerbated features when compared to KS patients, it raises the question on the validity of this model to study the KS pathophysiology. Nowadays, there are several biological models to study human diseases, one of which is the zebrafish (*Danio rerio*). Compared to the mice model, zebrafish can develop externally, hatch within 48-56 hpf, generates dozens to hundreds of offspring, allow straight and easy genetic editing, is a well-established bone model and holds one single gene for *mgp*, making it an interesting model to study KS pathophysiology and overcome some of the limitations posed by the *Mgp* $^{-/-}$ mice model.

Therefore, the main goals for our work are: (i) contribute to the establishment for the first time of a zebrafish model to study KS pathophysiology; and (ii) investigate whether MGP is a crucial inhibitor of vascular and cartilage calcification in the zebrafish model. For that we will:

a) Characterize a zebrafish mutant carrying the mutant form of *mgp*;
b) Identify the sites and extent of ectopic calcification upon treatment with warfarin, focusing on cartilage and vascular systems;
c) Determine whether Mgp and Elastin co-localize in wild type zebrafish and zebrafish expressing the mutant form of *mgp*.

Chapter 3 - Materials and Methods

3.1. Zebrafish lines and husbandry

Mutant Dre_mgpΔ18 (Chr 3: 1415226-1415243) +/CGGTTCTCAGGTGGCCTA, hereafter known as (*mgp* $^{+/m}$ or *mgp* $^{m/m}$) was generated by Stainier's Lab at Max Planck institute. Adult wild-type (*mgp* $^{+/+}$) zebrafish AB strain, and heterozygous (*mgp* $^{+/m}$) and homozygous (*mgp* $^{m/m}$) mutants were maintained in a 980 L ZebTEC® recirculating system (Tecniplast, Italy) through reverse osmosis. The system is composed by a salt mixture (Tropic Marin Pro Reef Sea Salt; Tropical Marine Center, United Kingdom) to keep the conductivity at 7001 S/cm, and sodium bicarbonate (Sigma-Aldrich, Spain) to buffer the pH at 7.5. The fish were submitted to a photoperiod of 14 hours of light and 10 hours of darkness. The fish were kept in 3,5 L plastic tanks, where they were fed twice a day. Fish were kept at a density of 10-14 adult fish and/or 20-28 larvae per tank [116,117].

3.2. Biological sample acquisition

Adult fish were anesthetized in 4,2% Tricaine solution (Tricaine 1M, pH 7.4) diluted in system water, for 2-5 minutes. Once anesthetized, the fish were laid under a magnifier and the biological samples were obtained through a uniform transversal cut, two segments post bifurcation of the second ray of the caudal fin (fin clip).

3.3. Genomic DNA extraction and yield concentration analysis

To obtain the genomic DNA content, the biological samples were incubated in Alkaline lysis buffer (250 mM NaOH and 2 mM EDTA, pH 7.7) at 95º C, for 15 minutes, with intervals of mixing in between. To neutralize the lysis process, Neutralization buffer (400 mM Tris-HCL, pH 8) was added. The samples were mixed using a vortex and spinned down once more. The DNA concentration was determined by spectrophotometry using the *Nanodrop* (Thermofischer, USA). The process schematization is summarized in Figure 3.1.

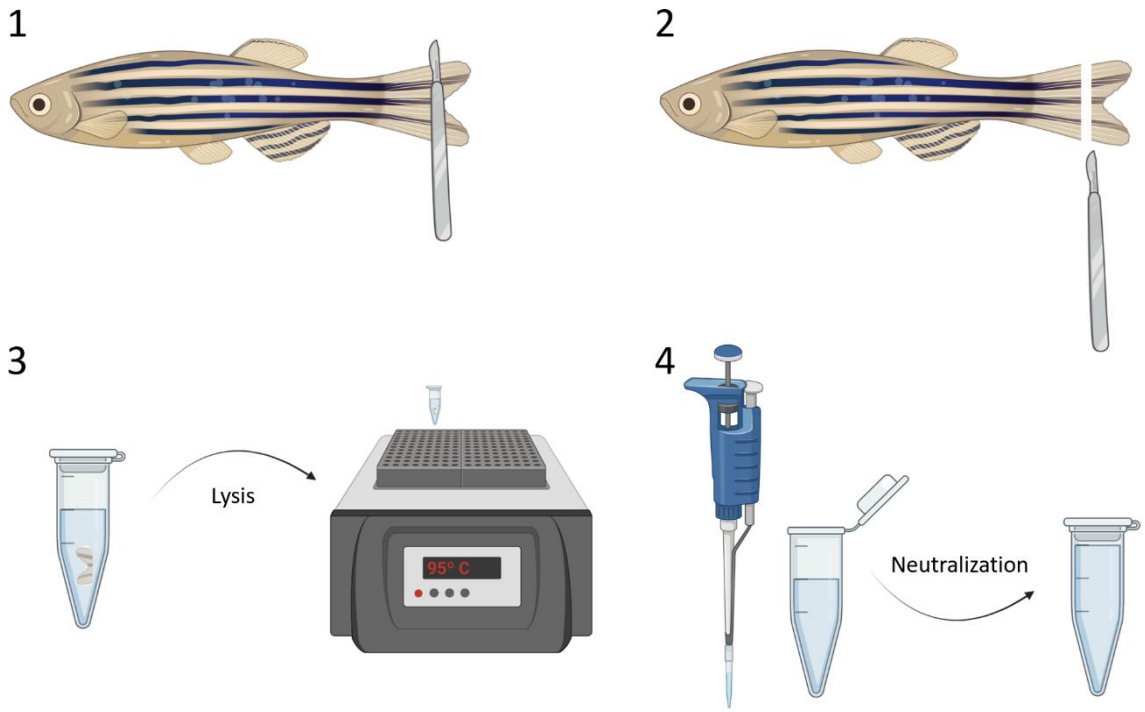

Figure 3.1. Genomic DNA extraction. (1) Adult zebrafish were anesthetized and laid under the magnifier, (2) fin clip of the caudal fin with a scalpel, (3) lysis of the fin clip and incubation at 95º C for 15 minutes and (4) neutralization of the lysis process.

3.4. Real-time qPCR

A 20 µL reaction mixture was prepared using 10 µL of Master Mix (NZYSpeedy qPCR Green Master Mix, MB222), 6,4 µL of RNAse free-water (Sigma), 0,8 µL of forward and reverse primer (10 µM) (FW 5-CGG AGG TGT GTG AGG ACT TC-3; REV 5-CGG GCT GAA GAA CTG ATA G-3), for each sample well. We added 2 µL of DNA template (samples) was added to each reaction. The qPCR reaction began by heating up the samples to 95º C for 2 minutes, followed by 39 cycles occurred in which: (i) the temperature was maintained at 95º C for 10 seconds (denaturation); (ii) the temperature dropped to 60º C for 30 seconds (annealing), as seen in Figure 3.2. In the end, the melting curve was set to start at 70º C with an increment of 0.1º C each 15 seconds until reaching 95º C. Graphical data was analyzed by Bio-Rad CFX Maestro software. Samples were sent for Sanger sequencing using the same forward primer sequence (5-CGG AGG TGT GTG AGG ACT TC-3), for further characterization.

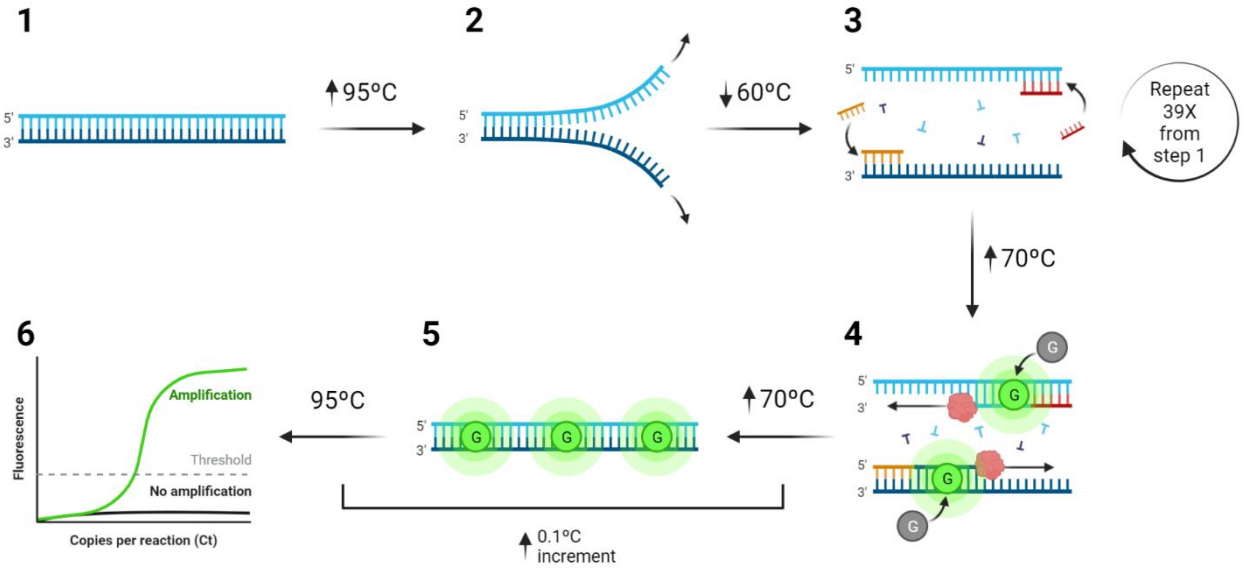

Figure 3.2. Real Time-qPCR protocol used to identify the zebrafish mutants. (1) DNA molecule at the initial stage, (2) denaturation stage at 95º C, (3) temperature dropped to 60º C to favor the annealing of the primers. Steps (1-3) repeated for 39 cycles. (4) Temperature rose to 70º C, where elongation stage occurs. (5) The temperature increased until 95º C, with a 0.1º C increment at each 15 seconds. (4-5) Melting curve interval.

3.5. Sequencing Alignment and Peptide Bioinformatic Analysis

Sequences analysis and alignment was performed using Clustal Omega online platform and peptide bioinformatic analysis predicted through InterProScan version 89.0 program.

3.6. Morphometric analysis

Adult fish (5 mpf) and larvae fish (5 dpf, 9 dpf, 15 dpf, 20 dpf and 30 dpf) were anesthetized as previously described, set under a stereomicroscope (Leica Model: MSV269) and the images obtained using VWR VisiCam 5 Plus camera. Images were uploaded to the ImageJ software, and different morphological parameters were measured: head length (HL), width (W), eye diameter (ED), standard length (SL), total length (TL), fork length (FL), top lobe caudal fin (TCF) and bottom lobe caudal fin (BCF), as seen in Figure 3.3.

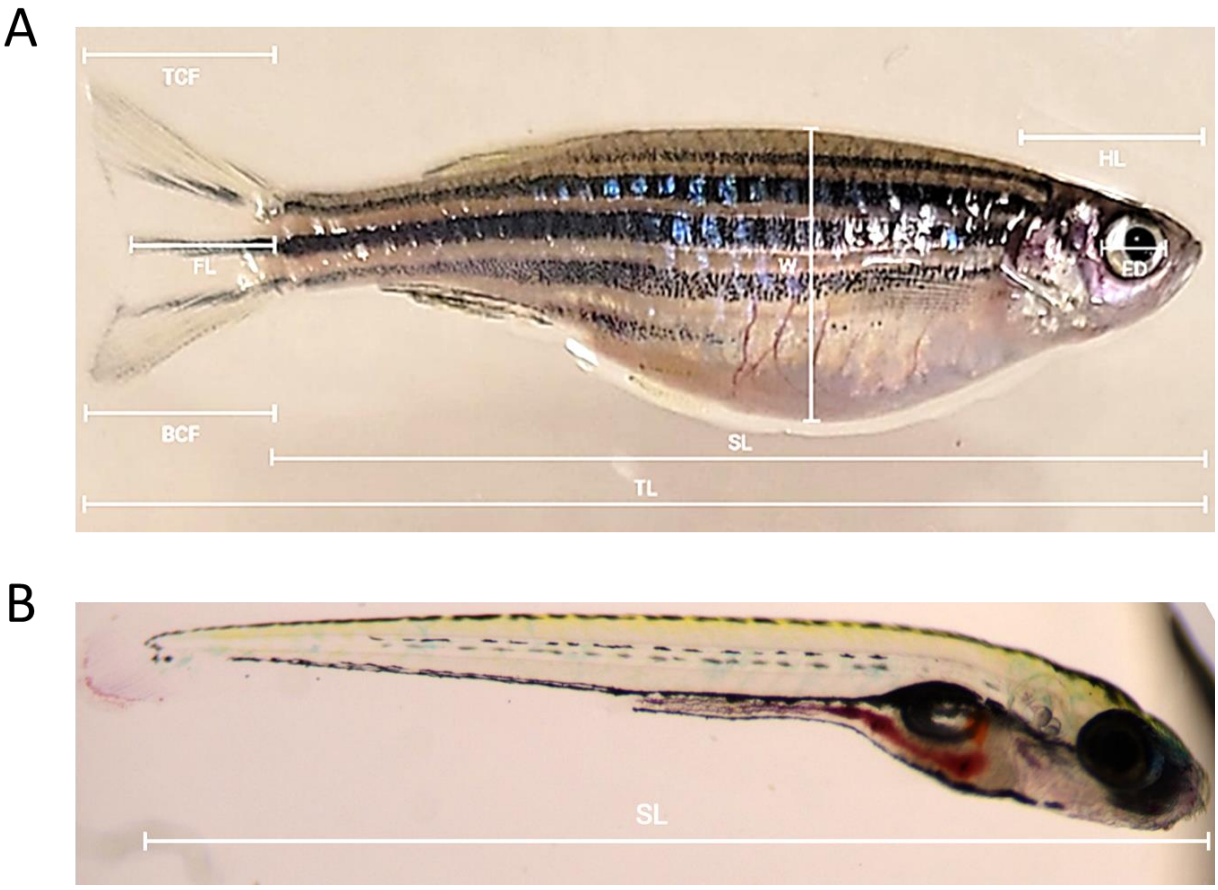

Figure 3.3. Morphological measured parameters of zebrafish. (A) 5 months adult fish (B) 9 dpf larvae. HL=head length; W=width; ED=eye diameter; SL=standard length; TL=total length; FL=fork length; TCF=top lobe caudal fin; BCF=bottom lobe caudal fin.

3.7. Hatching rate, egg mortality and larvae mortality

To evaluate hatching rate, the total number of eggs were counted at 0 hpf, and their viability was checked at 24 hpf and 48 hpf. To determine embryo mortality, 200 zebrafish embryos at 0 hpf were added to a 1 L tank with 0,1% methylene blue (w/v). Embryo and larvae mortality was daily assessed, until 48 hpf and at 48 hpf to 30 dpf, respectively.

3.8. Warfarin treatment

Fish tanks containing 20 to 30 zebrafish larvae with 7 dpf or 19 dpf were treated with system water supplemented with 25 mg/L of warfarin for a period 14 days, seen in Figure 3.4. The water bath containing warfarin was changed every day. Morphological changes and mortality rate was daily assessed. At the end of the experiment, fish were euthanized with a 10% Tricaine solution (Tricaine 1M, pH 7.4), and kept for further histological analysis,

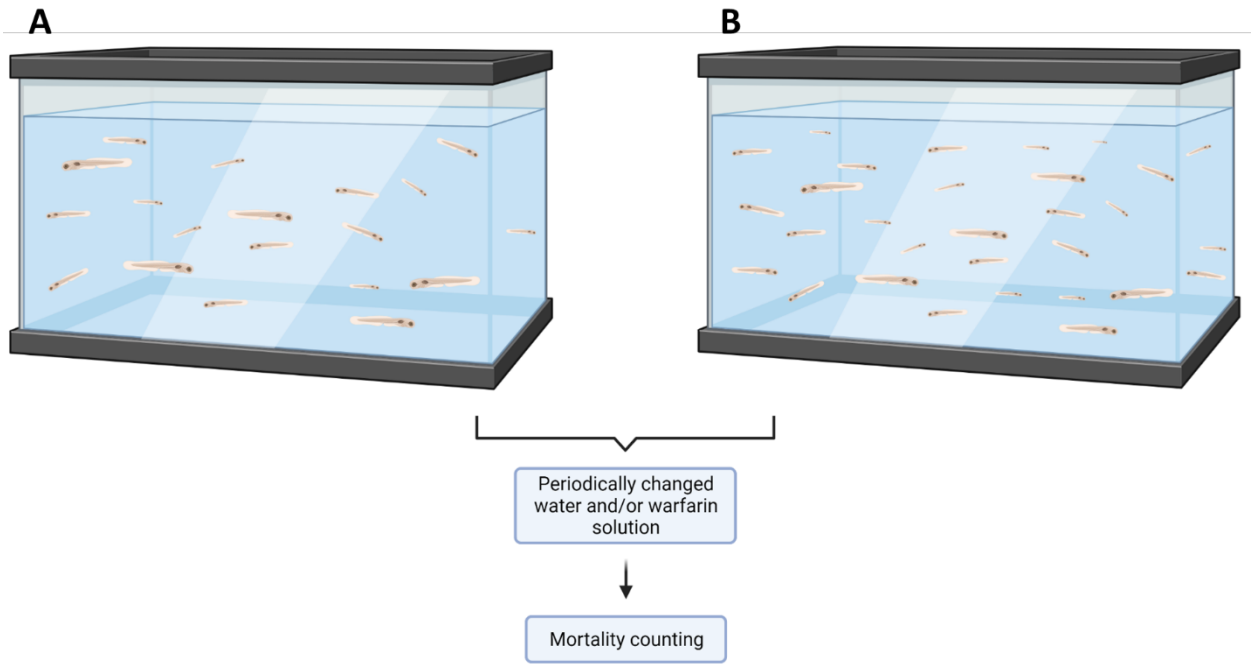

Figure 3.4. Treatment with warfarin. (A) 20 larvae with 19 dpf were treated with 25 mg/L for 14 days. (B) 30 larvae with 7 dpf were treated with 25 mg/L of warfarin for 15 days. Water bath and warfarin solution was daily renewed. Larvae mortality was assessed every day.

3.9. Alizarin Red *in vivo* Staining

Living zebrafish larvae were stained using alizarin red S (1.75 mM, pH 7.4) for a duration of 20 min. After, larvae were washed with system water for 5 minutes to remove the excess of Alizarin red and anesthetized in 1% Tricaine solution (Tricaine 1M, pH 7.4) in system water. Alizarin red signal was detected through the fluorescent magnifier (Leica MZ10) and mCherry channel which emits and excites at wavelengths of 550-650 and 540-590 nm, respectively. The experimental layout for each sample group is shown in Figure 3.5. Images of the whole larvae, vertebras and caudal fin were taken and analyzed through ImageJ software analysis. Vertebrae inter space, area and fluorescence intensity, and caudal fin rays' area and fluorescence intensity were determined through ImageJ software analysis.

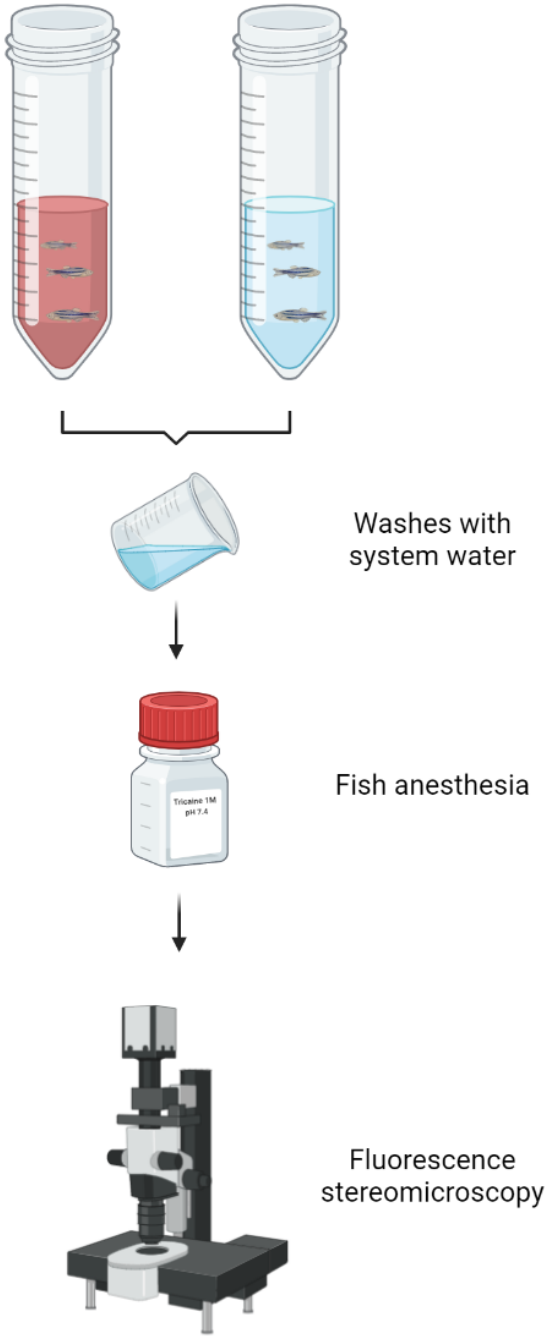

Figure 3.5. Experimental layout of the Alizarin red staining. Living fish larvae were submitted to alizarin red staining. Consecutive washings were performed to remove excessive alizarin red. The fish were anesthetized with 1% Tricaine solution and images were capture under the fluorescent stereomicroscope (Leica Model: MSV269).

3.10. Immunohistochemistry

Fish samples were fixed in 4% Paraformaldehyde (PFA) for 1 h, at room temperature, and washed consecutively with phosphate buffer saline (PBS) to remove the non-impregnated PFA and preserved in Methanol at -20º C, until further analysis.

The biological samples preserved in Methanol, were washed 5 times in Acetone, for 15 minutes, at room temperature. The acetone was replaced by cold GMA monomer (270 mg of benzoylperoxide [Sigma-Aldrich], 80 mL of (2-hydroethyl)-methacrylate [Sigma-Aldrich] and 12 mL of ethylenglycol mono butyl ether [Sigma-Aldrich]) 2 times, for 15 minutes each, at room temperature. New cold GMA monomer was added at 4º C, for 1 hour. The final substitution of cold GMA monomer occurred, and samples were stored at 4º C, for 48 hours.

Samples were laid in polypropylene embedding molds as described in Figure 3.6. Then a solution of GMA monomer with 2% catalyst (10 mL of Polyethylene glycol [Sigma-Aldrich], 1 mL N,N-Dimethylalanine [Sigma-Aldrich]) (always on ice) was putted into each well slowly, to prevent air bubbles to form. The position of the biological samples was adjusted, and a precisely well-molded plastic film was added to cover the top and to maintain the anoxia conditions. The polypropylene embedding molds were then stored at 4º C, for 24 hours and after for 24 hours.

Afterwards, 5 µm of thickness histological sections of the fish samples were obtained through the microtome (MICROM HM 340 E, Ser. Nr. 11119, Germany) and stored at 4º C.

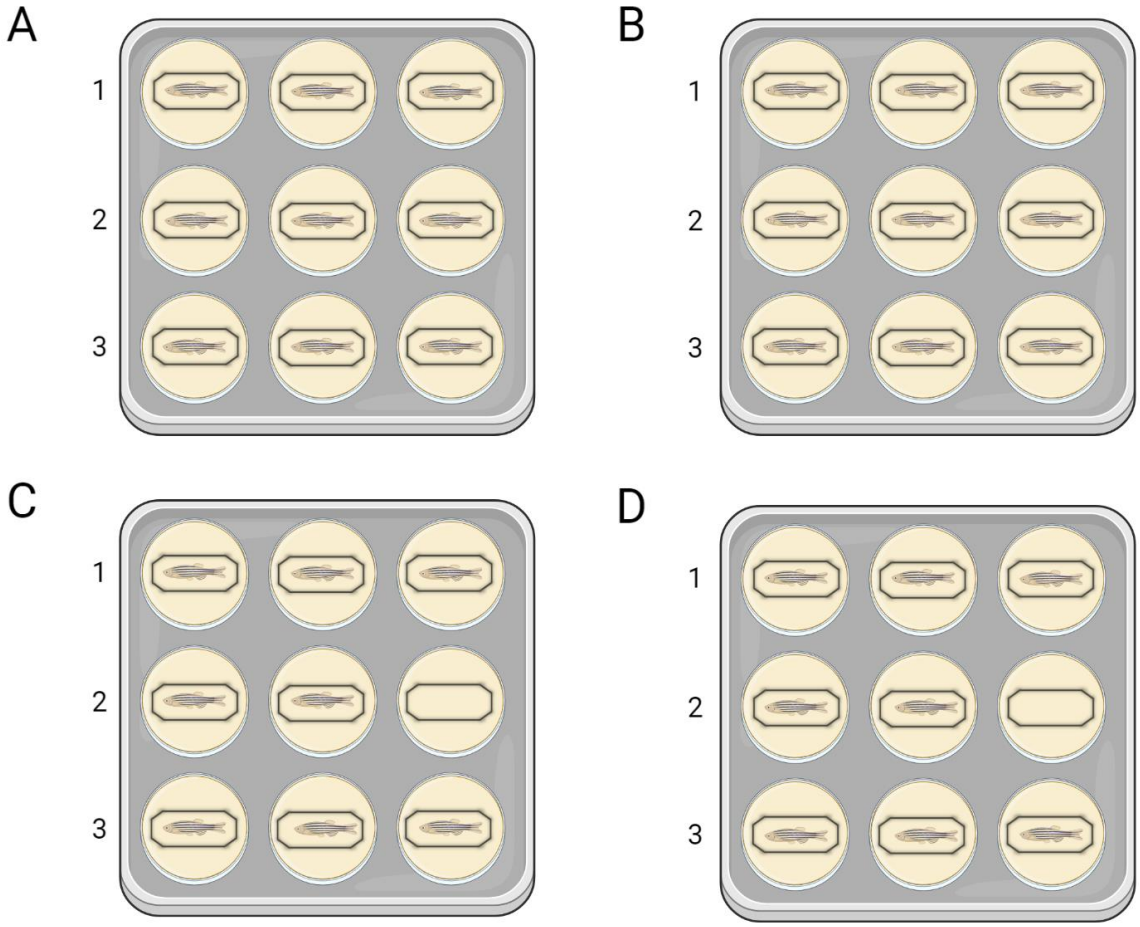

Figure 3.6. F3 generation larvae in polypropylene embedding molds with GMA monomer and 2% catalyst. (Line 1) *mgp* $^{m/m}$ mutants, (line 2) *mgp* $^{+/m}$ mutants and (line 3) *mgp* $^{+/+}$. Polypropylene embedding molds were separated for each experimental condition, (A) were the Alizarin red treated and warfarin treated samples, (B) were the Alizarin red treated and no warfarin treated samples, (C) were the non-treated with Alizarin red and warfarin treated samples and (D) were the non-treated with Alizarin red and no warfarin treated samples.

Slides were washed consecutively with TCT and then saturated in TCT with 0,5% Bovine serum albumin (BSA), for 30 minutes, at room temperature. Afterwards, the samples were incubated with 1:100 lab produced primary antibody (anti-BGP 27 rabbit polyclonal antibody), overnight. Next day, after TCT washings, slides were incubated with 1:200 secondary antibody with fluorochrome (anti-rabbit monoclonal secondary antibody 488 Alexa) for 2 hours, at room temperature and protected from sunlight. Slides were lastly mounted using a glycerol solution, constantly protected from light, and observed through stereomicroscopy (Axioscope 5). Images were uploaded and managed at netScope Viewer version 1.9.8171.41547.

3.11. von Kossa's staining and toluidine coloring

A 2% Silver Nitrate solution (Sigma-Aldrich) was applied to the slides for 30 min, under the UV sunlight. The excess of 2% silver nitrate solution was removed and the slides were stained with 1% toluidine blue solution, for 3-5 seconds and quickly washed in ddH_2O. The samples were observed through standard microscopy (Zeiss Axiolab). The von Kossa staining protocol is schematized in Figure 3.7.

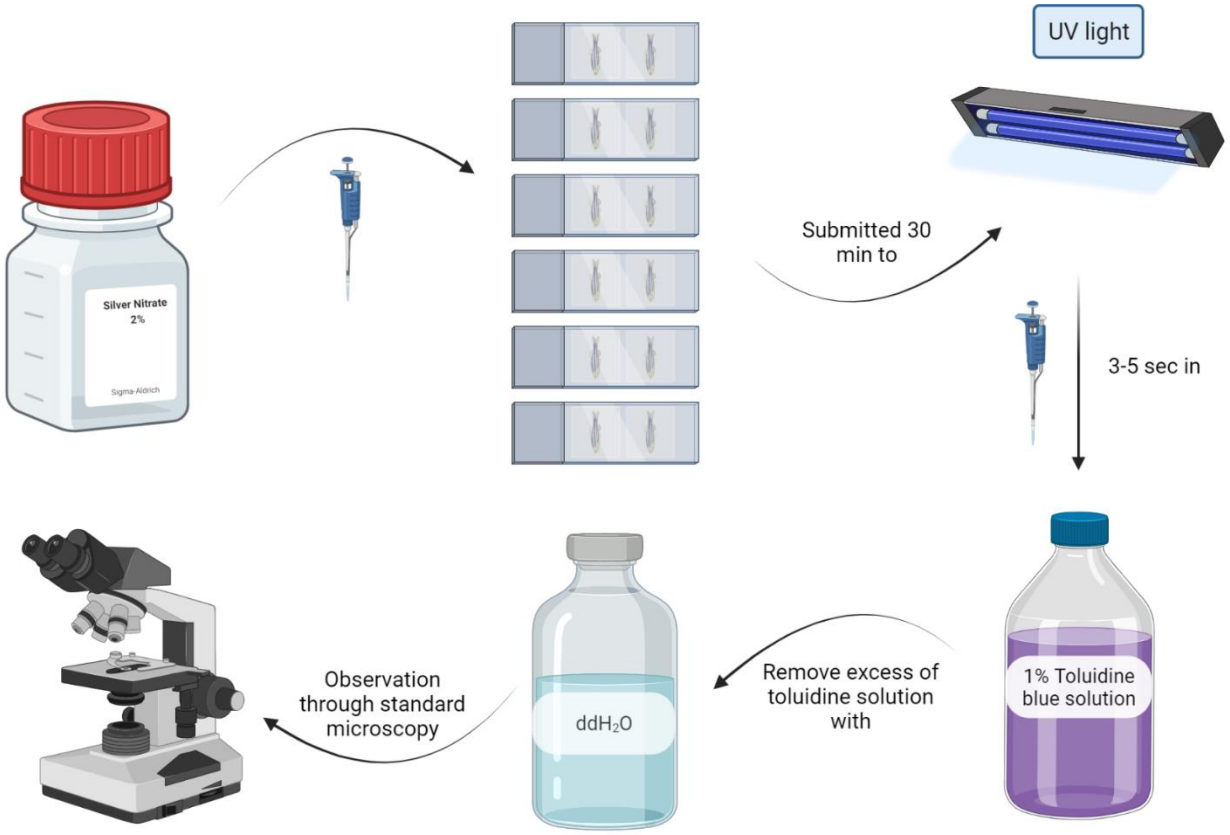

Figure 3.7. Von Kossa staining and toluidine coloring protocol to the zebrafish sections.

3.12. Statistical analysis

Statistical analysis was conducted using Prism 8.4.2 (GraphPad Software). Data is presented as mean ± Standard Deviation (SD) and significant differences were determined by a Student T-test or Chi-square test (hatching rate analysis) with a 95% degree of confidence. Differences were considered statistically significant for $p < 0.05$.

Chapter 4 – Results and Discussion

4.1. Identification and genomic characterization of the *mgp* mutants

Prior to our work, in collaboration with the Stainier's lab (Max Planck Institute), we obtained a zebrafish mutant in which exon 4 of the *mgp* gene was mutated using CRISPR-Cas9 methodology. As characterization of the mutation and the consequent changes to the Mgp protein structure had yet to be addressed, we performed a qPCR and analyzed the melting curve of the genomic DNA of the F1 *mgp* mutants in search of the existence of two or more amplicons.

After analyzing the melting curves, we identified two distinct curve patterns (Figure 4.1.1). We observed a single well-defined curve pattern (Figure 4.1.1. A) or two smaller curves (Figure 4.1.1. B). According to Farrar and Wittwer [118], the melting curve patterns obtained suggest that the single peak (one amplicon), amplified at higher temperatures was likely to correspond to a wild-type zebrafish (Figure 4.1.1. A), and that the double-peak melting curve (2 amplicons), suggested the presence of two distinct alleles which suggests a potential *mgp* $^{+/m}$ mutant (Figure 4.1.1. B), each peak corresponding to a different allele. As in Figure 4.1.1. B, the second amplicon matches the one observed in Figure 4.1.1. A, it is likely that it corresponds to the wild-type allele. On the other hand, the first amplicon amplifies at lower temperatures than the second amplicon which suggests that it may be relatively shorter than the other or that their GC content may greatly vary [118].

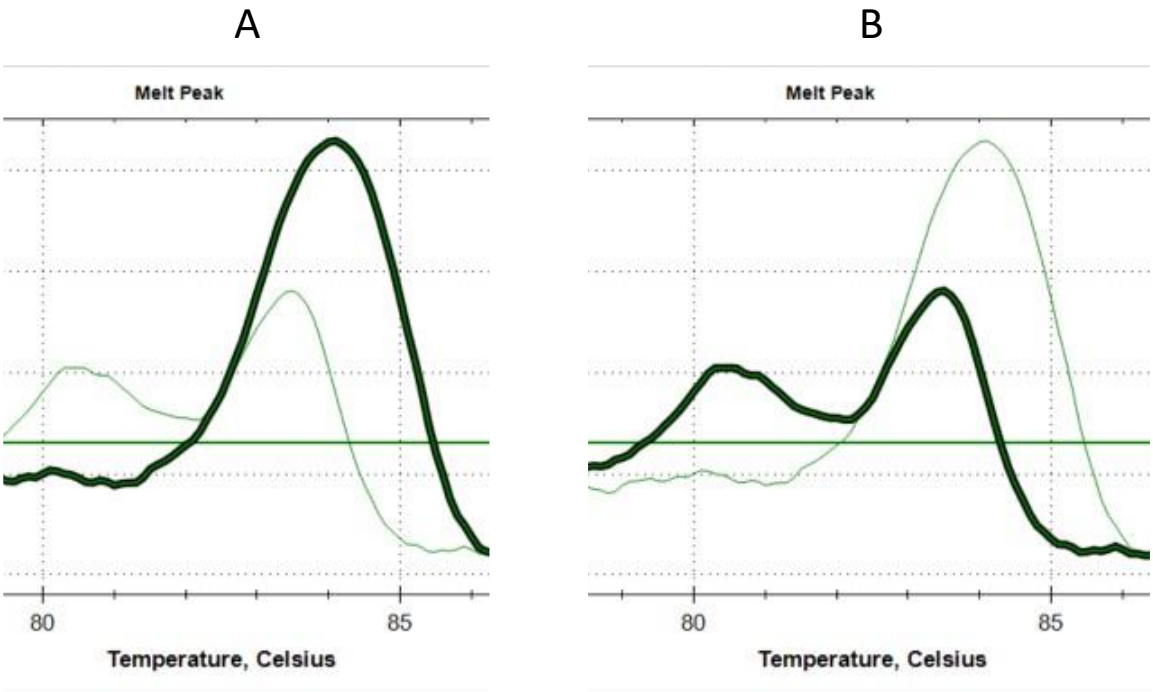

Figure 4.1.1. qPCR melting curve of the F1 *mgp* zebrafish mutants. (A) Melting curve displaying one single amplicon (curve pattern 1) and (B) melting curve displaying two different amplicons (curve pattern 2), corresponding to two different alleles. The Y axis provides the RFU signal from the SYBR Green intercalation.

To confirm the presence of two different alleles and to characterize the mutation, samples were sent for standard sequencing. For that, samples from the putative wild-type and *mgp* $^{+/m}$ zebrafish were sequenced and analyzed using BioEdit software, adding to the *mgp* sequence that was already sequenced from the NCBI database. By aligning and evaluating the chromatogram nucleotide peaks we observed an 18-nucleotide deletion in the *mgp* $^{+/m}$ sequence, as seen in Figure 4.1.2.

Based on previous studies that characterize the *mgp* sequence from zebrafish, we inferred that the mutation found had indeed occurred in exon 4 at the 3'-terminal of the gene, as an 18-nucleotide deletion from 243bp to 261bp (Figure 4.1.2).

Further analysis, using NCBI Blast and Clustal Omega platforms crosslinked the Mgp sequence from wild-type zebrafish (*Danio rerio*=Dre WT) with the *mgp* mutant zebrafish (Dre MT), mice (*Mus musculus*=Mus) and human (*Homo sapiens*=Has) and InterProScan platform was used to predict the protein domains. As predicted, the signal peptide, the cysteines that form the disulfide bond and the phosphorylation domain are common in all species compared, the putative cleavage sites are present within the three species although the arginine-arginine (R-R) cleavage

sites occurs later in the zebrafish when compared to mice and human, as seen in Figure 4.1.3. Wild type zebrafish have a 105 amino acid immature Mgp protein, while the *mgp* mutants' protein only have 99 amino acids. We have confirmed that this deleterious mutation withdraws 6 amino acids at positions 81-87 of the immature Mgp, at the C-terminal of the Mgp peptide sequence.

Interestingly, the mutation was not as initially desired, as it did not affect conserved domains with anti-mineralization properties such as the phosphorylation nor the Gla domains. Although the mutation was not as desired, we pursued our work, because the mutation deleted 3 highly conserved domains amongst vertebrates, that may possibly have an important role in the protein function and/or its tridimensional arrangement [22,34,83]. Congruently, the site of the mutation may suggest an alteration in protein function as a study from Weaver and co-authors [5] in human patients for KS found a deleterious mutation at exon 4, which affects residues 57-104 of MGP (C-terminal). The patient carrying this mutation displayed severe pulmonary calcification, midfacial retrusion and brachytelephalangism and many other features seen in KS patients. So far, no study has predicted or confirmed what is the function of the C-terminal after the Gla domain of MGP, but we believe that it may affect the tridimensional arrangement of the protein and consequently its function.

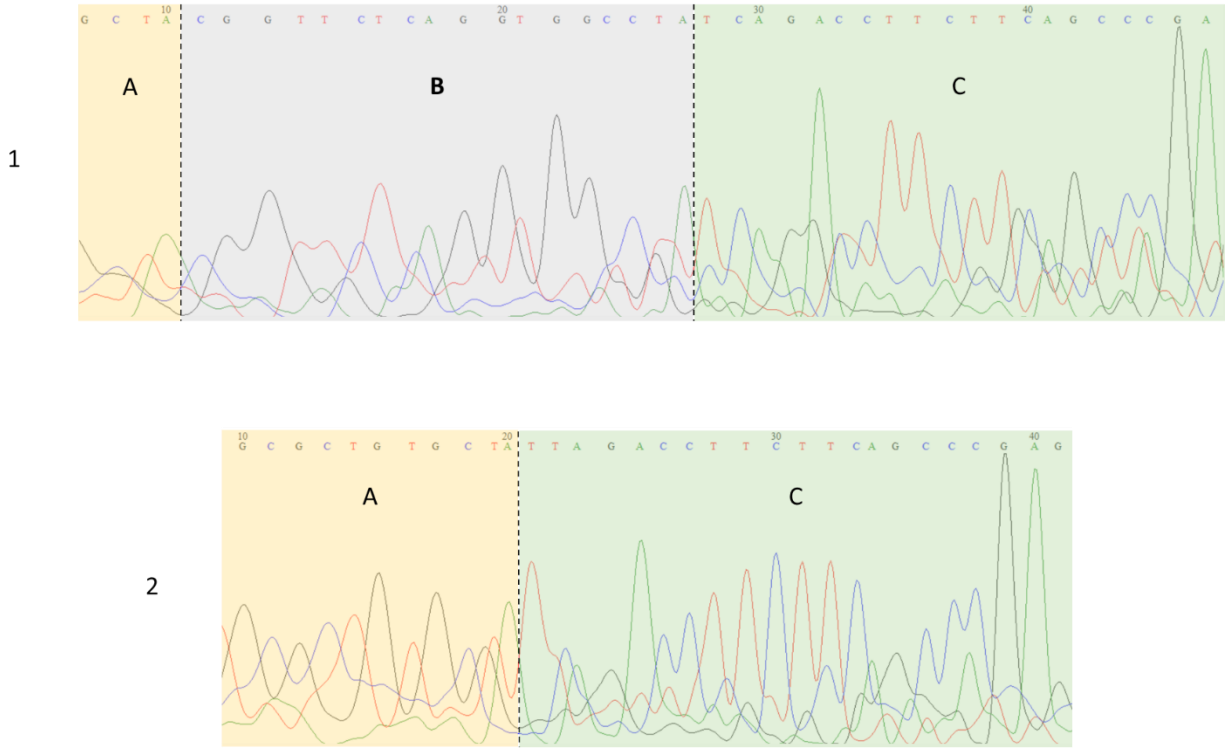

Figure 4.1.2. Chromatogram of the *mgp* exon 4 in the *mgp* zebrafish mutants. (1) *mgp* wild-type sequence with domains A, B and C of the exon 4 of *mgp*. (2) *mgp* $^{+/m}$ sequence without domain B.

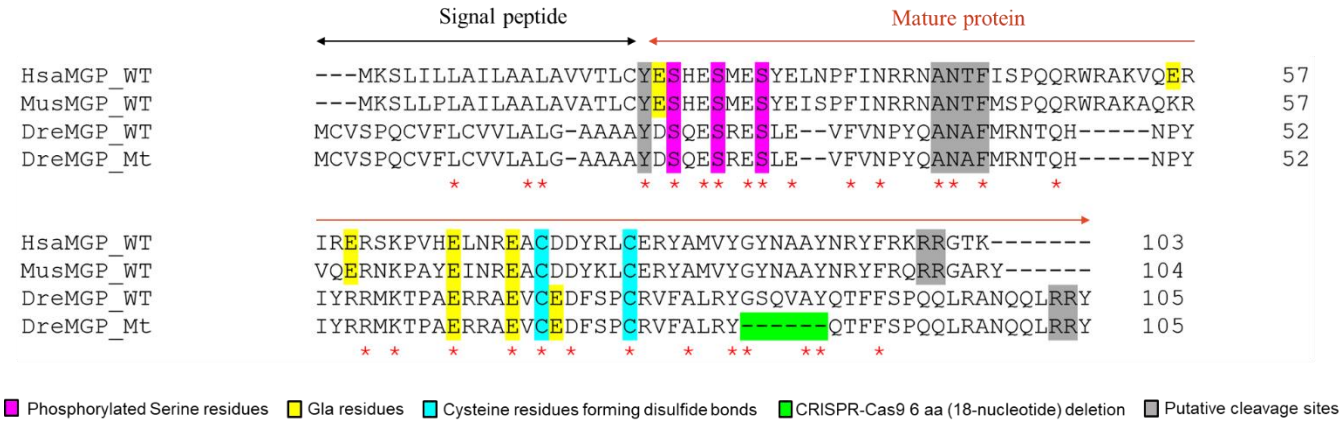

Figure 4.1.3. MGP peptide sequence alignment with other vertebrates. *mgp* mutant (DreMGP_Mt) has a 6 amino acid deletion (Has=*Homo sapiens*; Mus=*Mus musculus*; Dre=*Danio rerio*; WT=Wild-

type; Mt=Mutant; *=conserved residues).

4.2. *mgp* mutant larvae developmental characterization

Since the KS manifests since childhood, we first investigated the impact of the *mgp* mutation in early embryonic and larval stages of zebrafish development. For that, we generated, sequenced and identified *mgp* $^{m/m}$ from the F2 generation, and generated an F3 generation line of zebrafish embryos and larvae in which the presence of one or both mutant alleles were known from the beginning (Figure A.1 in Appendix). Next, we set up three independent experiments with at least an N>100 eggs per group and we daily investigated the embryo and larvae mortality until 30 dpf.

We observed that at 48 hpf, wild-type embryos die significantly less than the *mgp* $^{+/m}$ and *mgp* $^{m/m}$ mutants. On the other hand, we found no statistically significant differences between *mgp* $^{+/m}$ and *mgp* $^{m/m}$ embryos, as seen in Figure 4.2.1. The results show statistically significant differences between the *mgp* $^{+/+}$ and the *mgp* $^{m/m}$ embryos, with a mortality approximately 1.5-fold higher (≈5,4%) for the *mgp* $^{m/m}$ embryos.

Since Mgp begins to be expressed at early stages of development (24-48 hpf), the potential deficiency or nullity of expression of Mgp in the *mgp* $^{+/m}$ and *mgp* $^{m/m}$ mutants, may contribute to their higher mortality, due to its importance in inhibiting abnormal calcium deposition. Moreover, *mgp* is a key regulator of important downstream genes such as *sox10* and *polr2f*, that are involved in the formation of tissues and organs during embryonic development [119–121].

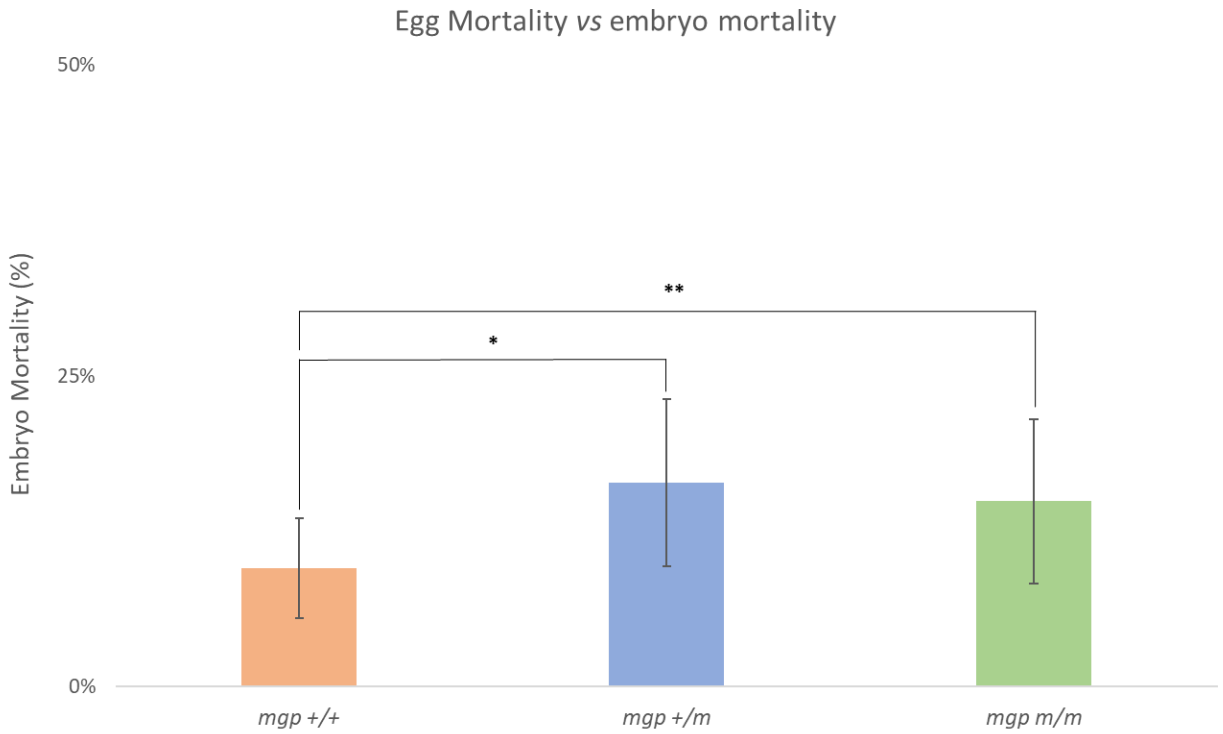

Figure 4.2.1. Impact of the loss of *mgp* function in embryo mortality. Percentage of dead embryos during 48 hpf. Error bars correspond to ± SD across three independent experiments in which the starting egg number was above 100 for each group (*mgp* $^{+/+}$, *mgp* $^{+/m}$ and *mgp* $^{m/m}$). Differences were considered statistically significant if $p<0.05$ (*=$p<0.05$; **=$p\leq0.01$). Non-statistically significant differences were not considered.

Next, we investigated whether there was a delay in the developmental process associated with the *mgp* mutation. For that, we analyzed the percentage of embryos that were able to hatch at 48 hpf. Figure 4.2.2. shows a clear difference in the hatching rate across the different groups, particularly between the *mgp* $^{+/+}$ and *mgp* $^{m/m}$ embryos, in which a 5-fold decrease was observed. The overall pattern of the hatching rate clearly suggests that the *mgp* $^{m/m}$ embryos had increased difficulty in hatching at 48 hpf, when compared to the *mgp* $^{+/+}$ embryos. Although the cumulative results show a clear difference between the groups considered, each individual experiment did not share this tendency. Nevertheless, to better confirm these results, more individual experiments should be conducted to compare if the results are as congruent as observed in Figure 4.2.2. Furthermore, these results may suggest that a delay in the biological development may take place within the *mgp* $^{m/m}$ embryos.

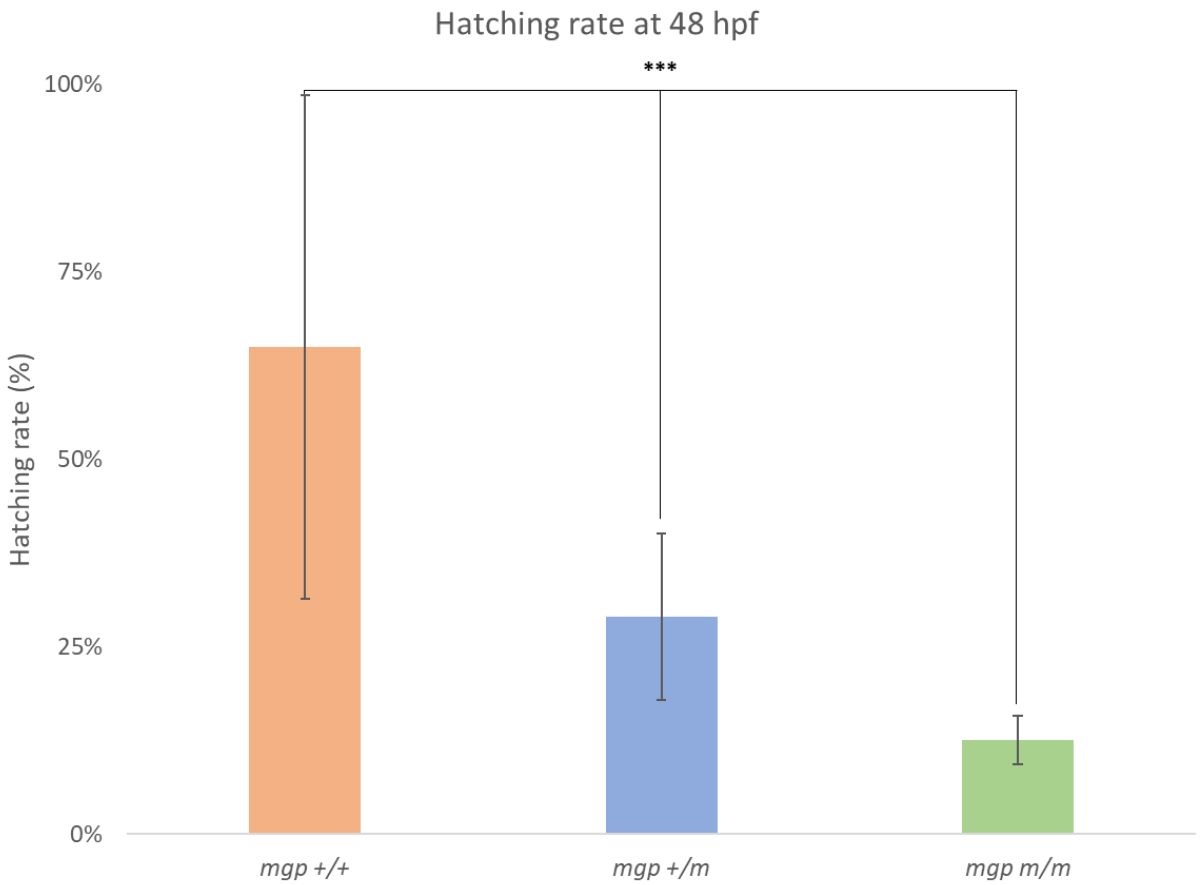

Figure 4.2.2. Impact of the loss of *mgp* function in the hatching rate at 48 hpf. Error bars correspond to ± SD across three independent experiments in which the starting egg number was above 100 for each group (*mgp* $^{+/+}$, *mgp* $^{+/m}$ and *mgp* $^{m/m}$). Differences were considered statistically significant if $p<0.05$ (***=$p\leq0.0002$).

After characterizing the potential phenotypic differences of the *mgp* mutants at the embryonic stage, we wanted to observe potential differences between the different groups (*mgp* $^{+/+}$, *mgp* $^{+/m}$ and *mgp* $^{m/m}$) during the larval developmental stage. For that, we considered three independent batches from the 48 hpf until 30 dpf. While larvae survival was assessed for a period of a month, we focused our attention between 7 to 11 dpf, as it is considered a critical timepoint for larvae development and a point in which significant differences were observed. We observed statistically significant differences between all groups (*mgp* $^{+/+}$, *mgp* $^{+/m}$ and *mgp* $^{m/m}$), as seen in Figure 4.2.3. The *mgp* $^{+/+}$ larvae had the lowest mortality in every timepoint measured, followed by the *mgp* $^{m/m}$ and *mgp* $^{+/m}$ larvae with a very slight difference (≈0.1%), at 7 and 8 dpf. This result suggests that the deficiency in the Mgp expression may contribute to a possible imbalance in the *mgp* mutants' biology, reducing its capability to thrive into mature stages of development, although

we were expecting the lowest survival rate belonging to the *mgp* $^{m/m}$ larvae, similar to the *Mgp* $^{-/-}$ mice [6,13].

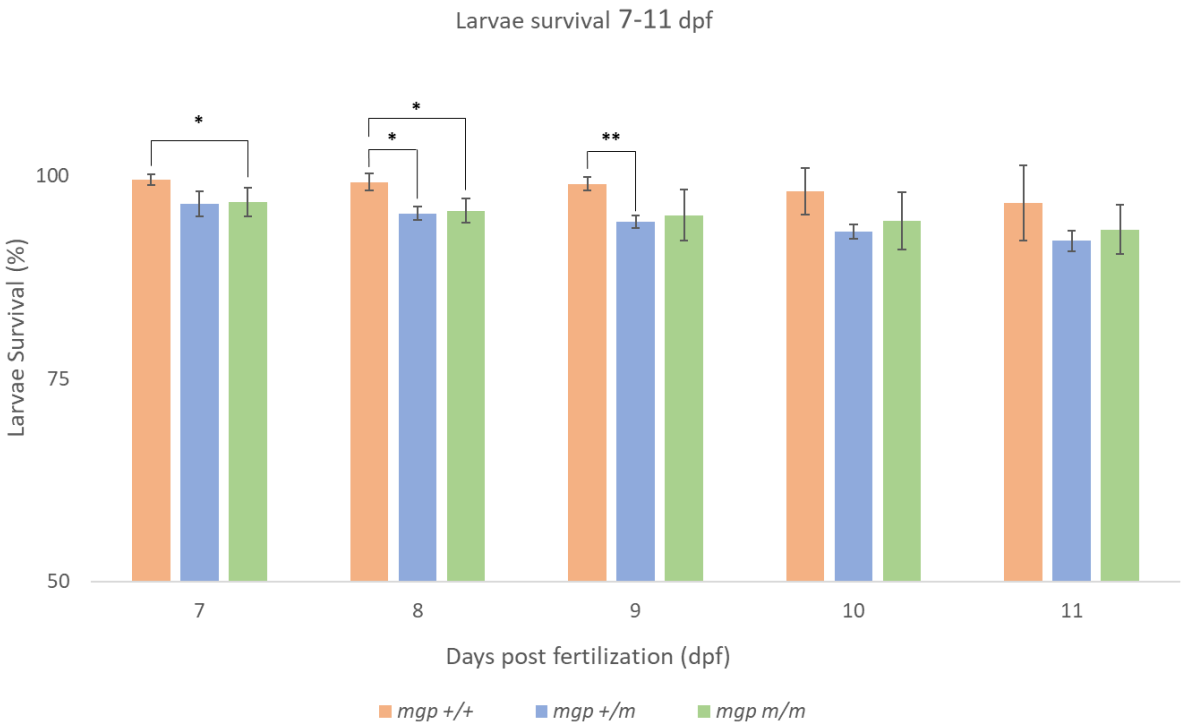

Figure 4.2.3. Larval mortality of the *mgp* mutants between **7 and 11 dpf.** Error bars correspond to ± SD across three independent experiments in which the starting egg number was above 100 for each group (*mgp* $^{+/+}$, *mgp* $^{+/m}$ and *mgp* $^{m/m}$). Differences were considered statistically significant for $p<0.05$ (*=$p<0.05$; **=$p\leq0.01$). Non-statistically significant differences were not considered.

4.3. Morphometric analysis of the *mgp* mutants

Once characterized the mutation in the *mgp* gene, we aimed to identify possible phenotypes associated with KS in the *mgp* mutants. For that, we examined 8 morphological parameters in the F1 *mgp* mutants such as the fork length (FL), top and bottom caudal fin (TCF and BCF), width (W), head length (HL), eye diameter (ED), standard length (SL) and total length (TL), as seen in Figure 4.3.1.

In overall, we observed that the size was identical or very similar for the FL, TCF, BCF, W, HL, ED and TL, between the wild type and the *mgp* mutation carriers. Differently, the SL was bigger in the wild type than in the *mgp* mutation carriers, although with no statistically significant difference.

We were not expecting to see differences within the parameters, particularly within the SL, TL and HL between the wild type and the *mgp* mutation carriers, since the features present in KS patients are manifested through homozygosity. In regard, this may suggest that haploinsufficiency for Mgp, is not sufficient to cause phenotypic changes to the fish, but it rather needs both mutated alleles (autosomal recessive disorder) for KS to manifest in human [1,2].

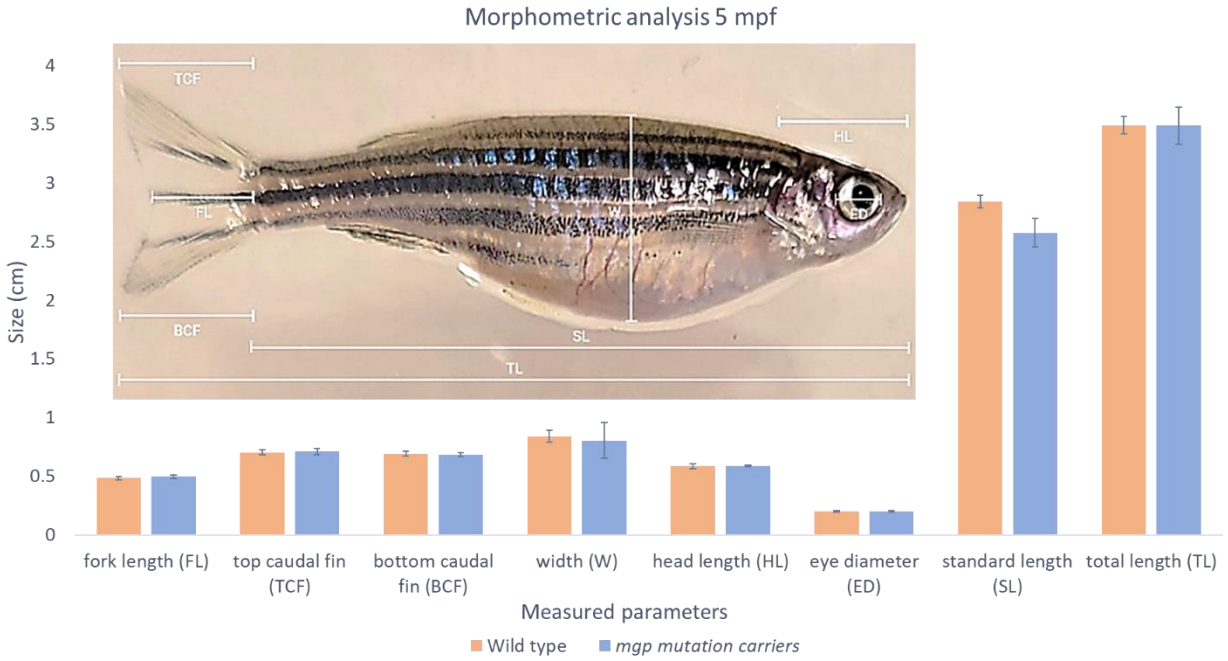

Figure 4.3.1. Morphometric analysis of the F1 *mgp* mutation carriers at 5 mpf. Analysis of 8 different parameters across 10 individuals randomly selected per group. Error bars correspond to ± SD. Non-statistically significant differences were not considered.

As such, we analyzed the potential phenotype of the F3 *mgp* mutants at the larval stages of development. We started by measuring the SL of each genotypic group (*mgp* $^{+/+}$, *mgp* $^{+/m}$ and *mgp* $^{m/m}$) at 5 dpf, 9 dpf, 15 dpf, 20 dpf and 30 dpf. For that, we measured the SL of 3 different batches of F3 *mgp* mutants, for a total of 30 larvae per genotype (10 larvae for each batch), as seen in Figure 4.3.2.

We have found that the *mgp* $^{m/m}$ were shorter when compared with the *mgp* $^{+/+}$ and *mgp* $^{+/m}$, especially at 5 and 15 dpf, in which statistical differences were observed.

These findings were not as evident to what has been found on mice, where the *Mgp* $^{-/-}$ mice was considerably shorter than their wild-type siblings. However, the phenotypic display of KS in mice are much more severe than what is seen in humans with KS, which is also relatable to what we have seen in the *mgp* $^{m/m}$ mutants. Although no statistically significant differences were found

at later stages of development, the *mgp* $^{m/m}$ larvae were consistently shorter in every timepoint measured.

Although the mutant mice are smaller, the same phenotype is often not present in KS patients. This could indicate that zebrafish mutant phenotype is closer to KS patients than the mutant mice. Secondly, the smaller and more prone to defects fish, could have died by the 15 dpf, as Figure 4.2.3 showed, as that is the critical period of larvae development. Lastly, the *mgp* mutant could have adapt to the lack of Mgp expression by the 15 dpf [6,13].

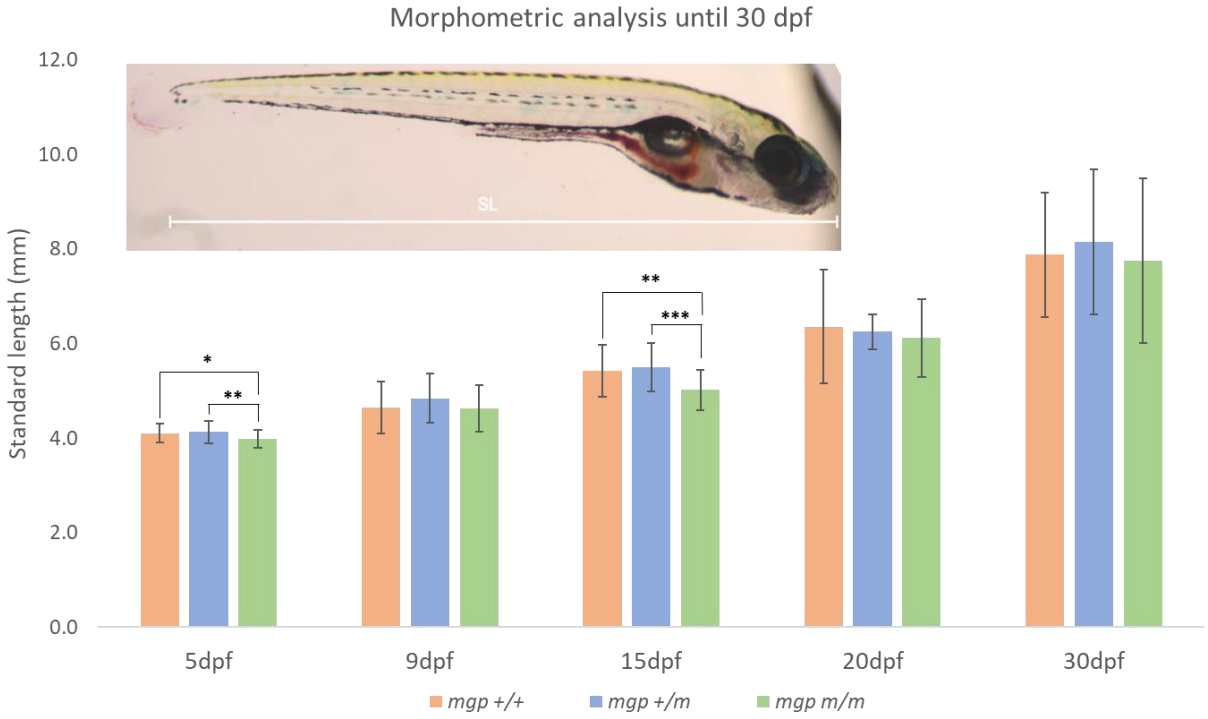

Figure 4.3.2. Morphometric analysis of the F3 *mgp* mutants until 30 dpf. The standard length from 30 fish per group was measured at 5, 9, 15, 20 and 30 dpf. Error bars correspond to ± SD across three independent experiments (dpf=days post fertilization). Differences were considered statistically significant for $p<0.05$ (*=$p<0.05$; **=$p\leq0.01$; ***=$p\leq0.001$). Non-statistically significant differences were not considered.

Since we measured the adult *mgp* mutants from the F1 generation and did not observe a potential phenotypic trait, we wanted to confirm if the *mgp* mutants from the F3 generation, particularly the *mgp* $^{m/m}$ zebrafish, had any significant difference when compared to the other genotypic groups (*mgp* $^{+/+}$ and *mgp* $^{+/m}$). We measured 10 adult zebrafish at 5 mpf, per group (*mgp* $^{+/+}$, *mgp* $^{+/m}$ and *mgp* $^{m/m}$) for the same 8 parameters measured on the *mgp* mutants from the F1 generation (Figure 4.4.1), as seen in Figure 4.3.3.

We observed that only the FL parameter was statistically significant between the *mgp* $^{+/+}$ and *mgp* $^{m/m}$ mutants and that the *mgp* $^{m/m}$ mutants were significantly bigger than the *mgp* $^{+/m}$ in FL, BCF and HL.

These findings were the opposite of what we expected and suggest that zebrafish may behave differently at the physiological level of the Mgp pathway, probably triggering other compensatory mechanisms. Interestingly, the *mgp* $^{+/m}$ mutants were the shortest in all measured parameters, which could suggest that the haploinsufficiency of the Mgp can possibly compromise the physical development of the zebrafish.

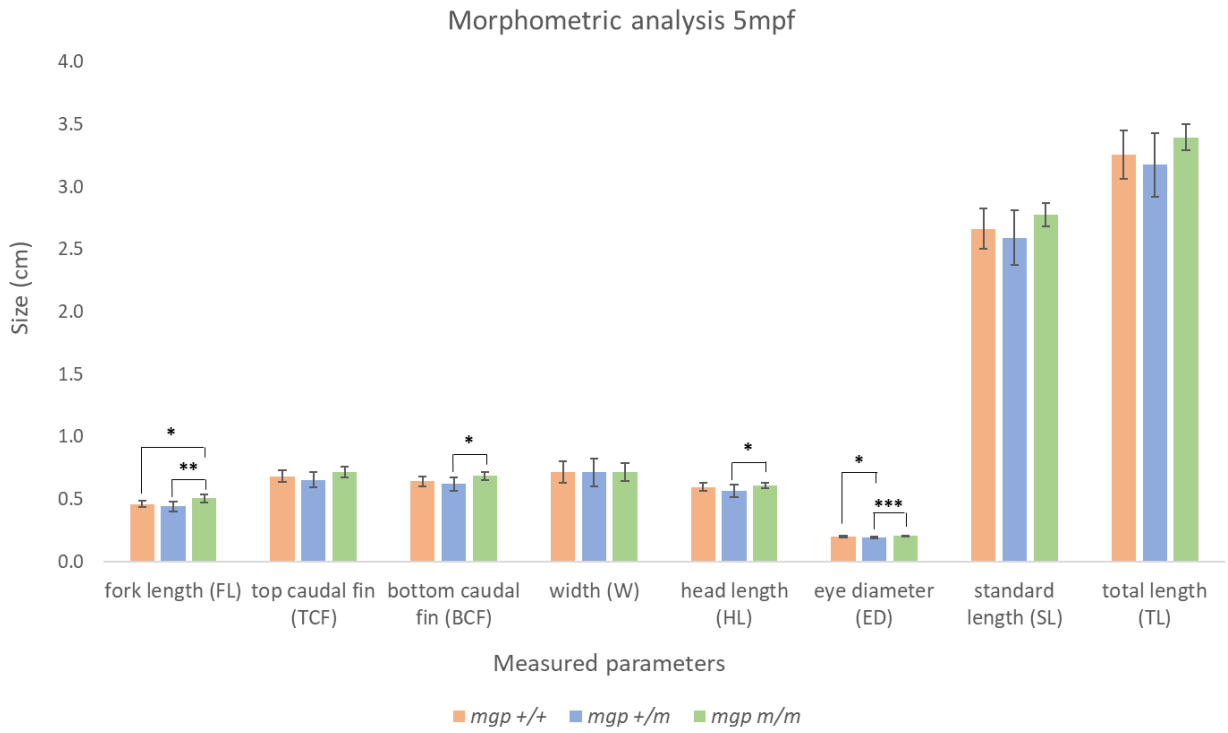

Figure 4.3.3. Morphometric analysis of the F3 *mgp* mutants at 5 mpf. The 8 parameters were measured in 10 fish per group (mpf=months post fertilization). Error bars correspond to ± SD. Differences were considered statistically significant for $p<0.05$ (*=$p<0.05$; **=$p\leq0.01$; ***=$p\leq0.001$) and non-statistically significant differences were not considered.

4.4. Inducing ectopic calcification to the *mgp* mutants

To analyze the extent of ectopic calcification within the *mgp* zebrafish mutants, the fish were treated (T) with warfarin. Warfarin acts as a mimic of conditions where Mgp is absent or non-functional. To analyze the impact of the mutation in the process of ectopic calcification, two

different batches of 20 larvae each containing 19 dpf F3 *mgp* mutants, were T with 25 mg/L of warfarin for 14 days and compared to warfarin T control fish.

We observed that the *mgp* $^{m/m}$ mutants, T with warfarin, died more, and began to die earlier when compared to other T groups, especially the controls (Figure 4.4.1). Furthermore, we observed statistically significant difference at days 7 and 9 (26 and 28 days of treatment), where the *mgp* $^{m/m}$ had the lowest survival rate compared to the *mgp* $^{+/+}$ and *mgp* $^{+/m}$.

The premature mortality and low survival of the *mgp* $^{m/m}$ suggest that this group is more susceptible to the warfarin treatment probably due to the lack of a functional Mgp. This suggests that the *mgp* $^{m/m}$ larvae are probably surviving due to the compensatory actions of the other Gla proteins such as the anticoagulation factors proteins S and C, and coagulation factors II, VII, IX and X, which could make them more susceptible for the induction of ectopic calcification, triggered by the warfarin. Afterall, both *Mgp* $^{-/-}$ mice and KS patients are likely more prone to the development of ectopic calcification, although the former endures severe ectopic calcification and dies prematurely [6,13]. This also suggests that the warfarin is favorably preventing VK recycling and therefore diminishing the γ-carboxylation of the glutamate residues important for the correct function of the Gla-dependent proteins [9].

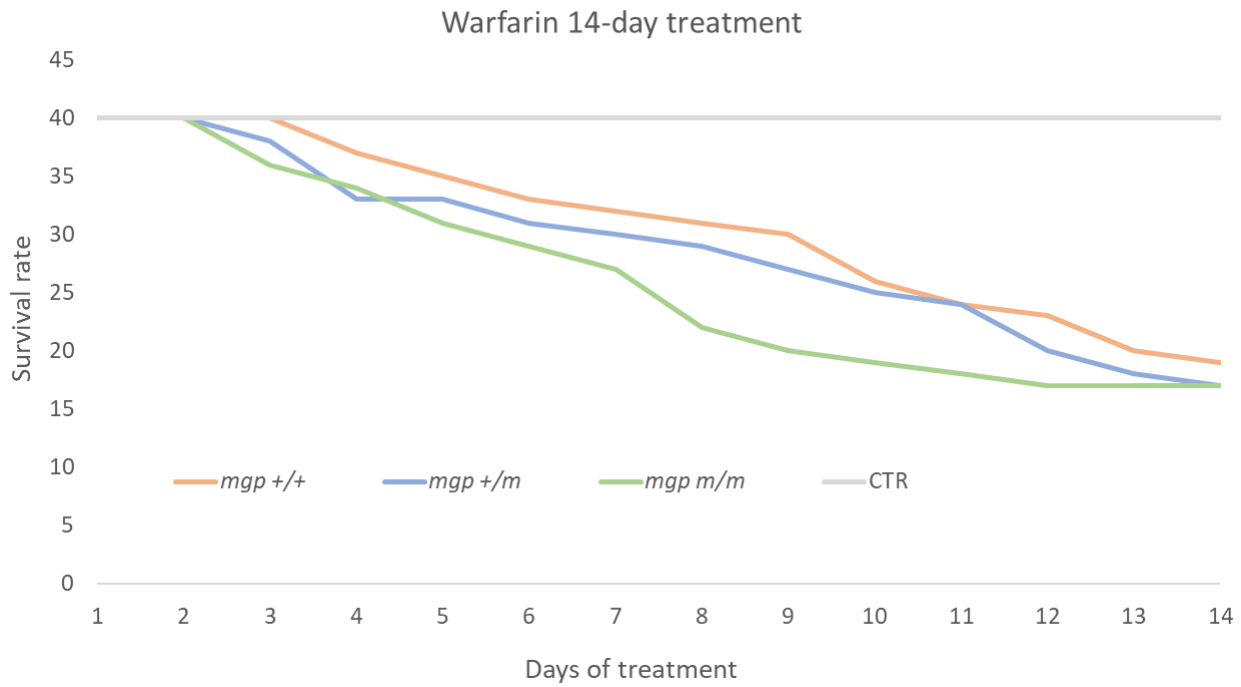

Figure 4.4.1. Inducing ectopic calcification to the *mgp* mutants at 19 dpf. Data across two independent experiments. 20 larvae per experiment were T with warfarin per group (*mgp* $^{+/+}$, *mgp* $^{+/m}$ and *mgp* $^{m/m}$) and 20 larvae per experiment were used as control (CTR) for each group. The warfarin treatment lasted 14 days until 33 dpf.

4.5. Analysis of ectopic calcification in the *mgp* mutant zebrafish

4.5.1. Abdominal vertebrae

In vivo Alizarin red staining was performed in F3 *mgp* mutants to determine the potential calcium accumulation differences between the *mgp* mutants after treatment with warfarin. For that, 22 dpf *mgp* $^{+/+}$, *mgp* $^{+/m}$ and *mgp* $^{m/m}$ larvae, T and non-treated (NT) with warfarin, were stained with Alizarin red S (1.75 mM, pH 7.4). Collected images suggested that the *mgp* $^{m/m}$ mutants (Figure 4.5.1.1 C and D) had less intervertebral space and a higher signal intensity, when compared to *mgp* $^{+/+}$ (Figure 4.5.1.1 A and B).

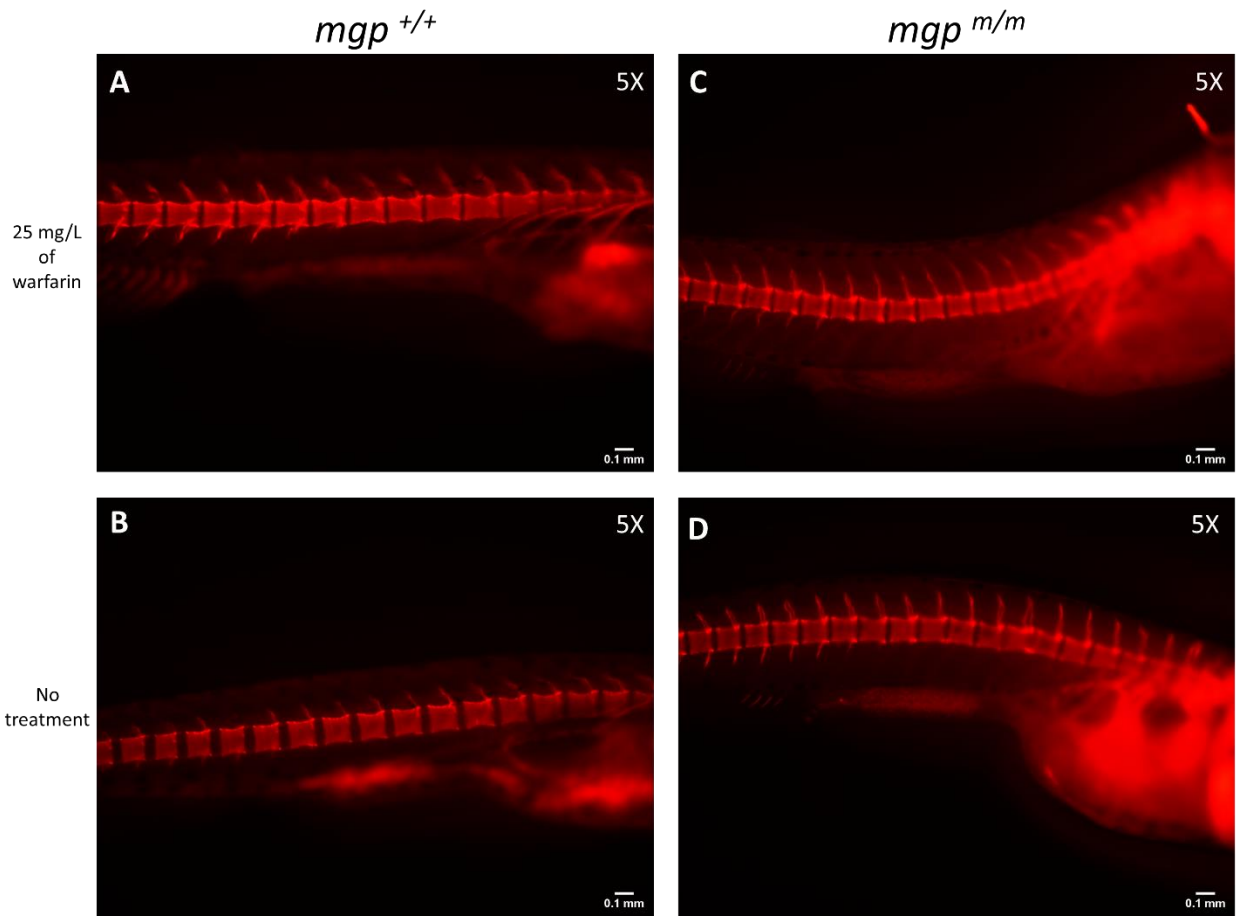

Figure 4.5.1.1. *In vivo* alizarin red staining of *mgp* mutant larvae at 22 dpf. Alizarin red stained images of the abdominal vertebrae area of *mgp* $^{+/+}$ larvae, (A) post warfarin treatment and (B) without treatment. (C-D). Alizarin red stained images of the abdominal vertebrae area of *mgp* $^{m/m}$ mutants, (C) post warfarin treatment and (D) without warfarin treatment. Images were taken with 5 times magnification.

4.5.1.1. Distances between vertebrae

To measure the distance between vertebrae we used ImageJ software to measure the intervertebral distance of 3 vertebrae in the abdominal vertebrae of 5 larvae per group. We observed that the *mgp* $^{m/m}$ larvae had the lowest intervertebral distance of the compared groups. Additionally, the *mgp* $^{m/m}$ larvae NT had almost the same intervertebral distance as the T group with warfarin. In overall, we observed that the larvae T with warfarin had significantly smaller intervertebral space than the NT with warfarin groups, except between the *mgp* $^{m/m}$ groups, which can be seen in Figure 4.5.1.2. Furthermore, the *mgp* $^{m/m}$ larvae NT with warfarin (Figure 4.5.1.1 D) had approximately the same intervertebral distance as their *mgp* $^{+/+}$ T with warfarin (Figure

4.5.1.1 A), but the effect of warfarin did not significantly decrease the intervertebral space on the *mgp* $^{m/m}$, as occurred in the *mgp* $^{+/+}$ and *mgp* $^{+/m}$ groups.

These findings suggest that the absence or non-functionality of Mgp in the organism mimics the effect of warfarin. As there is a non-functional or no Mgp protein, the effect caused by warfarin that is inhibit the pool recycling of VK, is irrelevant for the *mgp* $^{m/m}$ larvae.

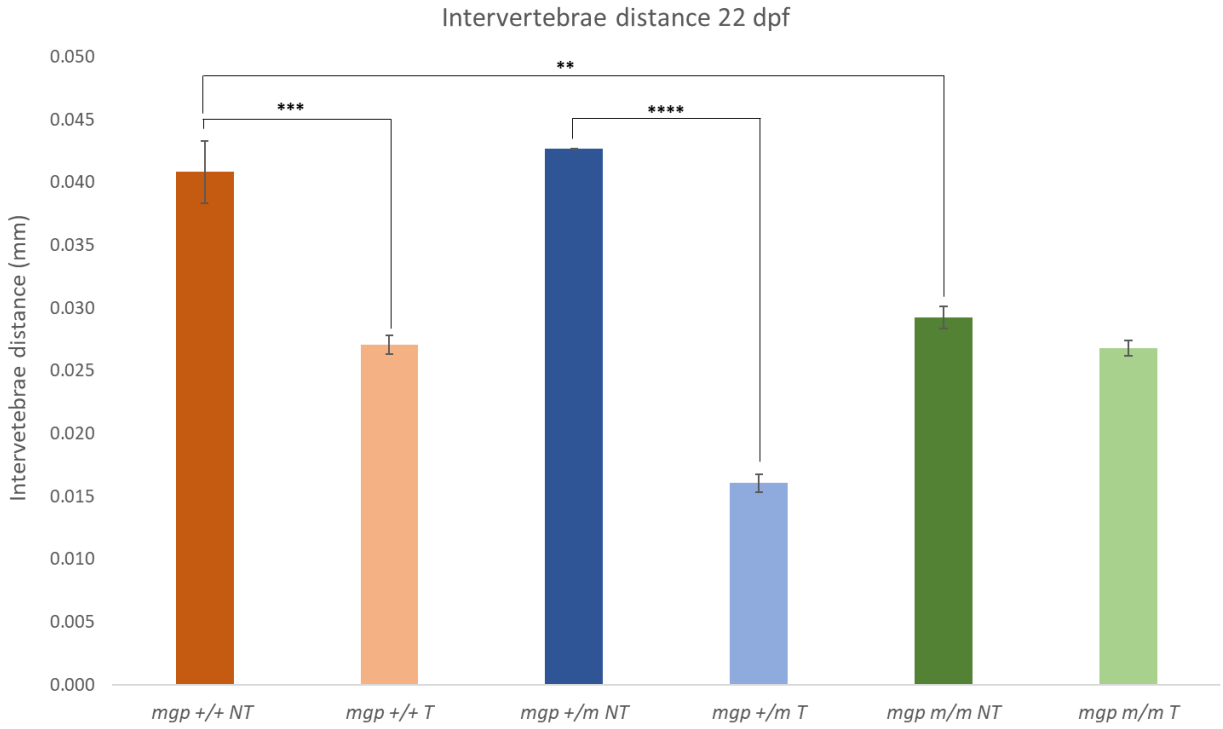

Figure 4.5.1.2. Intervertebral measurement of the *mgp* mutants at 22 dpf. We used an N=5 and measured 3 intervertebral spaces per fish. Error bars correspond to ± SD. Differences were considered statistically significant for $p<0.05$ (**=$p\leq0.01$; ***=$p\leq0.001$; ****=$p\geq0.0001$) and non-statistically significant differences were not considered. NT=Non-treated; T=Treated.

4.5.1.2. Area of the vertebrae

Next, we investigated whether there was an increase of the abdominal vertebrae overall size. For that we measured 10 vertebrae from 5 independent larvae per group. We observed no statistically significant differences in vertebrate area across *mgp* $^{+/+}$, *mgp* $^{+/m}$ and *mgp* $^{m/m}$ larvae. Similarly, the treatment with warfarin did not affect the vertebrate overall size in *mgp* $^{+/+}$ and *mgp* $^{m/m}$ larvae but a slight increase in the area *mgp* $^{+/m}$ larvae was observe post warfarin treatment.

Contrarily to what was expected, the intragroup patterns are practically the same, except for the *mgp* $^{+/m}$ larvae, which was significantly different between the NT and T groups. As the spine is still forming around the developmental stage where the fish were assessed (22 dpf), the imbalance of calcium levels from normal to abnormal may only occur after the total formation of the spinal cord. However, studies must be conducted at more mature stages of development regarding the area of the abdominal vertebrae.

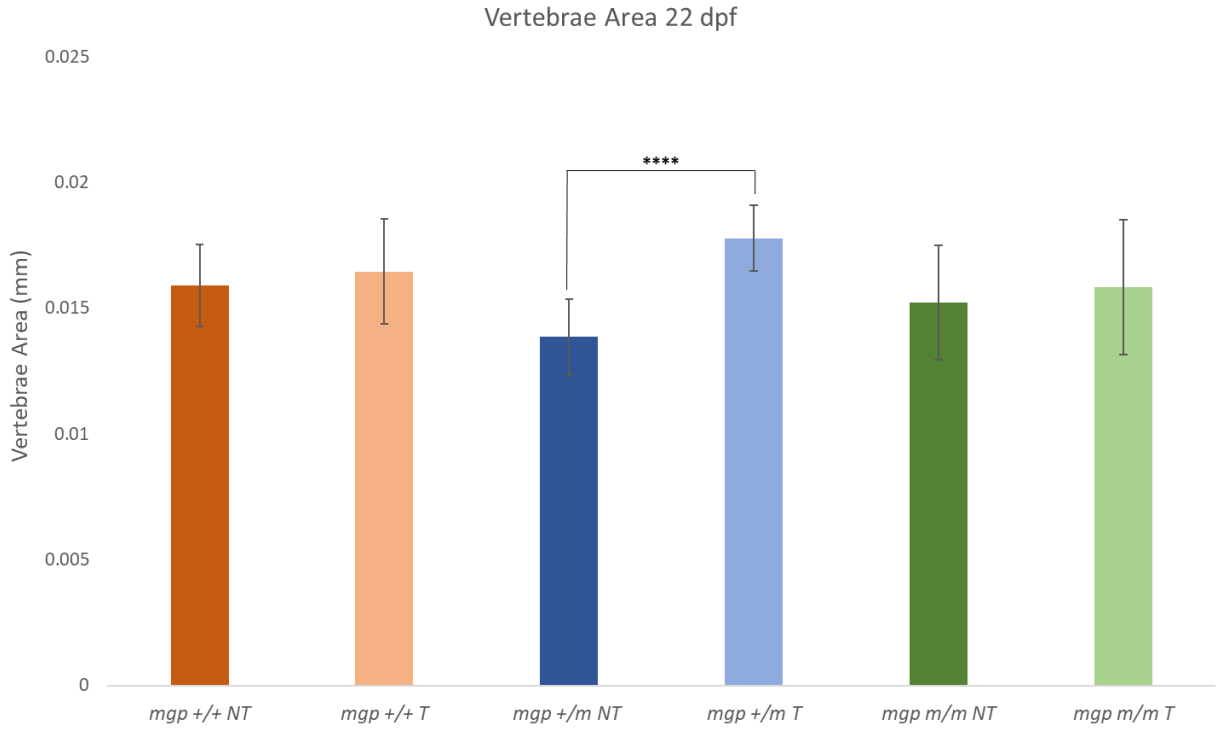

Figure 4.5.1.3. Vertebrae area of the *mgp* mutants at 22 dpf. A total of 10 vertebrae for each 5 fish of each group (*mgp* $^{+/+}$, *mgp* $^{+/m}$ and *mgp* $^{m/m}$) T and NT with warfarin. Error bars correspond to ± SD. Differences were considered statistically significant for $p<0.05$ (****=$p\geq0.0001$) and non-statistically significant differences were not considered. NT=Non-treated; T=Treated.

4.5.1.3. Mineralization quantification of the vertebrae

Lastly, we investigated whether there was an increase in the accumulation of calcium in the abdominal vertebrae of *mgp* mutants. For that, we obtained the Integrated Density (sum of the values of the pixels within the selection), Area and Mean of the vertebrae and the background, for the calculation of the Corrected Total Cell Fluorescence (CTCF), which gives the total fluorescence, particularly the total amount of calcium in the vertebrae. We calculated the CTCF of 5 vertebrae from 5 independent larvae per group, as seen in Figure 4.5.1.4.

As previously observed, CTCF was significantly higher in *mgp* $^{m/m}$ larvae when compared to *mgp* $^{+/+}$, *mgp* $^{+/m}$ larvae. Furthermore, while there was an increase in CTCF in *mgp* $^{+/+}$ *mgp* $^{+/m}$ larvae post warfarin treatment, no statistically significant differences were observed in the *mgp* $^{m/m}$ upon treatment with warfarin which reinforces the suggestion that the *mgp* $^{m/m}$ larvae do not have functional Mgp, which contributes to more ectopic calcification. Since the *mgp* $^{m/m}$ larvae may not have Mgp, warfarin cannot continue to contribute to the accumulation of calcium levels, probably due to a compensation mechanism triggered in these mutants. Overall, a dose of 25 mg/L of warfarin, a potent inhibitor of Mgp, mimics the effects observed in the *mgp* $^{m/m}$, but cannot induce more mineralization, which suggests that the 6-amino acids deletion in the *mgp* $^{m/m}$ likely lead to the production of a non-functional Mgp.

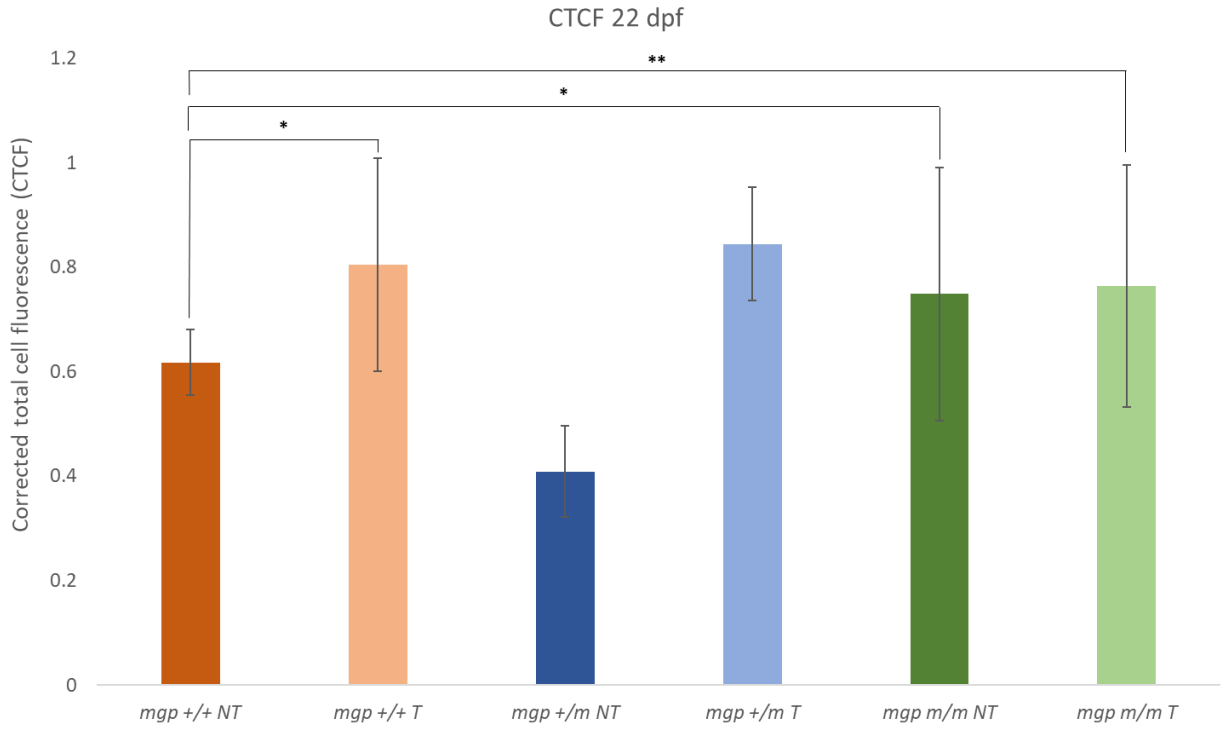

Figure 4.5.1.4. Calcification quantification of the abdominal vertebrae of the *mgp* mutants at 22 dpf. Analysis of 5 abdominal vertebrae for each 5 fish per group. Error bars correspond to ± SD. Differences were considered statistically significant for $p<0.05$ (*=$p<0.05$; **=$p\leq0.01$) and non-statistically significant differences were not considered. NT=Non-treated; T=Treated.

4.5.2. Caudal fin rays

The Alizarin red staining protocol was applied the same way as were described in section 4.6.1., since it was performed simultaneously. We observed the caudal fin rays to see potential

differences between the *mgp* $^{+/+}$ and *mgp* $^{m/m}$, T and NT groups with warfarin. For this analysis we did not use the *mgp* $^{+/m}$ mutants.

Preliminary observation of the collected images suggested that the wild type (Figure 4.5.2.1. B) siblings NT with warfarin had caudal fin rays of smaller size compared with the *mgp* $^{m/m}$ T and NT groups (Figure 4.5.2.1. C and D, respectively). Also, the images suggested that the *mgp* $^{+/+}$ NT with warfarin had a weaker mineralization signal (red signal) at the caudal fin rays when compared to the *mgp* $^{m/m}$ T and NT groups. To further investigate these potential differences, we measured the area and the signal intensity of the caudal fin rays.

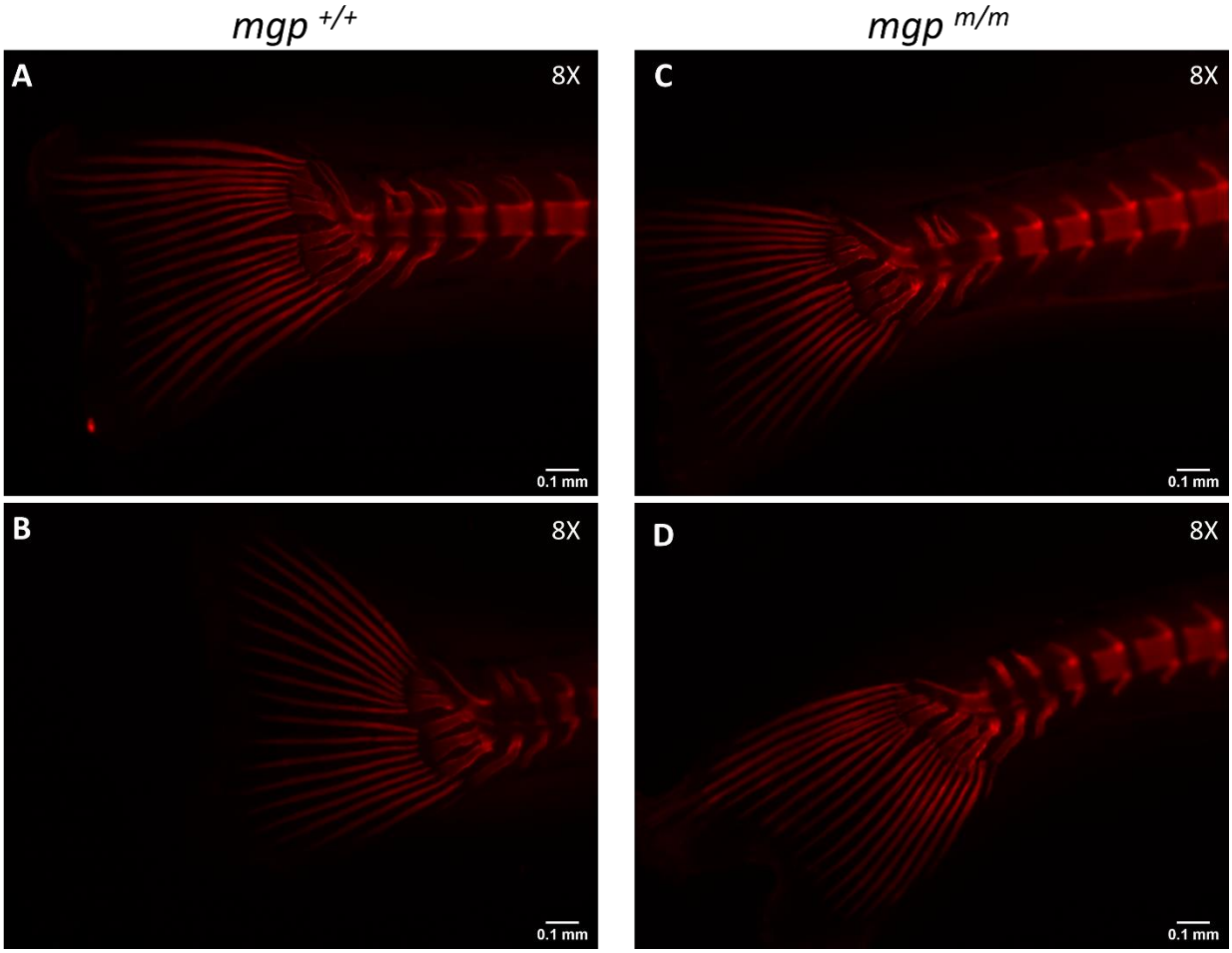

Figure 4.5.2.1. Alizarin red staining *in vivo* of the *mgp* mutant larvae at 22 dpf. (A and B) Alizarin red stained *mgp* $^{+/+}$ to the caudal fin rays, (A) with prior warfarin treatment and (B) without treatment. (C-D) Alizarin red stained *mgp* $^{m/m}$ mutants to the caudal fin rays are, (C) with prior warfarin treatment and (D) without warfarin treatment. Images were taken with 8 times magnification.

4.5.2.1. Area of the caudal fin rays

We quantified the area of the caudal fin rays of the *mgp* mutants at 22 dpf. For that, ImageJ software was used to measure the external outline of the rays. We measured 10 caudal fin rays from the bottom lobe from 3 larvae of each group (*mgp* $^{+/+}$ and *mgp* $^{m/m}$) T and NT with warfarin. Statistically significant differences were observed between the *mgp* $^{+/+}$ and *mgp* $^{m/m}$ larvae groups, as seen in Figure 4.5.2.2. The area of the rays of the *mgp* $^{m/m}$ NT larvae is 1.5-fold higher than the *mgp* $^{+/+}$ NT with warfarin. Interestingly, there is no statistically significant difference between the *mgp* $^{+/+}$ T with warfarin and the *mgp* $^{m/m}$ larvae groups, because the area is approximately the same between these groups. Both *mgp* $^{+/+}$ and *mgp* $^{m/m}$ T groups with warfarin displayed the same ray area, and the *mgp* $^{m/m}$ NT larvae had approximately the same ray area. These observations once again suggests that the Mgp deficiency may potentially favor osteoblast accumulation, contributing to an increased mineralization process. Furthermore, this suggests that Mgp may be absent from the *mgp* $^{m/m}$, as the caudal fin area is 50 % bigger than the *mgp* $^{+/+}$, suggesting more ectopic calcification and that these mutants behave as they were T with warfarin.

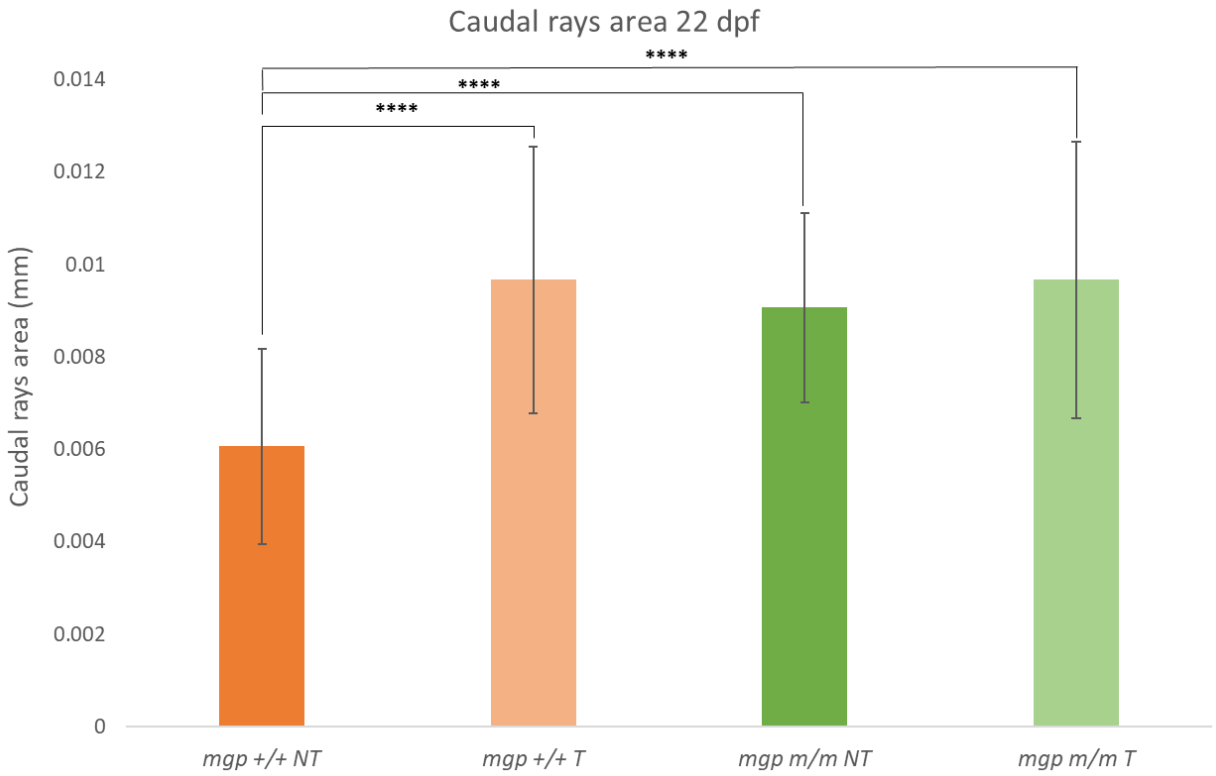

Figure 4.5.2.2. Area of the caudal fin rays of the *mgp* mutants at 22 dpf. A total of 10 caudal fin rays from the bottom lobe for each 3 fish of each group (*mgp* $^{+/+}$ and *mgp* $^{m/m}$) T and NT with warfarin. Error bars correspond to ± SD. Differences were considered statistically significant for $p<0.05$ (****=$p\geq0.0001$) and non-statistically significant differences were not considered. NT=Non-treated; T=Treated.

4.5.2.2. Mineralization quantification of the caudal fin rays

We analyzed the accumulation of calcium in the rays of the caudal fin in the *mgp* mutants. For that, we used the ImageJ software and obtained the Integrated Density, Area and Mean of the vertebrae and the backgrounds for the calculation of the CTCF. We calculated the CTCF for 5 rays per larvae and 3 larvae for each group (*mgp* $^{+/+}$ and *mgp* $^{m/m}$) T and NT with warfarin, seen in Figure 4.5.2.3.

Statistically significant differences were observed between the groups, except for the T *mgp* $^{+/+}$ and *mgp* $^{m/m}$ larvae groups. The *mgp* $^{+/+}$ T larvae had the highest accumulation of calcium in the caudal fin rays. The *mgp* $^{m/m}$ NT larvae had a high accumulation of calcium, but below the levels observed in the *mgp* $^{+/+}$ T larvae. The *mgp* $^{m/m}$ T larvae had similar calcium accumulation than the *mgp* $^{+/+}$ NT.

Despite this statistically significant difference, the expected results were supposed to be contrary, i.e., that the *mgp* $^{m/m}$ larvae would have higher CTCF corresponding to an increase ray mineralization than the *mgp* $^{+/+}$, congruent with the results seen in Figure 4.5.1.4. A possible explanation for this result is that the Alizarin red signal began to fade, as this group was the last one to be managed, since the NT *mgp* $^{m/m}$ larvae displayed a higher CTCF than the NT *mgp* $^{+/+}$. These results suggest that there is no difference in accumulation of calcium at the caudal fin rays between the *mgp* $^{+/+}$ and *mgp* $^{m/m}$ larvae groups, although another experiment should be conducted with the same exposure time and a higher N.

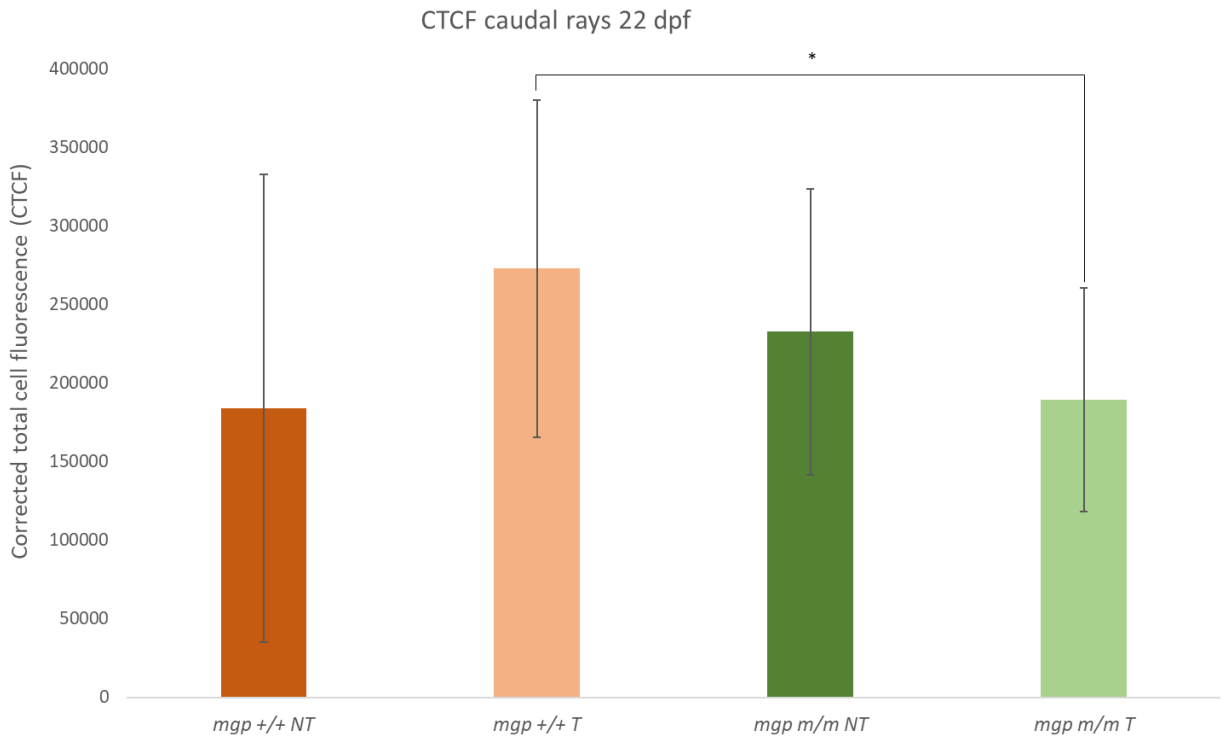

Figure 4.5.2.3. Calcification quantification of the caudal fin rays of *mgp* mutants at 22 dpf. Error bars correspond to ± SD. Differences were considered statistically significant for $p<0.05$ (*=$p<0.05$) and non-statistically significant differences were not considered. NT=Non-treated; T=Treated.

4.6. Mgp expression

To address whether our mutant express Mgp, we performed immunofluorescence analysis of *mgp* mutants, at 33 dpf. We observed that while *mgp* $^{+/+}$ sections had a green fluorescent signal (Figure 4.6.1. A and B) at the branchial arch, cardiac muscle, posterior kidney (Figure 4.6.1. A) and at the caudal vertebrae (Figure 4.6.1. B), whereas *mgp* $^{m/m}$ sections did not displayed any fluorescent signal. Mgp signal was found to be expressed in mineralized tissues such as bone and

calcified cartilage from the branchial arches overall suggesting that the while the mutation did not induce any frame shift, it affected amino acids important for mature protein function.

In this study, we tested several home-produced antibodies against Mgp and Bgp and only antibody Bgp27 signal was detected, and in control samples. We hypothesize that the antibody tested does in fact recognize Mgp. First, while Bgp and Mgp are proteins with similar size and function, there is no logical explanation to the reason why there is no Bgp signal detected in the *mgp* mutants. Second, the antibody samples are old with limited information, and at some point, there might have been a mislabel and that in fact that antibody against Mgp. Third, as both proteins have similar structure and domains, the antibody could recognize both Mgp and Bgp proteins. Lastly, we detected signal in the cardiac muscle, which can be expected for Mgp but not for Bgp which is expressed in the matrix of skeletal structures [83,122].

As such, it is important, in the future, to verify whether this antibody recognizes the Mgp protein, for example through Western blot.

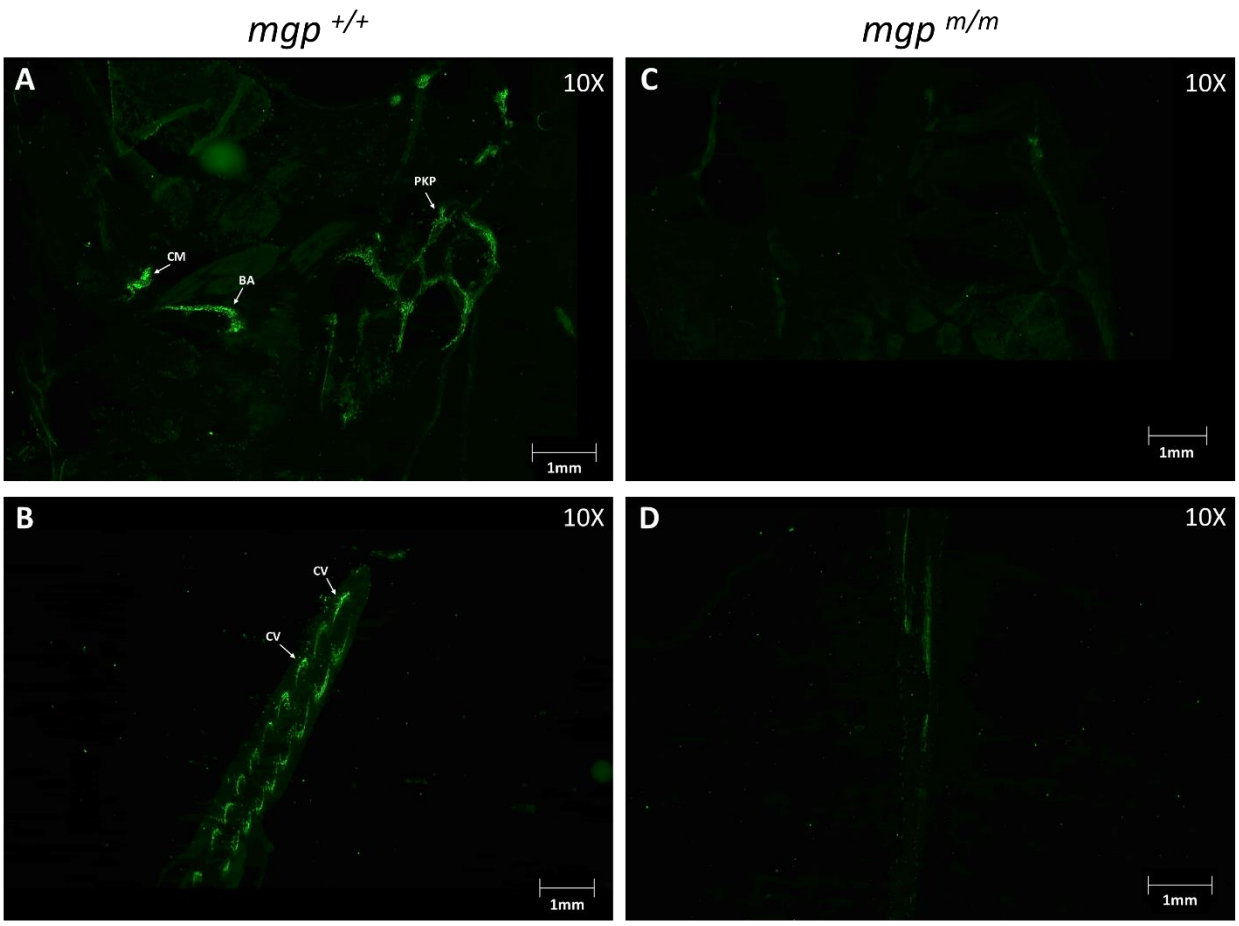

Figure 4.6.1. Immunohistochemistry for Mgp in the *mgp* mutants at 33 dpf, *ex vivo*. (A-B) *mgp* $^{+/+}$ zebrafish with the presence of Mgp (green signal) at (A) the branchial arch, cardiac muscle and posterior kidney and at (B) the caudal vertebrae near the caudal fin. (C-D) *mgp* $^{m/m}$ zebrafish with no presence of Mgp (absence of green signal) at (C) the branchial arch, cardiac muscle and posterior kidney and at (D) the caudal vertebrae near the caudal fin. Images were taken with 10 times magnification. Arrows point to tissues were Mgp is accumulated in the zebrafish mutants. BA=Branchial arch; CM=Cardiac muscle; CV=Caudal vertebrae; PKP=Posterior kidney periphery.

4.7. Ectopic calcification assessment in the *mgp* mutants

To identify possible ectopic calcification sites in the *mgp* mutants, we performed the von Kossa staining protocol [83], concomitantly with toluidine blue coloring, to observe ectopic calcification in the section of the *mgp* mutants. For that, we used histological sections from fish at 33 dpf (*mgp* $^{+/+}$ and *mgp* $^{m/m}$) T and NT with warfarin.

We observed that the *mgp* $^{m/m}$ juveniles had higher mineral concentration within tissues not normally mineralized tissues, such as the posterior kidney, heart, parasphenoidal cartilage and carotid artery. We observed that the T and NT *mgp* $^{m/m}$ juveniles (Figure 4.7.1 C and D,

respectively) had a higher density of mineral accumulation in the posterior kidney tissue (KT) than the T and especially the NT *mgp* $^{+/+}$ juveniles (Figure 4.7.1 A and B, respectively). At the kidney periphery (KP) the accumulation of mineral is very similar between the groups, although denser within the groups T with warfarin (Figure 4.7.1 A and C).

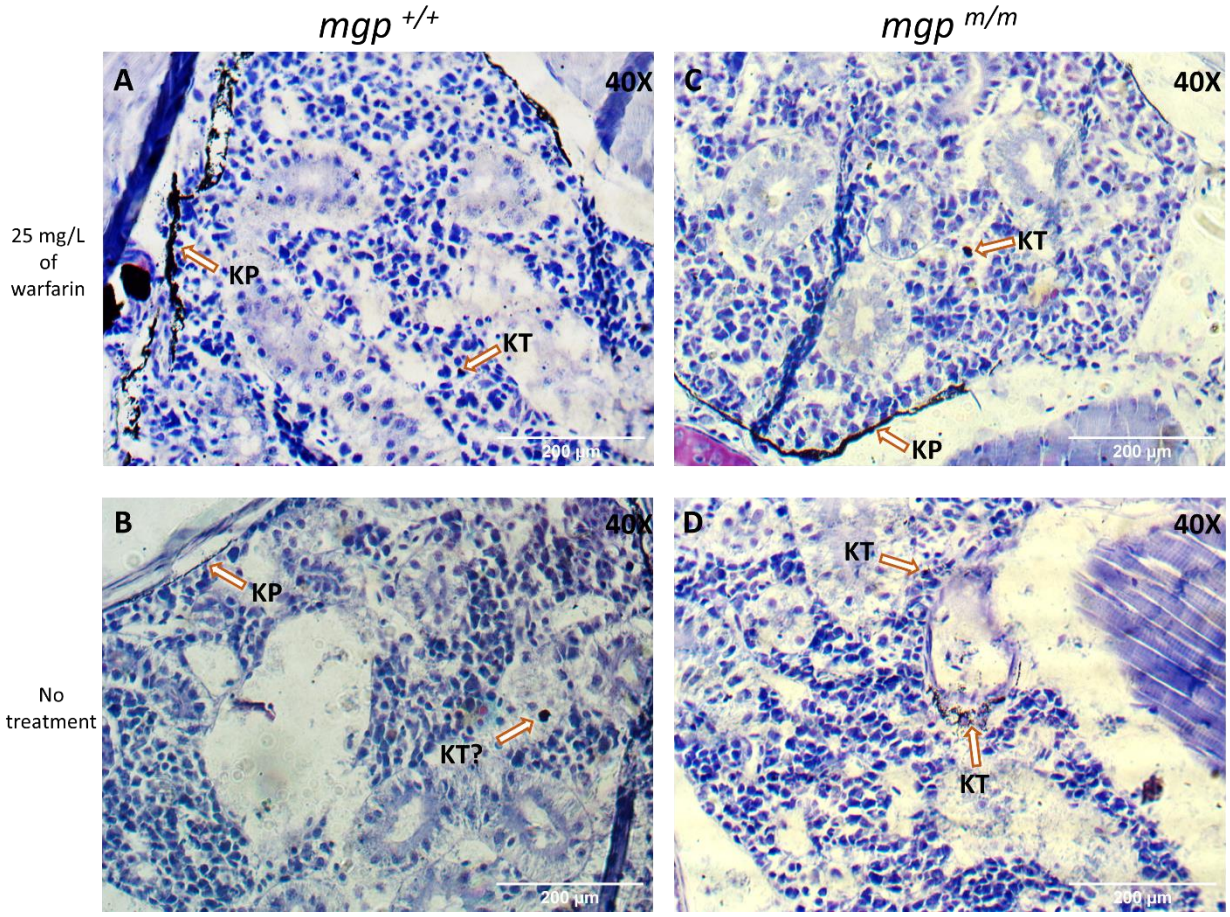

Figure 4.7.1. Ectopic calcification on the *mgp* mutants at 33 dpf, *ex vivo*. 40 times magnification. Scale at 200 µm. KP=Kidney Periphery; KT=Kidney Tissue.

We also observed that the *mgp* $^{m/m}$ juveniles had mineral deposition in the heart tissue (HT), a feature not observed in the *mgp* $^{+/+}$ juveniles, as seen in Figure 4.7.2. We have also observed that the heart periphery (HP) had mineral accumulation in the T *mgp* $^{m/m}$ (Figure 4.7.2 C) and T and NT *mgp* $^{+/+}$ juveniles (Figure 4.7.2 A and B, respectively), with higher accumulation in the groups T with warfarin (Figure 4.7.2 A and C). Although the concentration of blood cells in the heart is different within the sectioned groups, we could observe calcification near blood cells in the *mgp* $^{m/m}$ juveniles.

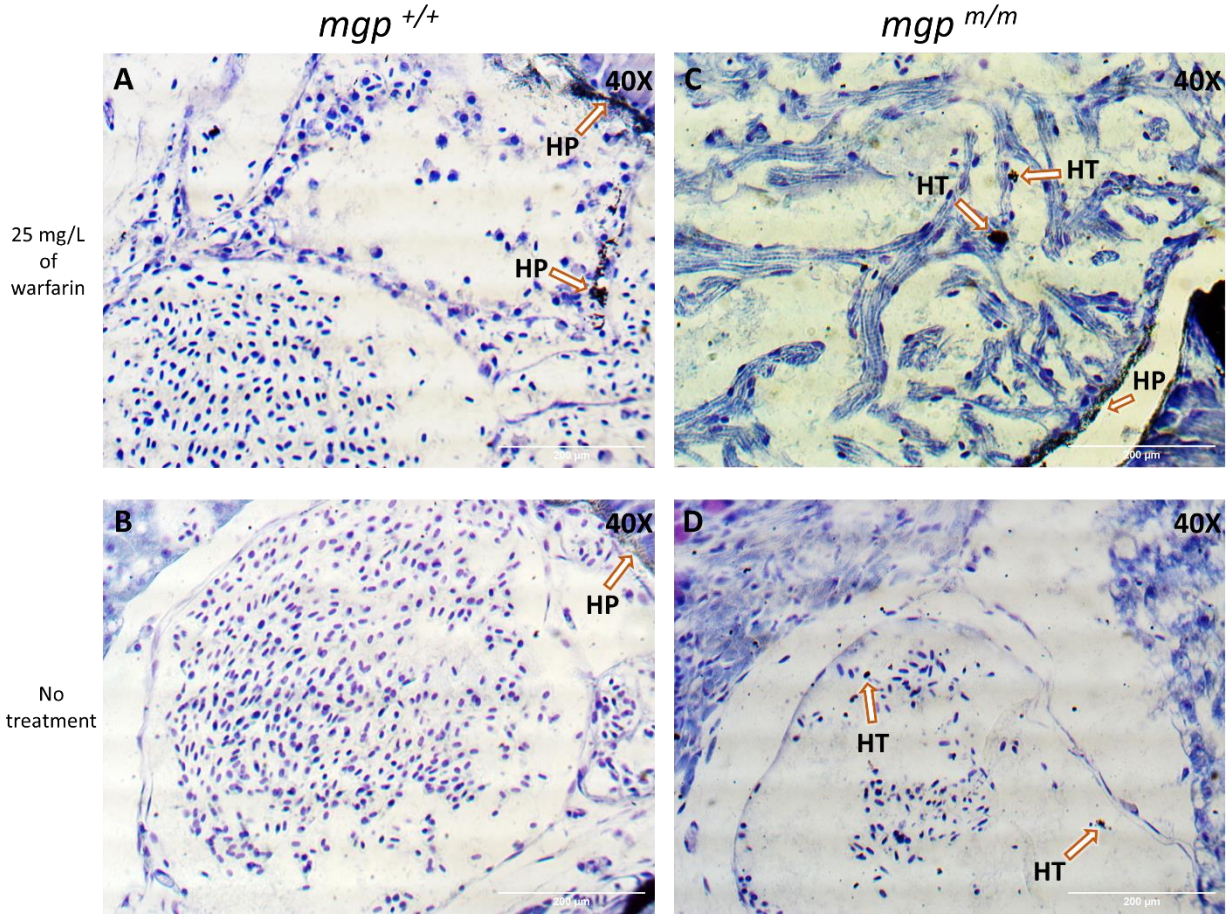

Figure 4.7.2. Ectopic calcification on the *mgp* mutants at 33 dpf, *ex vivo*. 40X magnification. Scale at 200 µm. HP=Heart Periphery; HT=Heart Tissue.

We also observed ectopic calcification in the parasphenoidal cartilage and carotid artery (CA) in all sectioned groups. We only observed erythrocyte (E) calcification in the groups T with warfarin (Figure 4.7.3 A and B). We also observed that, denser mineral accumulation occurred at the CA periphery of the *mgp* $^{m/m}$ than in the *mgp* $^{+/+}$juveniles. Both inferior and superior parasphenoidal cartilage (IP and SP, respectively) had the same similar densities of calcification within all groups.

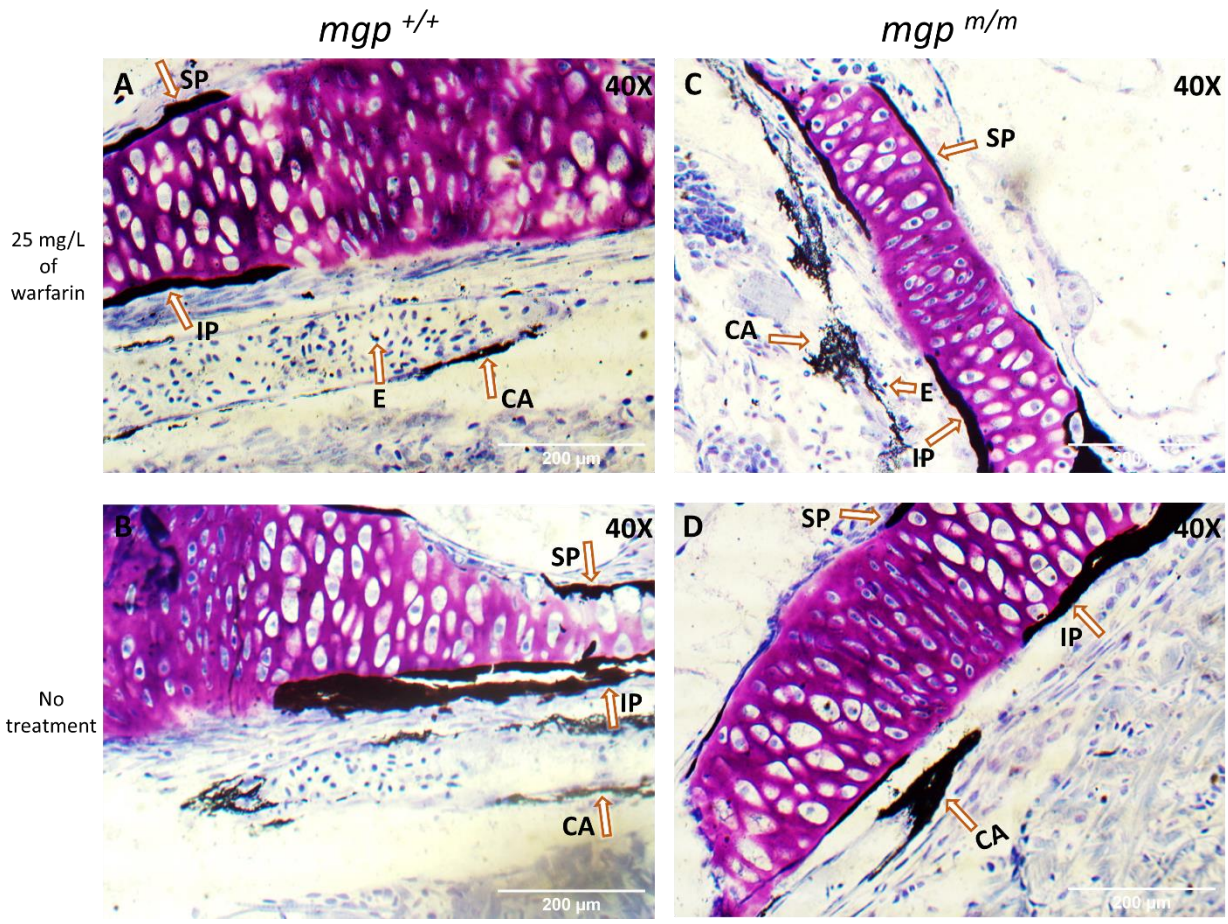

Figure 4.7.3. Ectopic calcification on the *mgp* mutants at 33 dpf, *ex vivo*. 40 times magnification. Scale at 200 µm. CA=Carotid artery; E=Erythrocytes; IP=Inferior Parasphenoidal cartilage; SP=Superior Parasphenoidal cartilage.

These results were congruent to what was expected, since the *mgp* $^{m/m}$ juveniles displayed an overall higher ectopic calcification than the *mgp* $^{+/+}$ juveniles, particularly in the heart. This outcome is supported by the lower larvae survival (Figure 4.2.3) and higher mineral accumulation within the abdominal intervertebral space (Figure 4.7.1.2) and caudal fin rays (Figure 4.7.2.2). As Mgp is non-functional in the *mgp* $^{m/m}$ mutants, greater mineral deposition occurs in soft tissues, since there is no inhibitor of calcification within the extracellular matrix of these tissues, where Mgp normally localizes. As more calcium accumulates in the heart, kidney and arteries, the chances of survival within these mutants are reduced, which makes them prone to diseases and eventually death, when compared with their *mgp* $^{+/+}$ siblings [123].

Chapter 5 - Conclusion

We have characterized an *mgp* mutant zebrafish that carries an 18-nucleotide deletion in exon 4 of the *mgp* gene. Although the mutation did not cause a frame shift or impact the GLA and Ser domains we were initially aiming for, it still removed several highly conserved amino acids present in all vertebrates. During a morphometric analysis we identified that *mgp* mutants have higher embryo and larvae mortality, a hatching retardation and are significantly shorter in early stages of development when compared to controls.

As Mgp is a strong inhibitor of calcification we investigated this premise and observed that these mutants present significantly more calcification than controls. In particular, we observed excessive calcification in the abdominal vertebrae and the caudal fin rays in *mgp* $^{m/m}$ when compared with the other groups. Additionally, the *mgp* $^{m/m}$ mutants did not respond to the warfarin treatment, a potent inductor of vascular calcification that mimics the loss of function of Mgp, suggesting that our mutants have a non-functional Mgp. To confirm the presence of Mgp, we performed an immunohistochemistry analysis which suggested that *mgp* $^{m/m}$ mutants do not express Mgp and that the *mgp* $^{+/+}$ expressed Mgp at the heart, kidney, and the cartilage of branchial arches. To deeper verify the presence of ectopic calcification, we performed the von Kossa staining protocol and observed that the *mgp* $^{m/m}$ mutants had higher ectopic calcification within the heart and parasphenoidal carotid artery than the *mgp* $^{+/+}$, and that the mutants T with warfarin were also prone to higher ectopic calcification effects.

With this work we have identified a knockout zebrafish mutant for Mgp and we have established a line for future experimental usage. The *mgp* $^{m/m}$ mutants displayed excessive calcification in several tissues such as: (i) the abdominal intervertebral space, which was much more reduced than the other experimental groups; (ii) the calcium accumulation in the NT *mgp* $^{m/m}$ mutants was much higher than the other NT groups; (iii) caudal fin rays area was much bigger in the NT *mgp* $^{m/m}$ mutants than the *mgp* $^{+/+}$; and (iv) in the heart and parasphenoidal carotid artery; which are phenotypes frequently associated with KS in humans like the ectopic calcification. Additionally, the morphological shortage observed at some timepoints of the development of the *mgp* $^{m/m}$ mutant larvae are another frequently displayed phenotype observed in KS human patients. This shows that the *mgp* mutant line developed can serve as a biological model to study the pathophysiology of KS, as summarized in Table 5.1. Furthermore, we have observed that the conserved domain of the protein where the mutation takes place, is likely important for the Mgp function, at least at the calcification level role.

Table 5.1. KS features comparison between KS human patients and the *mgp* mutants.

	KS Features	
	Human	Zebrafish
Ectopic calcification	Articular cartilage; Respiratory tract; Vascular system.	Abdominal intervertebral space; Parasphenoid cartilage; Cardiovascular system.
Developmental delay	Shortage; Mental retardation.	Shortage.
Mortality	Not associated.	At the embryonic and larval stages.
Brachytelephalangism	Frequent.	Not investigated.

Although described in the workflow objectives, we did not investigate the interaction between Mgp and Eln proteins, due to some unforeseen experimental setbacks, that have shortened the time to do so. Additionally, we also had trouble in the breeding events of the zebrafish, where sometimes some genotypic groups failed to produce viable eggs. Also, in future studies, we recommend measuring the size of the zebrafish mutant larvae before and after the warfarin treatment, to evaluate whether warfarin can influence growth, and if it is especially prone to negatively impact the development on the zebrafish carrying the *mgp* mutation. Moreover, it will also be interesting to measure and compare the sizes of the pectoral fins, as it can be a similar feature observed in KS patients (brachytelephalangism). Furthermore, we still do not know the effect of the mutation in the overall Mgp function, although the experiments performed in this work suggest that it is correlated with the inhibition of the calcification process.

The *mgp* mutant zebrafish model presents several advantages relatively to the mice model to study the KS features. Comparably to their wild-type siblings, the zebrafish mutants died more at early stages of development particularly at the embryonic stage, they displayed developmental delay at the larval stage, as they were consistently smaller than their wild-type siblings, and they endured severe calcification at the abdominal vertebrae and soft tissues like the heart and parasphenoidal carotid artery. Some of these features like the developmental delay and severe

calcification, are observed in the *Mgp* $^{-/-}$ mice model and KS patients, which makes the *mgp* $^{m/m}$ mutants a good model for parallel investigation of the *in vivo* Mgp mechanisms and the development of the KS. The *mgp* mutant zebrafish model can also be used to investigate the effects of over calcification to other diseases such as osteoporosis and pseudoxanthoma elasticum, as these fish share skeletal structural similarities with humans, and serve as a good template to study severe ectopic calcification, as it was observed in this work. The zebrafish mutants were capable to endure abnormal calcification more resiliently than the Mgp $^{-/-}$ mice model, favoring the longer-term study of abnormal mineralization and its effects on the soft tissues of these fish. Furthermore, the model of this work can be used to track down the molecules and proteins that may be involved within the Mgp synthesis pathway or other relevant unknown pathways that may be linked with KS. In time, this model can be of great help in finding a cure for KS.

Bibliography

1. Hur DJ, Raymond G v., Kahler SG, Riegert-Johnson DL, Cohen BA, Boyadjiev SA. A novel MGP mutation in a consanguineous family: Review of the clinical and molecular characteristics of Keutel syndrome. *Am J Med Genet*. 2005;135 A(1):36-40. doi:10.1002/ajmg.a.30680

2. Cancela ML, Laizé V, Conceição N, Kempf H, Murshed M. Keutel Syndrome, a Review of 50 Years of Literature. *Front Cell Dev Biol*. 2021;9(642136). doi:10.3389/fcell.2021.642136

3. Teebi AS, Lambert DM, Kaye GM, Al-Fifi S, Tewfik TL, Michel Azouz E. Keutel Syndrome: Further Characterization and Review. *American Journal of Medical Genetics* . 1998;77(2):182-187. doi:https://doi.org/10.1002/(SICI)1096-8628(19980630)78:2<182::AID-AJMG18>3.0.CO;2-J

4. Keutel J, Jörgensen G, Gabriel P. A new autosomal recessive syndrome: peripheral pulmonary stenoses, brachytelephalangism, neural hearing loss and abnormal cartilage calcifications-ossification. *Birth Defects*. 1972;8(5):60-68.

5. Weaver KN, el Hallek M, Hopkin RJ, et al. Keutel syndrome: Report of two novel MGP mutations and discussion of clinical overlap with arylsulfatase E deficiency and relapsing polychondritis. *Am J Med Genet A*. 2014;164(4):1062-1068. doi:10.1002/ajmg.a.36390

6. Koos R, Mahnken AH, Mühlenbruch G, et al. Relation of oral anticoagulation to cardiac valvular and coronary calcium assessed by multislice spiral computed tomography. *American Journal of Cardiology*. 2005;96(6):747-749. doi:10.1016/j.amjcard.2005.05.014

7. Sun LF, Chen X. Tracheobronchial Stenosis in Keutel Syndrome. *Indian Pediatr*. 2012;49:759-759. Accessed January 13, 2022. https://www.indianpediatrics.net/sep2012/sep-759.htm

8. Orphanet. Keutel Syndrome. Rare diseases. Published September 2007. Accessed January 21, 2022. https://www.orpha.net/consor/cgi-bin/Disease_Search.php?lng=EN&data_id=11660&Disease_Disease_Search_diseaseGroup=keutel-Syndrome&Disease_Disease_Search_diseaseType=Pat&Disease

9. Munroe PB, Olgunturk RO, Fryns JP, et al. Mutations in the gene encoding the human matrix Gla protein cause Keutel syndrome. *Nat Genet*. 1999;21:142-144. doi:https://doi.org/10.1038/5102

10. Khosroshahi HE, Sahin SC, Akyuz Y, Ede H. Long term follow-up of four patients with Keutel syndrome. *Am J Med Genet A*. 2014;164(11):2849-2856. doi:10.1002/ajmg.a.36699

11. Zebboudj AF, Imura M, Boström K. Matrix GLA protein, a regulatory protein for bone morphogenetic protein-2. *Journal of Biological Chemistry*. 2002;277(6):4388-4394. doi:10.1074/jbc.M109683200

12. Bosemani T, Felling RJ, Wyse E, et al. Neuroimaging findings in children with Keutel syndrome. *Pediatr Radiol*. 2014;44(1):73-78. doi:10.1007/s00247-013-2768-0

13. Luo G, Ducy P, Mckeet MD, et al. Spontaneous calcification of arteries and cartilage in mice lacking matrix GLA protein. *Nature*. 1997;386:78-81. doi:https://doi.org/10.1038/386078a0

14. Hale JE, Fraser JD, Price PA, Hale JE, Williamson MK. The Identification of Matrix Gla Protein in Cartilage. *J Biol Chem*. 1988;263(12):5820-5824. doi:https://doi.org/10.1016/S0021-9258(18)60639-8

15. Correia E, Conceição N, Cancela ML, Belo JA. Matrix Gla protein expression pattern in the early avian embryo. *International Journal of Developmental Biology*. 2016;60(1-3):71-76. doi:10.1387/ijdb.150365jb

16. Cranenburg ECM, Koos R, Schurgers LJ, et al. Characterisation and potential diagnostic value of circulating matrix Gla protein (MGP) species. *Thromb Haemost*. 2010;104(4):811-822. doi:10.1160/TH09-11-0786

17. Kuronuma K, Yokoi A, Fukuoka T, et al. Matrix Gla protein maintains normal and malignant hematopoietic progenitor cells by interacting with bone morphogenetic protein-4. *Heliyon*. 2020;6(4):1-11. doi:10.1016/j.heliyon.2020.e03743

18. Price PA, Urist MR, Otawara Y. MATRIX GLA PROTEIN, A NEW y-CARBOXYGLUTAMIC ACID-CONTAINING PROTEIN WHICH IS ASSOCIATED WITH THE ORGANIC MATRIX OF BONE. *Biochem Biophys Res Commun*. 1983;117(3):765-771. doi:https://doi.org/10.1016/0006-291X(83)91663-7

19. Fraser JD, Otawara Y, Price PA. 1,25-Dihydroxyvitamin D3 Stimulates the Synthesis of Matrix y-Carboxyglutamic Acid Protein by Osteosarcoma Cells MUTUALLY EXCLUSIVE EXPRESSION OF VITAMIN K-DEPENDENT BONE PROTEINS BY CLONAL OSTEOBLASTIC CELL LINES. *J Biol Chem*. 1988;263(2):911-916. doi:https://doi.org/10.1016/S0021-9258(19)35439-0

20. Cancela ML, Laizé V, Conceição N. Matrix Gla protein and osteocalcin: From gene duplication to neofunctionalization. *Arch Biochem Biophys*. 2014;561:56-63. doi:10.1016/j.abb.2014.07.020

21. White RJ, Collins JE, Sealy IM, et al. A high-resolution mRNA expression time course of embryonic development in zebrafish. Published online 2017. doi:10.7554/eLife.30860.001

22. Leurs N, Martinand-Mari C, Ventéo S, Haitina T, Debiais-Thibaud M. Evolution of Matrix Gla and Bone Gla Protein Genes in Jawed Vertebrates. *Front Genet*. 2021;12. doi:10.3389/fgene.2021.620659

23. Cancela L, Hsiehg CL, Francket U, Pricesv PA. Molecular Structure, Chromosome Assignment, and Promoter Organization of the Human Matrix Gla Protein Gene*. *J Biol Chem*. 1990;265(25):15040-15048. doi:https://doi.org/10.1016/S0021-9258(18)77221-9

24. Schurgers LJ, Cranenburg ECM, Vermeer C. Matrix Gla-protein: The calcification inhibitor in need of vitamin K. *Thromb Haemost*. 2008;100(4):593-603. doi:10.1160/TH08-02-0087

25. Herrmann SM, Whatling C, Brand E, et al. Polymorphisms of the Human Matrix Gla Protein (MGP) Gene, Vascular Calcification, and Myocardial Infarction. *Arterioscler Thromb Vasc Biol*. 2000;20(11):2386-2394. doi:https://doi.org/10.1161/01.ATV.20.11.2386

26. Wallin R, Schurgers LJ, Loeser RF. Biosynthesis of the vitamin K-dependent matrix Gla protein (MGP) in chondrocytes: A fetuin-MGP protein complex is assembled in vesicles shed from normal but not from osteoarthritic chondrocytes. *Osteoarthritis Cartilage*. 2010;18(8):1096-1103. doi:10.1016/j.joca.2010.05.013

27. Speer MY, Yang HY, Brabb T, et al. Smooth muscle cells give rise to osteochondrogenic precursors and chondrocytes in calcifying arteries. *Circ Res*. 2009;104(6):733-741. doi:10.1161/CIRCRESAHA.108.183053

28. Yagami K, Suh JY, Enomoto-Iwamoto M, et al. *Matrix GLA Protein Is a Developmental Regulator of Chondrocyte Mineralization and, When Constitutively Expressed, Blocks Endochondral and Intramembranous Ossification in the Limb*. Vol 147.; 1999. doi:10.1083/jcb.147.5.1097

29. Cranenburg ECM, van Spaendonck-Zwarts KY, Bonafe L, et al. Circulating matrix γ-carboxyglutamate protein (MGP) species are refractory to vitamin K treatment in a new case of Keutel syndrome. *Journal of Thrombosis and Haemostasis*. 2011;9(6):1225-1235. doi:10.1111/j.1538-7836.2011.04263.x

30. NCBI. MGP matrix Gla protein [Homo sapiens (human)]. Published January 2022. Accessed December 17, 2021. https://www.ncbi.nlm.nih.gov/gene/4256#gene-expression

31. Schurgers LJ, Uitto J, Reutelingsperger CP. Vitamin K-dependent carboxylation of matrix Gla-protein: A crucial switch to control ectopic mineralization. *Trends Mol Med*. 2013;19(4):217-226. doi:10.1016/j.molmed.2012.12.008

32. El Asmar MS, Naoum JJ, Arbid EJ. Vitamin K dependent proteins and the role of vitamin K2 in the modulation of vascular calcification: A review. *Oman Med J*. 2014;29(3):172-177. doi:10.5001/omj.2014.44

33. Vilder EY de, Vanakker OM. From variome to phenome: Pathogenesis, diagnosis and management of ectopic mineralization disorders. *World J Clin Cases*. 2015;3(7):556. doi:10.12998/wjcc.v3.i7.556

34. Laizé V, Martel P, Viegas CSB, Price PA, Cancela ML. Evolution of matrix and bone γ-carboxyglutamic acid proteins in vertebrates. *Journal of Biological Chemistry*. 2005;280(29):26659-26668. doi:10.1074/jbc.M500257200

35. Proudfoot D, Shanahan CM. Molecular mechanisms mediating vascular calcification: Role of matrix Gla protein (review article). *Nephrology*. 2006;11(5):455-461. doi:10.1111/j.1440-1797.2006.00660.x

36. O'rourke C, Shelton G, Hutcheson JD, et al. Calcification of vascular smooth muscle cells and imaging of aortic calcification and inflammation. *Journal of Visualized Experiments*. 2016;2016(111):1-13. doi:10.3791/54017

37. Wen L, Chen J, Duan L, Li S. Vitamin K-dependent proteins involved in bone and cardiovascular health (Review). *Mol Med Rep*. 2018;18(1):3-15. doi:10.3892/mmr.2018.8940

38. Yao Y, Zebboudj AF, Torres A, Shao E, Boström K. Activin-like kinase receptor 1 (ALK1) in atherosclerotic lesions and vascular mesenchymal cells. *Cardiovasc Res*. 2007;74(2):279-289. doi:10.1016/j.cardiores.2006.09.014

39. Wajih N, Borras T, Xue W, Hutson SM, Wallin R. Processing and transport of matrix γ-carboxyglutamic acid protein and bone morphogenetic protein-2 in cultured human vascular smooth muscle cells: Evidence for an uptake mechanism for serum fetuin. *Journal of Biological Chemistry*. 2004;279(41):43052-43060. doi:10.1074/jbc.M407180200

40. Marulanda J, Murshed M. Role of Matrix Gla protein in midface development: Recent advances. *Oral Dis*. 2018;24(1-2):78-83. doi:10.1111/odi.12758

41. Schurgers LJ, Teunissen KJF, Knapen MHJ, et al. Novel conformation-specific antibodies against matrix γ- carboxyglutamic acid (Gla) protein: Undercarboitylated matrix Gla protein as marker for vascular calcification. *Arterioscler Thromb Vasc Biol*. 2005;25(8):1629-1633. doi:10.1161/01.ATV.0000173313.46222.43

42. Schurgers LJ, Spronk HMH, Skepper JN, et al. Post-translational modifications regulate matrix Gla protein function: importance for inhibition of vascular smooth muscle cell calcification. *Journal of Thrombosis and Haemostasis*. 2007;5(12):2503-2511. doi:https://doi.org/10.1111/j.1538-7836.2007.02758.x

43. Danziger J. Vitamin K-dependent proteins, warfarin, and vascular calcification. *Clinical Journal of the American Society of Nephrology*. 2008;3(5):1504-1510. doi:10.2215/CJN.00770208

44. Tie JK, Jin DY, Straight DL, Stafford DW. Functional study of the vitamin K cycle in mammalian cells. *Blood*. 2011;117(10):2967-2974. doi:10.1182/blood-2010-08-304303

45. Tew BY, Hong TB, Otto-Duessel M, et al. Vitamin K epoxide reductase regulation of androgen receptor activity. *Oncotarget*. 2017;8(8):13818-13831. doi:10.18632/oncotarget.14639

46. Link KP. The Discovery of Dicumarol and Its Sequels. *Circulation*. 1959;19(1):97-107. doi:10.1161/01.cir.19.1.97

47. Chatrou MLL, Winckers K, Hackeng TM, Reutelingsperger CP, Schurgers LJ. Vascular calcification: The price to pay for anticoagulation therapy with vitamin K-antagonists. *Blood Rev*. 2012;26(4):155-166. doi:10.1016/j.blre.2012.03.002

48. Chen X, Liu Y, Furukawa N, et al. A novel vitamin K derived anticoagulant tolerant to genetic variations of vitamin K epoxide reductase. *Journal of Thrombosis and Haemostasis*. 2021;19(3):689-700. doi:10.1111/jth.15209

49. Nollet L, Gils M van, Verschuere S, Vanakker O. The role of vitamin k and its related compounds in mendelian and acquired ectopic mineralization disorders. *Int J Mol Sci*. 2019;20(9). doi:10.3390/ijms20092142

50. Price PA, Faus SA, Williamson MK. Warfarin Causes Rapid Calcification of the Elastic Lamellae in Rat Arteries and Heart Valves. *Arterioscler Thromb Vasc Biol*. 1998;18(9):1400-1407. doi:https://doi.org/10.1161/01.ATV.18.9.1400

51. Schurgers LJ, Aebert H, Vermeer C, Bültmann B, Janzen J. Oral anticoagulant treatment: Friend or foe in cardiovascular disease? *Blood*. 2004;104(10):3231-3232. doi:10.1182/blood-2004-04-1277

52. Han KH, O'Neill WC. Increased peripheral arterial calcification in patients receiving warfarin. *J Am Heart Assoc*. 2016;5(1):1-8. doi:10.1161/JAHA.115.002665

53. Walfisch A, Koren G. The "Warfarin Window" in Pregnancy: The Importance of Half-life. *Journal of Obstetrics and Gynaecology Canada*. 2010;32(10):988-989. doi:10.1016/S1701-2163(16)34689-8

54. Shian Chan W, Anand S, Ginsberg JS. *Anticoagulation of Pregnant Women With Mechanical Heart Valves A Systematic Review of the Literature*.; 2000. https://jamanetwork.com/

55. Murshed M, Schinke T, McKee MD, Karsenty G. Extracellular matrix mineralization is regulated locally; different roles of two gla-containing proteins. *Journal of Cell Biology*. 2004;165(5):625-630. doi:10.1083/jcb.200402046

56. Kapustin AN, Davies JD, Reynolds JL, et al. Calcium regulates key components of vascular smooth muscle cell-derived matrix vesicles to enhance mineralization. *Circ Res*. 2011;109(1):1-12. doi:10.1161/CIRCRESAHA.110.238808

57. van Varik BJ, Rennenberg RJMW, Reutelingsperger CP, Kroon AA, de Leeuw PW, Schurgers LJ. Mechanisms of arterial remodeling: Lessons from genetic diseases. *Front Genet*. 2012;3(290):1-10. doi:10.3389/fgene.2012.00290

58. Parashar A, Gourgas O, Lau K, et al. Elastin calcification in in vitro models and its prevention by MGP's N-terminal peptide. *J Struct Biol*. 2021;213(1):1-9. doi:10.1016/j.jsb.2020.107637

59. Kumric M, Borovac JA, Kurir TT, et al. Role of matrix gla protein in the complex network of coronary artery disease: A comprehensive review. *Life*. 2021;11(8). doi:10.3390/life11080737

60. Basalyga DM, Simionescu DT, Xiong W, Baxter BT, Starcher BC, Vyavahare NR. Elastin degradation and calcification in an abdominal aorta injury model: Role of matrix metalloproteinases. *Circulation*. 2004;110(22):3480-3487. doi:10.1161/01.CIR.0000148367.08413.E9

61. Pencak P, Czerwieńska B, Ficek R, et al. Calcification of coronary arteries and abdominal aorta in relation to traditional and novel risk factors of atherosclerosis in hemodialysis patients. *BMC Nephrol*. 2013;14(1). doi:10.1186/1471-2369-14-10

62. Li Q, Jiang Q, Uitto J. Ectopic mineralization disorders of the extracellular matrix of connective tissue: Molecular genetics and pathomechanisms of aberrant calcification. *Matrix Biology*. 2014;33:23-28. doi:10.1016/j.matbio.2013.06.003

63. Giachelli CM. Ectopic calcification: new concepts in cellular regulation. *Z Kardiol*. 2001;90(3):31-37. doi:https://doi.org/10.1007/s003920170039

64. Pugsley MK, Tabrizchi R. The vascular system An overview of structure and function. *J Pharmacol Toxicol Methods*. 2000;2(44):333-340. doi:https://doi.org/10.1016/S1056-8719(00)00125-8

65. Tomanek RJ. Formation of the coronary vasculature: a brief review. *Cardiovasc Res*. 1996;1(31):46-51. doi:https://doi.org/10.1016/S0008-6363(95)00205-7

66. Hsu CPD, Hutcheson JD, Ramaswamy S. Oscillatory fluid-induced mechanobiology in heart valves with parallels to the vasculature. *Vascular Biology*. 2020;2(1):R59-R71. doi:10.1530/vb-19-0031

67. Urry DW. Molecular perspectives of vascular wall structure and disease: the elastic component. *Perspect Biol Med*. 1978;21(2):265-295. doi:10.1353/pbm.1978.0038

68. Dye B, Lincoln J. The endocardium and heart valves. *Cold Spring Harb Perspect Biol*. 2020;12(12):1-17. doi:10.1101/cshperspect.a036723

69. CARDIOVASCULAR SYSTEM. Published December 10, 2019. Accessed January 20, 2022. https://www.thenurseslab.com/2019/12/physical-assessment-part-5.html

70. Parvizi Javad, Kim GK. *High Yield Orthopaedics*. 1st ed. (Rebane T, ed.). Elsevier; 2010. doi:https://doi.org/10.1016/C2009-0-32243-6

71. Chang LR, Marston G, Martin A. *Anatomy, Cartilage*. StatPearls Publishing; 2021. Accessed February 2, 2022. https://www.ncbi.nlm.nih.gov/books/NBK532964/#!po=90.0000

72. Triche R, Mandelbaum BR. *Overview of Cartilage Biology and New Trends in Cartilage Stimulation*. Vol 18.; 2013. doi:10.1016/j.fcl.2012.12.001

73. Eschweiler J, Horn N, Rath B, et al. The biomechanics of cartilage-an overview. *Life*. 2021;11(4). doi:10.3390/life11040302

74. El-Maadawy S, Kaartinen MT, Schinke T, Murshed M, Karsenty G, McKee MD. Cartilage formation and calcification in arteries of mice lacking matrix Gla protein. *Connect Tissue Res*. 2003;44(SUPPL. 1):272-278. doi:10.1080/03008200390181762

75. Mitsuyama H, Healey RM, Terkeltaub RA, Coutts RD, Amiel D. Calcification of human articular knee cartilage is primarily an effect of aging rather than osteoarthritis. *Osteoarthritis Cartilage*. 2007;15(5):559-565. doi:10.1016/j.joca.2006.10.017

76. Liu Q, Wang R, Hou S, et al. Chondrocyte-derived exosomes promote cartilage calcification in temporomandibular joint osteoarthritis. *Arthritis Res Ther*. 2022;24(1). doi:10.1186/s13075-022-02738-5

77. Mithieux SM, Weiss AS. ELASTIN. In: Parry DAD, Squire JM, eds. *Fibrous Proteins: Coiled-Coils, Collagen and Elastomers*. Vol 70. 1st ed. Elsevier Academic Press; 2005:437-461. doi:10.1016/S0065-3233(04)70013-3

78. Khavandgar Z, Roman H, Li J, et al. Elastin haploinsufficiency impedes the progression of arterial calcification in mgp-deficient mice. *Journal of Bone and Mineral Research*. 2014;29(2):327-337. doi:10.1002/jbmr.2039

79. Janssen R, Vermeer C. Vitamin K deficit and elastolysis theory in pulmonary elasto-degenerative diseases. *Med Hypotheses*. 2017;108:38-41. doi:10.1016/j.mehy.2017.07.029

80. Hinton RB, Adelman-Brown J, Witt S, et al. Elastin haploinsufficiency results in progressive aortic valve malformation and latent valve disease in a mouse model. *Circ Res*. 2010;107(4):549-557. doi:10.1161/CIRCRESAHA.110.221358

81. Lieschke GJ, Currie PD. Animal models of human disease: Zebrafish swim into view. *Nat Rev Genet*. 2007;8(5):353-367. doi:10.1038/nrg2091

82. Busse B, Galloway JL, Gray RS, Harris MP, Kwon RY. Zebrafish: An Emerging Model for Orthopedic Research. *Journal of Orthopaedic Research*. 2020;38(5):925-936. doi:10.1002/jor.24539

83. Gavaia PJ, Simes DC, Ortiz-Delgado JB, et al. Osteocalcin and matrix Gla protein in zebrafish (Danio rerio) and Senegal sole (Solea senegalensis): Comparative gene and protein expression during larval development through adulthood. *Gene Expression Patterns*. 2006;6(6):637-652. doi:10.1016/j.modgep.2005.11.010

84. Hinits Y, Pan L, Walker C, Dowd J, Moens CB, Hughes SM. Zebrafish Mef2ca and Mef2cb are essential for both first and second heart field cardiomyocyte differentiation. *Dev Biol*. 2012;369(2):199-210. doi:10.1016/j.ydbio.2012.06.019

85. Gemberling M, Bailey TJ, Hyde DR, Poss KD. The zebrafish as a model for complex tissue regeneration. *Trends in Genetics*. 2013;29(11):611-620. doi:10.1016/j.tig.2013.07.003

86. MacRae CA, Peterson RT. Zebrafish as tools for drug discovery. *Nat Rev Drug Discov*. 2015;14(10):721-731. doi:10.1038/nrd4627

87. Meunier R. Stages in the development of a model organism as a platform for mechanistic models in developmental biology: Zebrafish, 1970-2000. *Studies in History and Philosophy of Science Part C :Studies in History and Philosophy of Biological and Biomedical Sciences*. 2012;43(2):522-531. doi:10.1016/j.shpsc.2011.11.013

88. Dam D, Dijck A, Deyn P. *Animal Models of Dementia*. Vol 48. 1st ed. (Deyn P, Dam D, eds.). Humana Totowa; 2011. doi:https://doi.org/10.1007/978-1-60761-898-0

89. Bradford YM, Toro S, Ramachandran S, et al. Zebrafish models of human disease: Gaining insight into human disease at ZFIN. *ILAR J*. 2017;58(1):4-16. doi:10.1093/ilar/ilw040

90. Goldsmith JR, Jobin C. Think small: Zebrafish as a model system of human pathology. *J Biomed Biotechnol*. 2012;2012. doi:10.1155/2012/817341

91. Howe K, Clark MD, Torroja CF, et al. The zebrafish reference genome sequence and its relationship to the human genome. *Nature*. 2013;496(7446):498-503. doi:10.1038/nature12111

92. Hosen MJ, Vanakker OM, Willaert A, Huysseune A, Coucke P, Paepe A de. Zebrafish models for ectopic mineralization disorders: Practical issues from morpholino design to post-injection observations. *Front Genet*. 2013;4(MAY). doi:10.3389/fgene.2013.00074

93. Shin JT, Fishman MC. From zebrafish to human: Modular medical models. *Annu Rev Genomics Hum Genet*. 2002;3:311-340. doi:10.1146/annurev.genom.3.031402.131506

94. Yesudhason BV, Selvan Christyraj JRS, Ganesan M, et al. Developmental stages of zebrafish (Danio rerio) embryos and toxicological studies using foldscope microscope. *Cell Biol Int*. 2020;44(10):1968-1980. doi:10.1002/cbin.11412

95. NCBI. mgp matrix Gla protein [Danio rerio (zebrafish)]. Published January 2022. Accessed December 18, 2021. https://www.ncbi.nlm.nih.gov/gene/402937

96. Simes DC, Williamson MK, Ortiz-Delgado JB, Viegas C, Price PA, Cancela ML. *Purification of Matrix Gla Protein From a Marine Teleost Fish, Argyrosomus Regius: Calcified Cartilage and Not Bone as the Primary Site of MGP Accumulation in Fish*. Vol 18.; 2003.

97. UniProt. Accessed January 21, 2022. https://www.uniprot.org/uniprotkb/Q6YND0/entry

98. ZFIN Gene: mgp. mgp. Accessed January 7, 2022. https://zfin.org/ZDB-GENE-060928-1

99. NCBI. elna elastin a [Danio rerio (zebrafish)]. Published January 2022. Accessed December 18, 2021. https://www.ncbi.nlm.nih.gov/gene/790915#genomic-regions-transcripts-products

100. NCBI. elnb elastin b [Danio rerio (zebrafish)]. Published January 2022. Accessed December 19, 2021. elnb elastin b [Danio rerio (zebrafish)]

101. Miao M, Bruce AEE, Bhanji T, Davis EC, Keeley FW. Differential expression of two tropoelastin genes in zebrafish. *Matrix Biology*. 2007;26(2):115-124. doi:10.1016/j.matbio.2006.09.011

102. Hong YJ, Choi YW, Myung KB, Choi HY. The immunohistochemical patterns of calcification-related molecules in the epidermis and dermis of the zebrafish (Danio rerio). *Ann Dermatol*. 2011;23(3):299-303. doi:10.5021/ad.2011.23.3.299

103. Apschner A, Huitema LFA, Ponsioen B, Peterson-Maduro J, Schulte-Merker S. Zebrafish enpp1 mutants exhibit pathological mineralization, mimicking features of generalized arterial calcification of infancy (GACI) and pseudoxanthoma elasticum (PXE). *DMM Disease Models and Mechanisms*. 2014;7(7):811-822. doi:10.1242/dmm.015693

104. Czimer D, Porok K, Csete D, et al. A New Zebrafish Model for Pseudoxanthoma Elasticum. *Front Cell Dev Biol*. 2021;9. doi:10.3389/fcell.2021.628699

105. The Zebrafish Information Network. ZFIN Fish Search Results. Accessed January 12, 2022. https://zfin.org/action/fish/do-search?geneOrFeatureName=&mutationType=Any&anatomyTermIDs=&anatomyTermNames=&searchTerm=&filter1=tgOnly&sortBy=BEST_MATCH&maxDisplayRecords=&page=1

106. The Zebrafish Information Network. ZFIN Feature: uw101Tg. Accessed January 12, 2022. https://zfin.org/ZDB-ALT-131213-1

107. Yan YL, Miller C, Nissen R, et al. Oskar anchoring restricts pole plasm to the posterior of the Drosophila oocyte A zebrafish sox9 gene required for cartilage morphogenesis. *Development*. 2002;129(21):5065-5079. doi:10.1242/dev.129.21.5065

108. McMillan SC, Zhang J, Phan HE, et al. A regulatory pathway involving retinoic acid and calcineurin demarcates and maintains joint cells and osteoblasts in regenerating fin. *Development (Cambridge)*. 2018;145(11). doi:10.1242/DEV.161158

109. Jagadeeswaran P, Lin S, Weinstein B, Hutson A, Kim S. Loss of GATA1 and gain of FLI1 expression during thrombocyte maturation. *Blood Cells Mol Dis*. 2010;44(3):175-180. doi:10.1016/j.bcmd.2009.12.012

110. Tsuji-Tamura K, Morino-Koga S, Suzuki S, Ogawa M. The canonical smooth muscle cell marker TAGLN is present in endothelial cells and is involved in angiogenesis. *J Cell Sci*. 2021;134(15). doi:10.1242/JCS.254920

111. Yin X, Hao J, Yao Y. CRISPR/Cas9 in zebrafish: An attractive model for FBN1 genetic defects in humans. *Mol Genet Genomic Med*. 2021;9(10). doi:10.1002/mgg3.1775

112. Rodríguez-Rodríguez DR, Ramírez-Solís R, Garza-Elizondo MA, Garza-Rodríguez MDL, Barrera-Saldaña HA. Genome editing: A perspective on the application of CRISPR/Cas9 to study human diseases (Review). *Int J Mol Med*. 2019;43(4):1559-1574. doi:10.3892/ijmm.2019.4112

113. Lee MH, Shin J il, Yang JW, et al. Genome Editing Using CRISPR-Cas9 and Autoimmune Diseases: A Comprehensive Review. *Int J Mol Sci*. 2022;23(3). doi:10.3390/ijms23031337

114. Lanham KA, Prasch AL, Weina KM, Peterson RE, Heideman W. A dominant negative zebrafish Ahr2 partially protects developing zebrafish from dioxin toxicity. *PLoS One*. 2011;6(12). doi:10.1371/journal.pone.0028020

115. Gene Silencing Methods: CRISPR vs. RNAi vs. TALEN. abm. Accessed January 20, 2022. https://old.abmgood.com/marketing/knowledge_base/Gene-Silencing-CRISPR-TALEN-RNAi.php

116. Tarasco M, Martins G, Gavaia PJ, Bebianno MJ, Cancela ML, Laizé V. ZEB316: A Small Stand-Alone Housing System to Study Microplastics in Small Teleosts. *Zebrafish*. 2020;17(1):18-26. doi:10.1089/zeb.2019.1801

117. Martins G, Diogo P, Santos T, et al. Microdiet Formulation with Phospholipid Modulate Zebrafish Skeletal Development and Reproduction. *Zebrafish*. 2020;17(1):27-37. doi:10.1089/zeb.2019.1794

118. Farrar JS, Wittwer CT. High-Resolution Melting Curve Analysis for Molecular Diagnostics. In: *Molecular Diagnostics: Third Edition*. Elsevier Inc.; 2017:79-102. doi:10.1016/B978-0-12-802971-8.00006-7

119. Pingault V, Zerad L, Bertani-Torres W, Bondurand N. SOX10: 20 years of phenotypic plurality and current understanding of its developmental function. *J Med Genet*. 2022;59(2):105-114. doi:10.1136/jmedgenet-2021-108105

120. Antonacopoulou AG, Grivas PD, Skarlas L, Kalofonos M, Scopa CD, Kalofonos HP. POLR2F, ATP6V0A1 and PRNP expression in colorectal cancer: new molecules with prognostic significance? *Anticancer Res*. 2008;28(2B):1221-1227.

121. Alieva AK, Filatova E v., Rudenok MM, Slominsky PA, Shadrina MI. Housekeeping genes for parkinson's disease in humans and mice. *Cells*. 2021;10(9). doi:10.3390/cells10092252

122. Simes DC, Williamson MK, Schaff BJ, et al. Characterization of Osteocalcin (BGP) and Matrix Gla Protein (MGP) Fish Specific Antibodies: Validation for Immunodetection Studies in Lower Vertebrates. *Calcif Tissue Int*. 2004;74(2):170-180. doi:10.1007/s00223-003-0079-4

123. Huang J, Kong Y, Xie C, Zhou L. Stem/progenitor cell in kidney: characteristics, homing, coordination, and maintenance. *Stem Cell Res Ther*. 2021;12(1). doi:10.1186/s13287-021-02266-0

Appendix

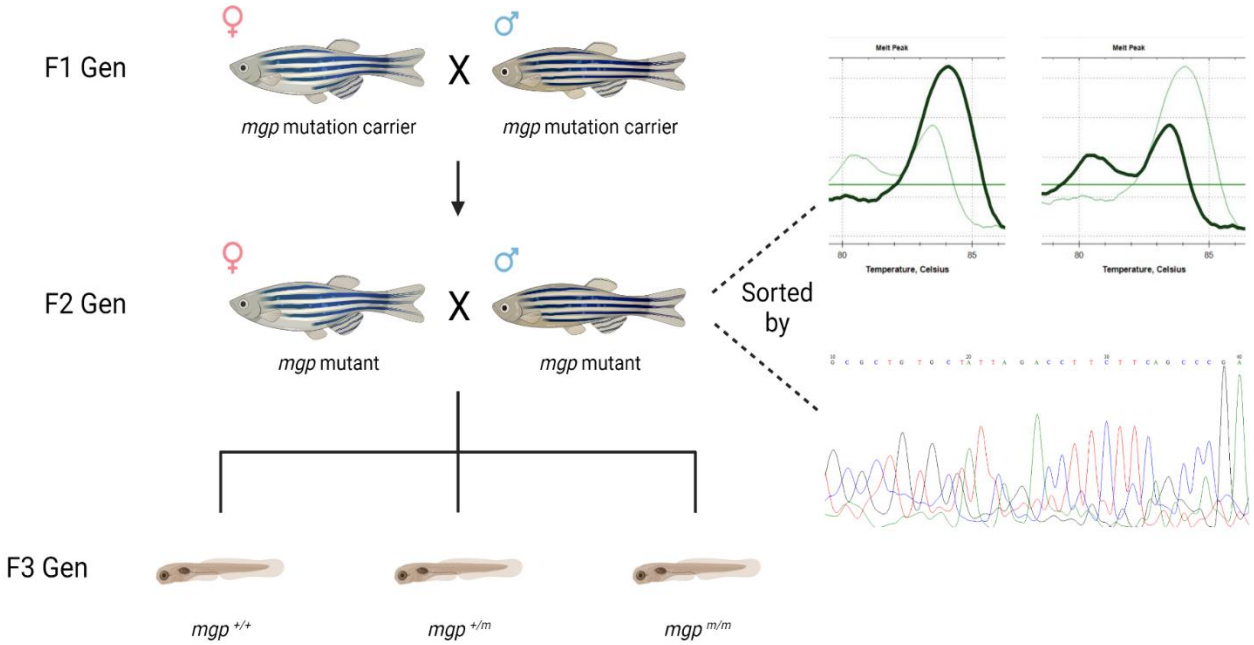

Figure A.1. Crossings of the *mgp* mutants to obtain the F3 generation zebrafish. The F1 Gen (*mgp* mutation carriers) were crossed to obtain the F2 generation. The F2 generation was sorted by Real-time qPCR and subsequently sequencing after 3 mpf, as performed for the sorting and genotyping of the F1 generation. Once the F2 generation was sorted, crossings were performed to obtain the F3 generation larvae for the 3 genotypes (*mgp* $^{m/m}$ mutants, *mgp* $^{+/m}$ mutants and *mgp* $^{+/+}$).

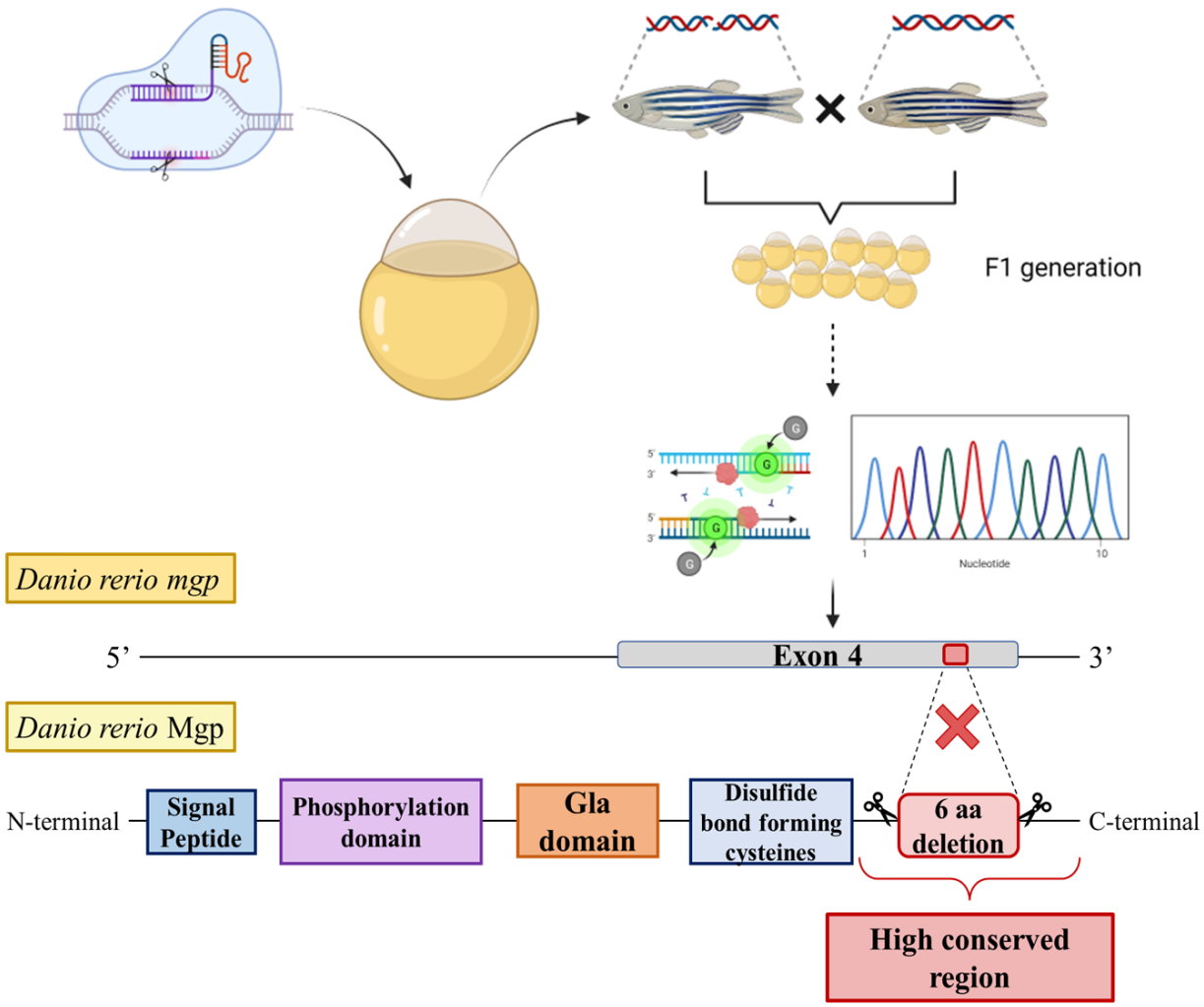

Figure A. 2. Summary image of the knockout *mgp* mutant generation. Mutant Dre_mgpΔ18 (Chr 3: 1415226-1415243) +/CGGTTCTCAGGTGGCCTA, were generated by Stainier's Lab at Max Planck institute. The *mgp* mutants were characterized by RT-PCR and sequencing. The mutation was identified in exon 4 as an 18-nucleotide deletion in zebrafish *mgp* gene and through sequence alignment predicted as a 6-amino acid deletion at the Mgp C-terminal.